AD-785 704

INVESTIGATION OF BACK-BLAST
ATTENUATORS FOR RECOILLESS RIFLES

A. T. Sutor

Rockwell International Corporation

Prepared for:

Watervliet Arsenal

June 1974

SECURITY CLASSIFICATION OF THIS PAGE (When Data Entered)

REPORT DOCUMENTATION PAGE

READ INSTRUCTIONS BEFORE COMPLETING FORM

1. REPORT NUMBER	2. GOVT ACCESSION NO.	3. RECIPIENT'S CATALOG NUMBER
WVT-CR-74018		AD-785 704

4. TITLE (and Subtitle)

Investigation of Back-Blast Attenuators for Recoilless Rifles

5. TYPE OF REPORT & PERIOD COVERED

Final

6. PERFORMING ORG. REPORT NUMBER

R-9343 (Sep 73)

7. AUTHOR(s)

A. T. Sutor

8. CONTRACT OR GRANT NUMBER(s)

Contract DAAF07-73-C-0159

9. PERFORMING ORGANIZATION NAME AND ADDRESS

Rocketdyne Division
Rockwell International
6633 Canoga Avenue, Canoga Park, California 91304

10. PROGRAM ELEMENT, PROJECT, TASK AREA & WORK UNIT NUMBERS

AMCMS No. 513F.12.05014.02
DA Project No. 1F163206D050
Pron No. EJ-2-50139-(01)-M7-M7

11. CONTROLLING OFFICE NAME AND ADDRESS

Benet Weapons Laboratory
Watervliet Arsenal
Watervliet, N.Y. 12189

12. REPORT DATE

June 1974

13. NUMBER OF PAGES

124

14. MONITORING AGENCY NAME & ADDRESS(if different from Controlling Office)

15. SECURITY CLASS. (of this report)

UNCLASSIFIED

15a. DECLASSIFICATION/DOWNGRADING SCHEDULE

16. DISTRIBUTION STATEMENT (of this Report)

Approved for release; distribution unlimited.

17. DISTRIBUTION STATEMENT (of the abstract entered in Block 20, if different from Report)

Reproduced by
NATIONAL TECHNICAL
INFORMATION SERVICE
U S Department of Commerce
Springfield VA 22151

18. SUPPLEMENTARY NOTES

Reproduced from
best available copy.

19. KEY WORDS (Continue on reverse side if necessary and identify by block number)

Blast Suppression
Recoilless Rifle, Back Blast Suppressor
Suppressor Design

20. ABSTRACT (Continue on reverse side if necessary and identify by block number)

Based on a series of water table tests, various configurations of recoilless rifle back blast suppressor models were designed and fabricated for shock tube experiments. Various lengths of suppressor were tested with enclosed cavities for damping the blast wave. Because the blast wave suppression was less than desired, a new series of mufflers, using commercial washers, was tested. Results were encouraging and attenuations of 62 to 74 per cent were measured in the regions of peak blast wave pressure. ——— SEE REVERSE SIDE

DD FORM 1 JAN 73 **1473** EDITION OF 1 NOV 65 IS OBSOLETE

ABSTRACT (Continued)

Block No. 20

   A design concept based on the best suppressor design tested was incorporated into a layout drawing. This suppressor design consisted of a multinozzle plate and adapter which attaches to the Army 105 mm recoilless rifle. Because the maximum allowable rifle length of 170 inches permitted a 21-inch increase in the current rifle length, this additional length was used for a multi-hole muffler. A full-scale Rocketdyne drawing was submitted with the report. The submitted back blast suppressor design was 16 inches in diameter and 23.5 inches long and contained 253 holes for the nozzle plate. The design was stressed for 12,000 psi chamber pressure and was designed to attenuate the original blast pressure to 5 psi anywhere along the helicopter surface.

   A recommended test procedure for the 105 mm recoilless rifle at Picatinny Arsenal included a series of tests at increasing chamber pressure. It was suggested that the test procedure, including free field pressure measurement location, be the same as that used for previous rifle tests. Measurement of the reflected blast wave pressures at specific locations was recommended, with the addition of two pressure transducers and three strain gages, all mounted on the suppressor.

DISCLAIMER

The findings in this report are not to be construed as an official
Department of the Army position unless so designated by other authorized
documents.

The use of trade name(s) and/or manufacturer(s) in this report does not
constitute an official indorsement or approval.

DISPOSITION

Destroy this report when it is no longer needed. Do not return it to
the originator.

iii

WVT-CR-74018

AD

INVESTIGATION OF BACK-BLAST ATTENUATORS
FOR RECOILLESS RIFLES

PREPARED BY

A. T. SUTOR
ROCKETDYNE DIVISION
ROCKWELL INTERNATIONAL
6633 CANOGA AVENUE
CANOGA PARK, CALIFORNIA 91304

PREPARED FOR

BENET WEAPONS LABORATORY
WATERVLIET ARSENAL
WATERVLIET, N.Y.   12189

JUNE 1974

TECHNICAL REPORT

iV

FOREWORD

This report is submitted in partial fulfillment of the requirements for Contract No. DAAF07-73-C-0159, sponsored by the Department of the Army, Watervliet Arsenal, Watervliet, New York. The Watervliet Arsenal Technical Representative was Mr. Donald Spring, with technical assistance provided by Major John R. Adams and Mr. Charles A. Andrade.

The work was performed by the Rocketdyne Division of Rockwell International. The Program Manager was Mr. L. P. Combs and the Principal Engineer was Mr. A. T. Sutor. The following Rocketdyne personnel contributed to the investigation: G. Ratekin, Water Table Testing; R. Kassner, Theoretical Analyses; S. Logan and C. Brown, Helium Shock Tube Tests; G. Hood and E. A. Rojec, Instrumentation; G. D. Artz, Propellant Firing Tests; and W. R. Wagner, Design Concepts, Heat Transfer, and Rocket-Assist Analysis.

CONTENTS

INTRODUCTION AND SUMMARY

Recoillessness is achieved in a recoilless rifle by discharging a portion of the gun propellant combustion product gases in the opposite direction to that of the projectile and propulsive gases issuing from the rifle's muzzle. To maximize the impulse obtained from the back-discharged gases, they are typically expelled through a convergent, divergent (de Laval) nozzle.

Flow through the back-flow nozzle, being determined by the breech pressure profile when a round is fired, is a short-duration transient pulse. Typically, the breech pressure rise is rapid enough that initiation of nozzle flow produces a moderately high-amplitude blast wave which propagates away from the nozzle, through the atmosphere surrounding the rifle. Although this back blast is aft-directed (i.e., is nonspherical) and is attenuated by wave-front expansion as it propagates away from the nozzle source, the wave pressure may be high enough to injure personnel or damage structures placed in its path. While the initial or frontal blast wave usually represents the strongest damage potential, additional, subsequent waves can be generated by the continuing flow through the nozzle, and the high temperature gases themselves may contribute to overall damage which might be sustained in the back-blast region.

This report is concerned with a predominantly experimental development of design concepts for devices capable of reducing the back-blast amplitude produced by a 105-mm recoilless rifle to levels that would permit it to be mounted on an outboard bomb shackle of a Cobra helicopter. The major goal was reduction of peak reflected pressures, at any point along the helicopter surface, from anticipated amplitudes on the order of 30 to 35 psi to no more than 5 psi. Candidate designs were constrained by a limitation that the weapon length not be increased by more than 21 inches. Secondary objectives were concerned with the durability of the attenuation device, its effects on recoillessness and, if the major objective could not be met for a pure recoilless rifle, how much breech pressure reduction, in conjunction with a rocket-assisted projectile, would permit blast amplitudes to be reduced below the allowable level.

The program conducted by Rocketdyne comprised a systematic series of subscale laboratory experiments of three types: (1) two-dimensional cold-flow screening tests on a water table, (2) three-dimensional cold-flow experiments with a helium/air shock apparatus in an evacuated chamber, and (3) gun propellant firings of the same shock apparatus in an atmospheric-pressure gun-firing range. The water table was used to obtain qualitative comparisons among several candidate design concepts and preliminary estimates of their required sizes. The more promising candidates were then tested in the three-dimensional shock apparatus to gain more-nearly quantitative assessments of their potential. From the data obtained, a full-scale attenuator design concept was evolved and submitted to Watervliet Arsenal as a candidate to be tested on the full-scale, 105-mm recoilless rifle.

Because of the attenuator length constraint, the full-scale design was based on replacing the rifle's back-flow nozzle with a multinozzle discharge plate, with each of a large number of small-diameter nozzles discharging into an individual attenuator tube packed with an alternating series of spacers and washers. (Small diameters were required to provide the moderately high attenuator length/nozzle diameter found necessary to accomplish the required level of back-blast attenuation.) Partly because of the complexity and estimated cost of a full-scale attenuator, and partly because of their changing recoilless rifle program requirements, Watervliet Arsenal decided to delay building and testing the full-scale attenuator and to conduct, instead, subscale gun propellant firing tests at Rocketdyne of a few tubes from the full-scale design.

The subscale gun propellant firing tests demonstrated conclusively that the attenuator design conceived under this program can provide more than the required back-blast attenuation and that it is structurally capable of withstanding the sequential firing of many rounds.

105-MM RECOILLESS RIFLE CHARACTERISTICS

The effort described in this report was oriented specifically toward attenuation of the back blast produced by firing a 105-mm recoilless rifle being developed by Watervliet Arsenal for potential application as armament for the Cobra helicopter. The Army's development testing employed a single-round combustion chamber/breech assembly shown in Fig. 1. The back-flow nozzle for providing thrust to counteract the rifle recoil is clearly evident on the left end of the assembly. A lightweight (~1/8-inch thick), sheet metal burst disk was clamped between the nozzle and the combustion chamber, primarily to prevent contamination of the gun propellant before it was fired.

Firing a 25-pound projectile, the rifle was designed to have peak breech pressures of approximately 12,000 psi and yield projectile muzzle velocities of 1800 ft/sec. In most of the Army tests, however, peak pressures ranged between 4000 and 8000 psi. Breech pressure rise rates were approximately 4×10^6 psi/sec preceding the peak pressure, and the durations of the pressure pulses were on the order of 10 to 20 milliseconds.

NOZZLE
SK-MGH-5671

O-RING
MS 28513-265
SEE NOTE 2

PROPELLAN
SK-MGH-56

HOUSING
SK-MGH-5658

DISC, BURST
SK-MGH-5672

IGN
SK-M

ADAPTER
SK-MGH-5668

SLEEVE
SK-MGH-5659

EXIT CONE
SK-MGH-5670

IGN
PAD

SECTION A-A

GUN PROPELLANT

CAP, SK-MGH-5682

IGNITION CHARGE
SEE NOTE 3

IGNITER TUBE
SK-MGH-5668
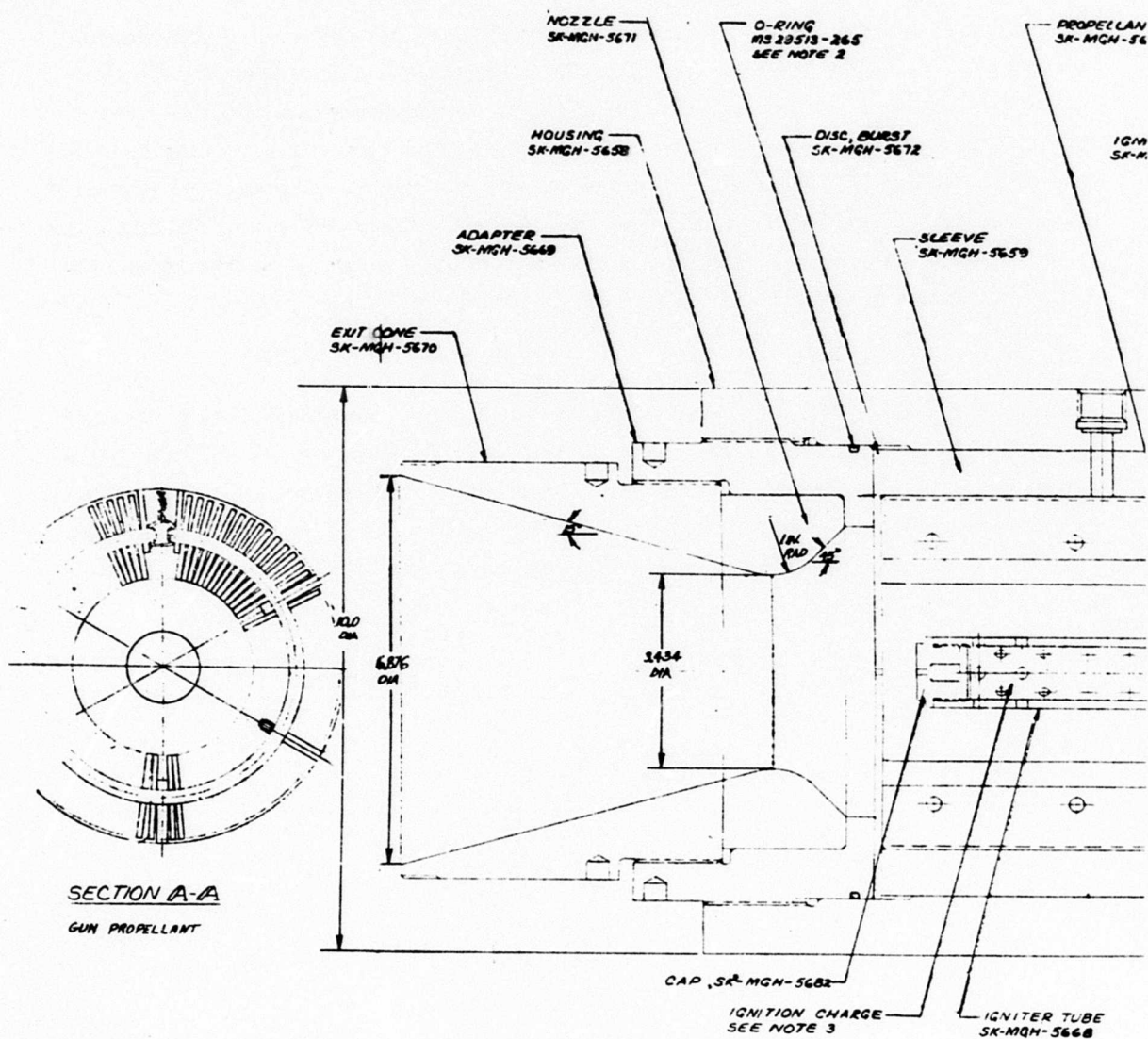
NOTES:-
1- SPEC MIL-A-2550 APPLIES.
2- AT ASSEMBLY COAT O-RING WITH SILICONE COMPOUND, SPEC MIL-S-8660.
3- TO BE SPECIFIED BY ENGINEER.
4- SPOTFACE AS REQUIRED TO SEAT CAP SCREWS.
5- LOCATE FROM CHANNEL, DWG NO. WTV-C20943 (2 PLACES).
6- INSTALL CAP SCREW MS 16997-191 BEFORE FASTENING ADAPTER SK-MGH-5657 TO REAR SUPPORT.
7- TO BE ASSEMBLED AT TEST SITE. USE METHOD OUTLINED FOR GENERAL ASSEMBLY ON DWG NO. WTV-F 16771.
   LOCATE AND DRILL HOLES FOR ROLL PINS FROM PILOT HOLES ON BASE PLATE OF REAR SUPPORT.
8- COMMERCIAL EQUIVALENT ACCEPTABLE.
9- APPLY SURFACE PRIMER N' SPEC MIL-S-22473 ALLOW PRIMER TO DRY FOR ONE MINUTE, FOLLOWED
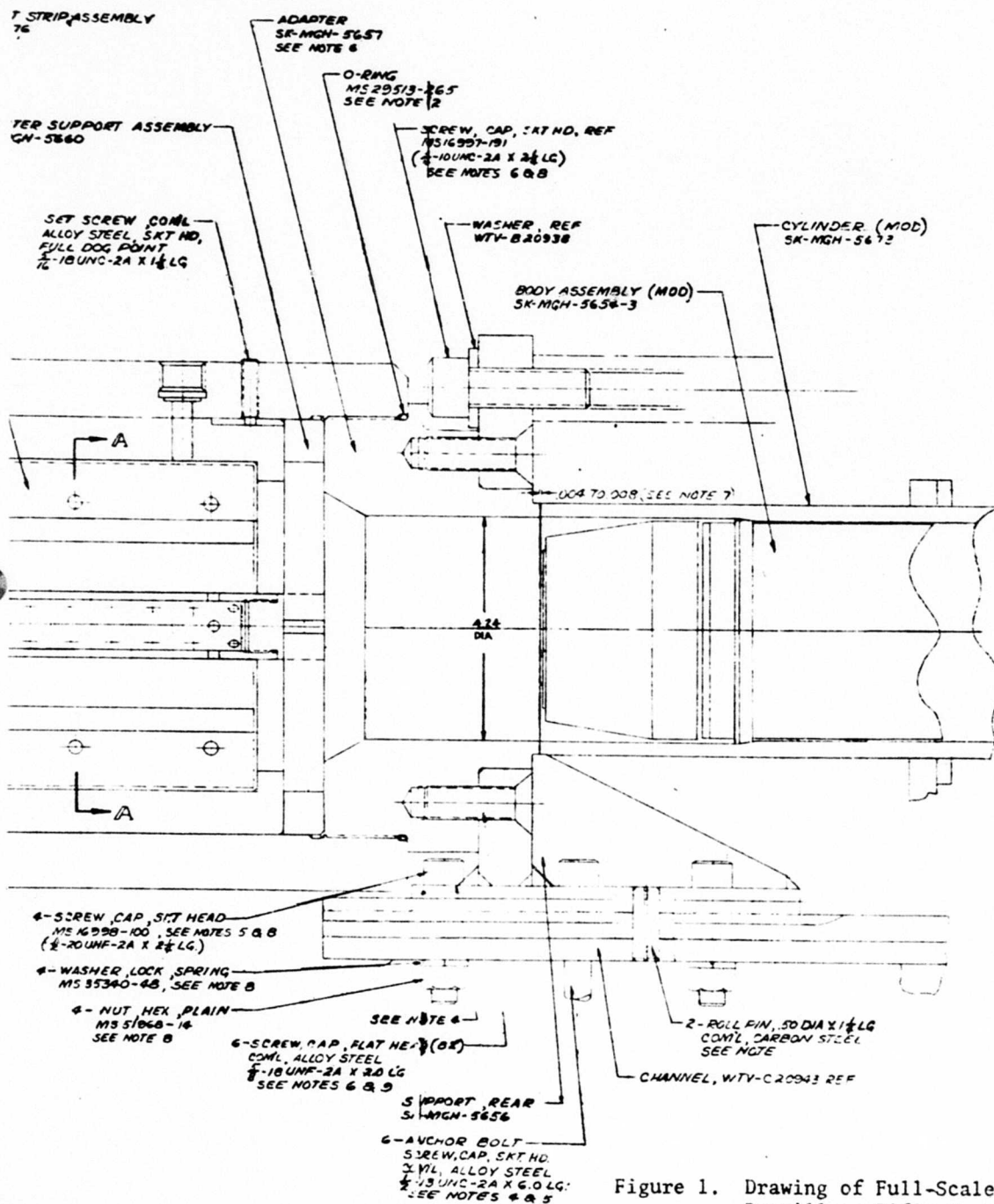   BY SEALING COMPOUND GRADE 'EV' SPEC MIL-S-22473 360° ON FIRST TWO THREADS OF ENGAGEMENT.

4

Figure 1. Drawing of Full-Scale 105-mm Recoilless Rifle Combustion Chamber/Breech Assembly

ANALYSIS TO SUPPORT MODEL TESTING

Analyses were performed to furnish answers to a number of questions regarding proper selection of basic parameters for the model tests.

SHOCK TUBE TEST PARAMETERS

It was to be determined whether shock waves of sufficient strength can be produced in the shock tube test so that the shocks produced by the rifle can be simulated. The curves of Fig. 2, correlating the shock-wave strengths produced in simple (constant-area) shock tubes for different driver gases, were established to answer this question. The subscripts in Fig. 2 are defined below:

1. The condition of the air at rest at low pressure

2. The condition of the air behind the shock front

3. The condition of the driver gas behind the contact surface with the air

4. The condition of the driver gas prior to bursting of the diaphragm

The curves show the effects of different gas properties. It can be seen that none of the driver gases exactly model the behavior of the hot gas. However, helium is superior to air insofar as the achievable shock-wave strengths come considerably closer to those of the hot-gas case. Helium was selected as the driver gas for the scheduled shock-tube tests.

Water table experiments conducted at Rocketdyne were scaled to gas pressure ratios and superimposed on the same chart. The water table can thus be used to establish wave-attenuation trends for shock-attenuation configurations.
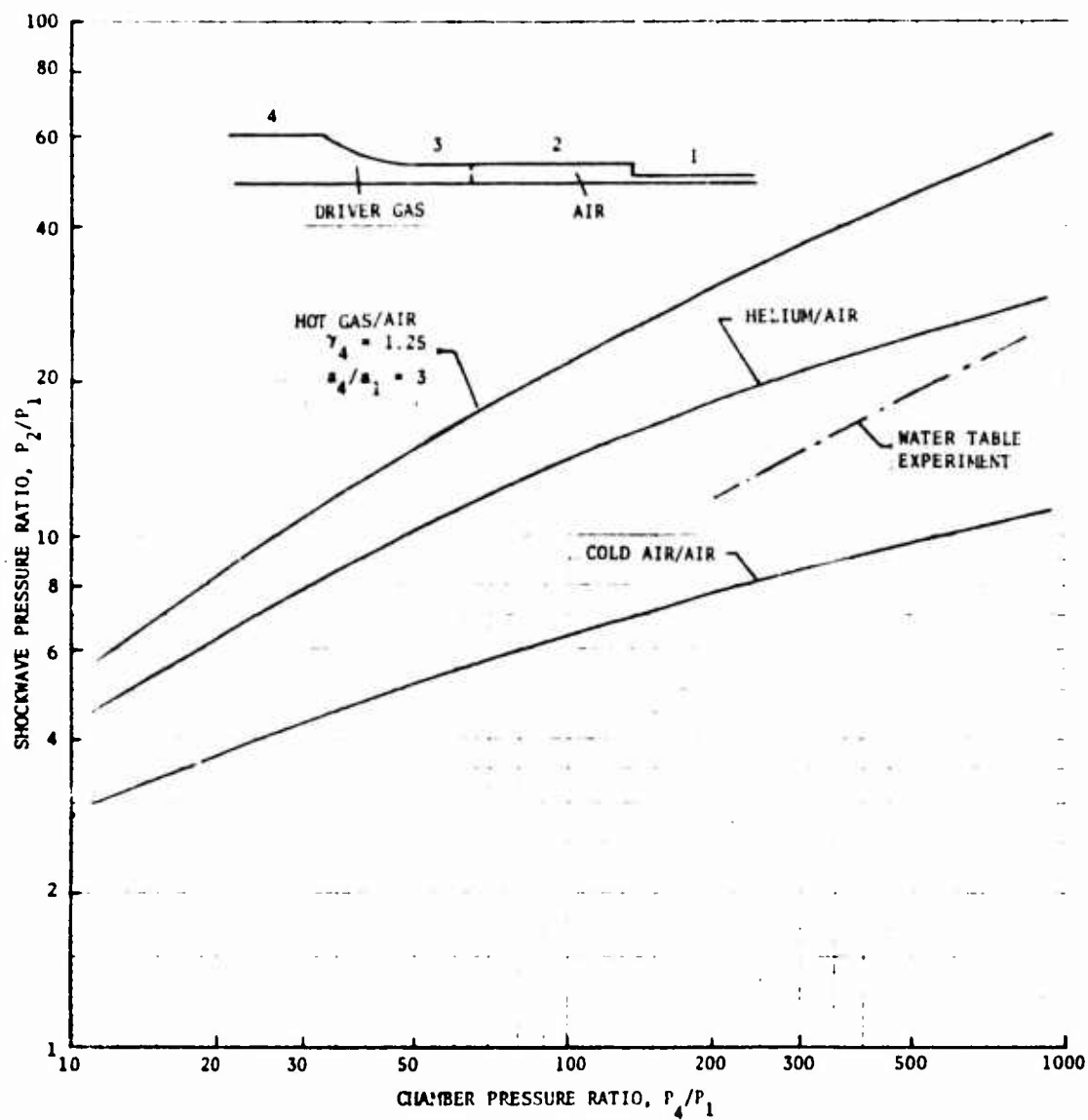
Figure 2. Shockwave Strength for Different Fluids

EFFECT OF AREA CHANGE IN THE SHOCK TUBE
ON SHOCK-WAVE STRENGTH

The design configuration to be employed in the shock-tube model features a larger cross section upstream of the diaphragm than that of the suppression device downstream of the nozzle. Therefore, the preceding analysis was extended to include the effect of such area changes on shock strength.

The analysis method by Alpher and White (Ref. 1) was applied. This analysis is based on certain ideal assumptions. All the area change is assumed to occur sufficiently close to the diaphragm section so that wave phenomena within the zone of area change can be neglected. Nonsteady waves then occur only upstream and downstream of the area change while, in each instant, the flow and state parameters immediately upstream and downstream of the variable-area zone are connected by the isentropic steady-state relationships. Although these assumptions are not quite realistic for the present application, it was felt that they would still properly reflect the trends.

It is seen in Fig. 3 that the overall contraction area ratio of $A_4/A_1 = 4$ (chamber cross section to suppressor cross section) would result in an enhancement of the shock-wave pressure ratio associated with a given diaphragm pressure ratio. For the case shown with helium as the driver gas, the shock-wave pressure ratio would increase from approximately 28 without contraction to approximately 38 with contraction, at a diaphragm pressure ratio of 800.

This increase was considered significant because it would enable a closer simulation by the model test of the actual shock strength at the suppressor entrance occurring in the rifle. Therefore, it would increase the confidence in the applicability of the test results.

1. Alpher, R. A. and D. R. White: "Flow in Shock Tubes With Area Change at the Diaphragm Section," J. of Fluid Mech., Vol. 3, February 1958, p. 457.
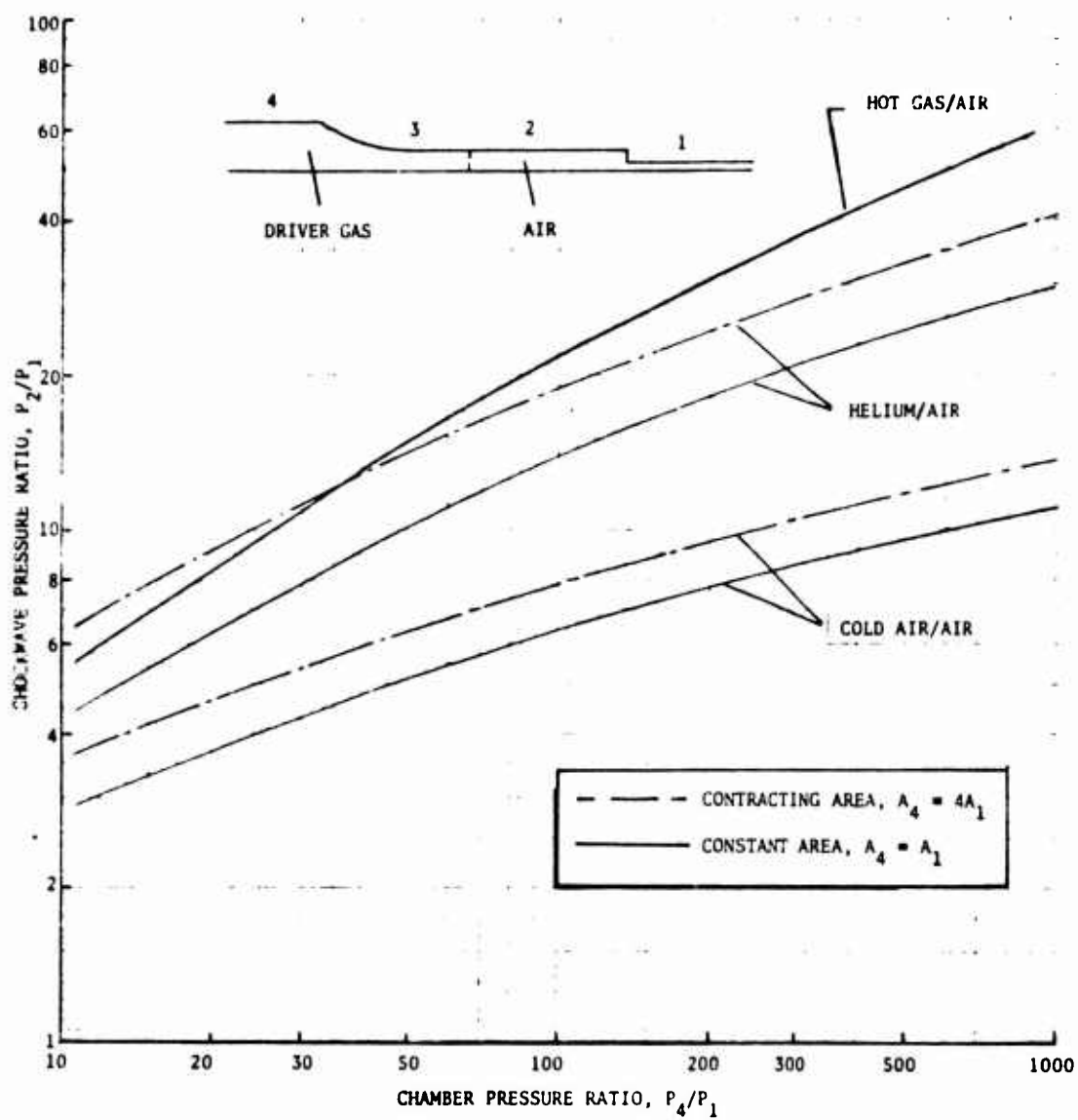
Figure 3. Effects of Area Change on Shockwave Strength

WATER TABLE TEST PROGRAM

In the water table experiment, a hydraulic shock is produced by sudden opening of a shutter which is the analog of the bursting of the diaphragm in the shock-tube test. The applicable analogy between water height ratios for the hydraulic-shock and air-shock pressure ratios is presented in Fig. 4.

However, there is no strict analogy between the water table and the gas shock tube regarding the processes taking place in the driver sections. There, the thermodynamic differences (specific heat ratios, γ, and ratios of sonic velocities) of driver gas and driven gas cannot be modeled by the water table. Also, very large local variations in water height and large slopes of the water surface are caused by expansion waves. These tend to produce strong deviations from the usual water table behavior by which a gas with $\gamma = 2$ is modeled, making analytical predictions difficult. Therefore, to obtain the true correlations governing the water table experiment, a simple shock tube experiment was conducted with a water channel of constant width. The wave strengths, Y_2/Y_1, were measured as functions of the "diaphragm" height ratios Y_4/Y_1. These were then converted to gas pressure ratios, using the conversion curve. The resulting curve, $P_2/P_1 = f (P_4/P_1)$, indicated in Fig. 2 is close to that for the subsequent air shock tube tests with helium gas as driver.

WATER TABLE SUPPRESSOR CONFIGURATION TEST RESULTS

A curve was established to give the experimental relationship of water wave strength (Y_e/Y_a) to the driving head (Y_c/Y_a). This is shown in Fig. 5 and indicates good agreement between the present data and previous OV-10 data. This curve was primarily a working curve for use with the remainder of the data. The recoilless rifle driving pressure ratio was nominally scaled to the water table using a water driving head ratio of 37. To simplify testing, the curve in Fig. 5 was established so it was not necessary to make each run with $Y_c/Y_a = 37$. For most of the test runs, the ratio Y_c/Y_a fell between 30 and 38, and the results were then scaled to a value of 37 using this curve.

TO CONVERT WATER HEIGHT RATIO TO SHOCK FRONT
PRESSURE, FIND PRESSURE RATIO CORRESPONDING
TO HEIGHT RATIO ON THIS CHART AND MULTIPLY
BY ATMOSPHERIC PRESSURE

BLAST WAVE PRESSURE RATIO (P/P_o)

P_o - ATMOSPHERIC PRESSURE

WATER TABLE WAVE HEIGHT RATIO (y/y_o)
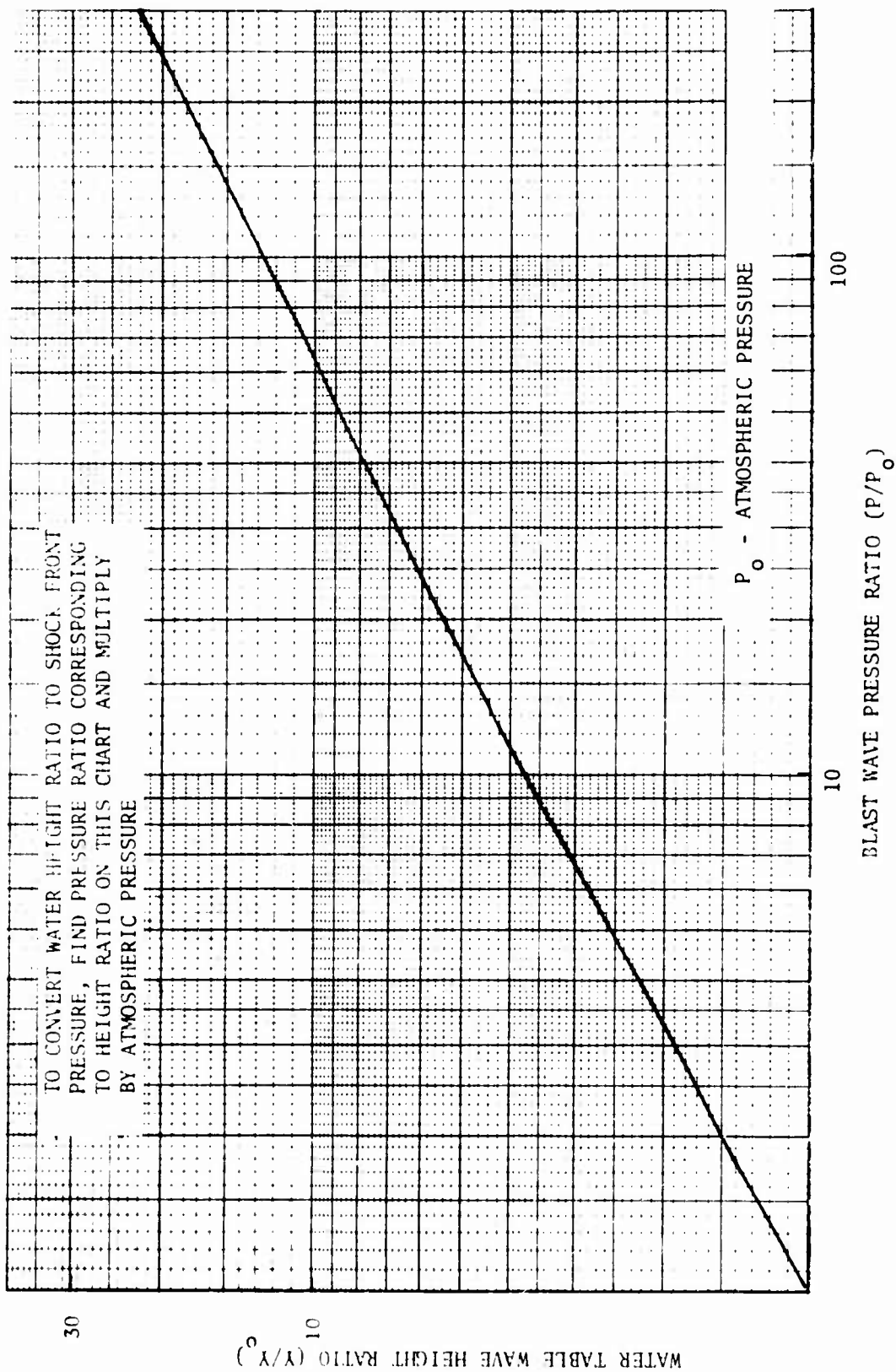
Figure 4.   Conversion of Water Table Wave Height Ratio to Gaseous Shock Front
Pressure Ratio

R-9343

Figure 5. Water Wave Height as a Function of Initial Head Pressure
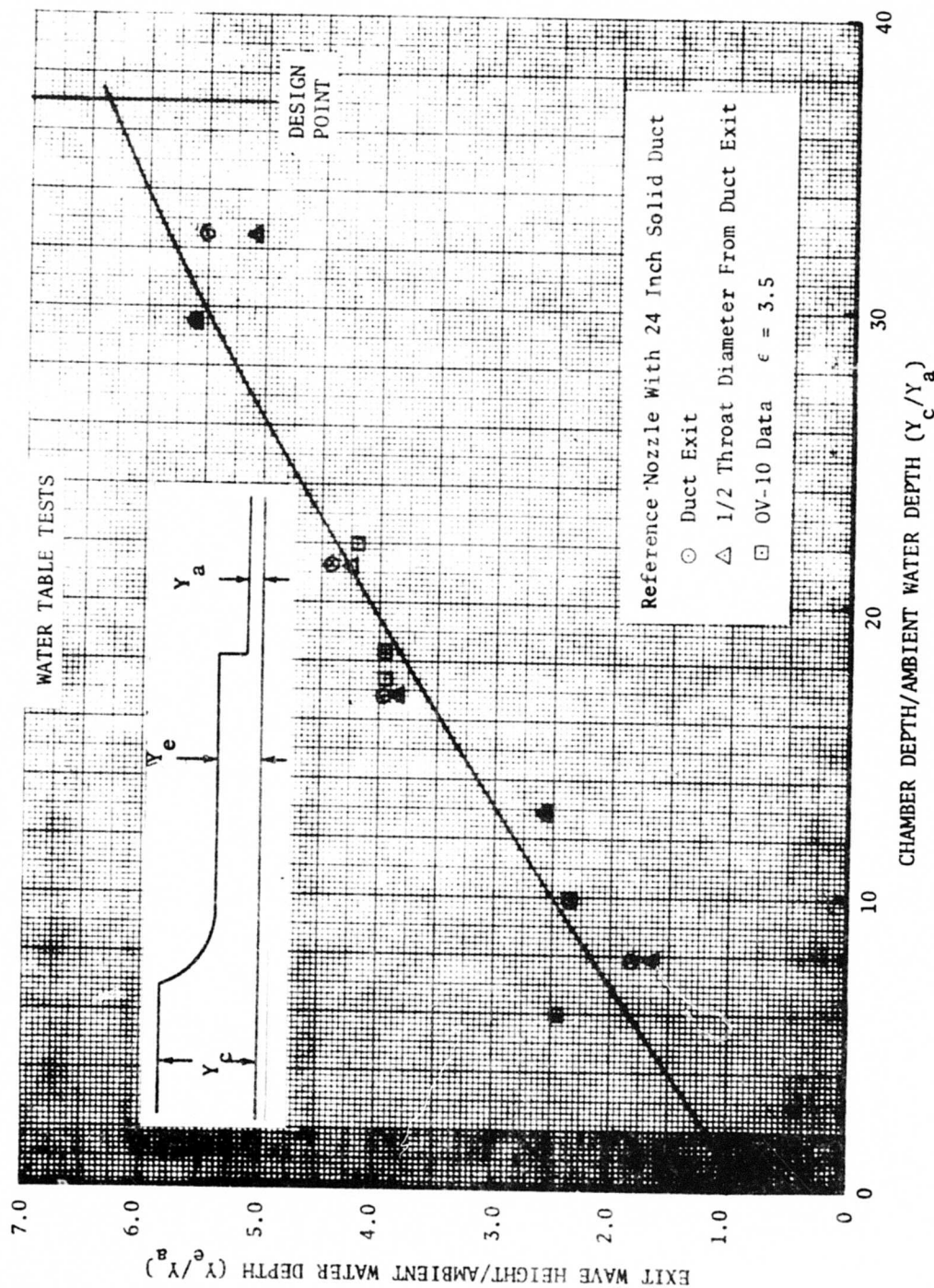
The basic suppressor designs tested and relative performance are shown in Fig. 6. The water table attenuation factor is defined as:

$$A_w = \frac{Y_2/Y_a}{(Y_e/Y_a)_{ref}}$$

where:

A_w = water table attenuation factor

Y_e/Y_a = wave strength at suppressor exit

$(Y_e/Y_a)_{ref}$ = wave strength at exit of straight-wall duct (the same length and inside diameter of the suppressor studied)

This factor was scaled to air (A_a) by scaling Y_e/Y_a to (P_e/P_a) and $(Y_e/Y_a)_{ref}$ to $(P_e/P_a)_{ref}$ by means of Fig. 4 and plotted in Fig. 6, where:

$$A_a = \frac{P_e/P_a}{(P_e/P_a)_{ref}}$$

The blast wave suppressor used for test 6 was not effective. The initial blast wave expanded into the suppressor cavity, forming a secondary wave, but this secondary wave traveled only slightly behind the primary wave that continued down the duct. The end result was recombination of the secondary wave with the primary wave and little reduction in the exiting wave strength.

The suppressor studied in test 19 behaved in a manner relative to that of test 6. However, part of the secondary wave was effectively suppressed in the outermost row of baffles where closed cavities existed, and the performance was considerably improved.

A multinozzle with interacting suppressor cavities was modeled in test 31. This suppressor design was of interest because of the simplicity of fabrication. Interaction and cancellation of the secondary waves between the nozzles was indicated and resulted in a considerable improvement over the design studied in test 6.
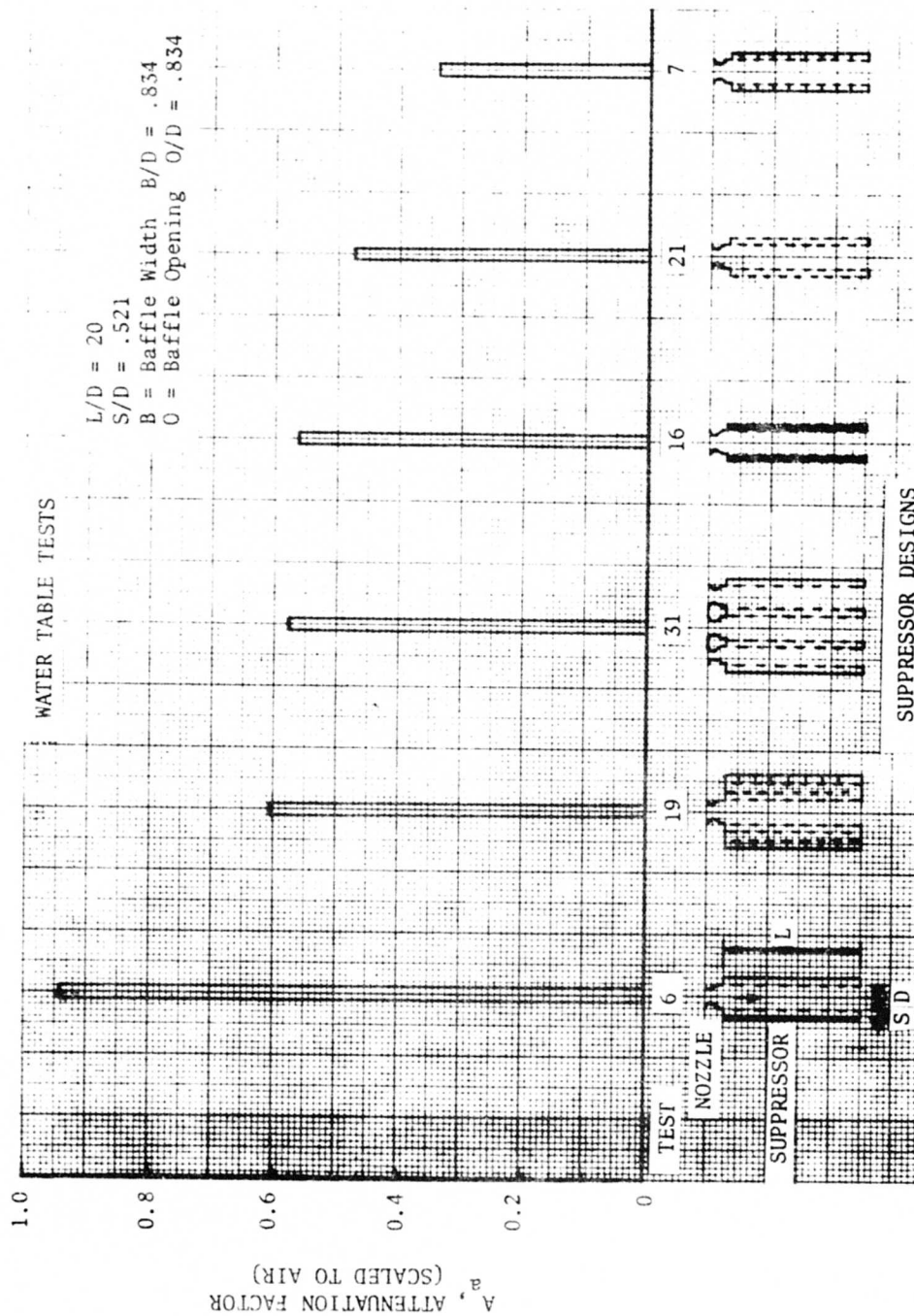
Figure 6. Comparison of Suppressor Designs

The same configuration was tested in tests 16 and 21. Packing was added for test 16. Both devices allowed the secondary wave to exit through the sides of the suppressor. It was considered that this accounted for the improved performance as compared to test 6. The packing in test 16 apparently gave slightly decreased attenuation because it tended to block the passage of the secondary wave through the suppressor sides. It is noted that neither of these designs represent a realistic design for application to a multinozzle because each suppressor is bordered on all sides by other suppressors, resulting in the configuration of test 31.

The final configuration shown in Fig. 6 (test 7) was clearly superior to the other designs. The design used a series of individual closed cavities. The primary wave expanded into each of the cavities, forming a series of secondary waves. Consequently, each cavity decreased the primary wave strength. Also, the cavities were designed so that considerable time, relative to the primary wave speed, was required for the secondary wave to travel in, and then back out of, a cavity. This configuration resulted in an attenuation of the scaled air wave to 34 percent of the unsuppressed strength. Because relatively large wave attenuations ($A_a \cong .10$ to 15 percent) are the goal of this study, this design was selected for further refinement.

The suppressor length relative to diameter (L/D) has a strong effect on suppressor attenuation. Four tests were made to develop the curve shown in Fig. 7. These runs used the same hardware, with the only variation being in the nozzle and suppressor widths (diameter). The curve was scaled to air and indicates that for this design, an L/D of 40 to 50 would be required to achieve the desired attenuation.

Increasing L/D in these tests resulted in larger cavities relative to the width (diameter) which resulted in increased attenuation. It was found that the same effect could be achieved by increasing the number of cavities of constant size. However, little or no improvement was achieved when the number of cavities was increased by proportionately decreasing the cavity size (no L/D increase). It may be possible to decrease the required L/D by improving the cavity design, but with the selected suppressor design, L/D appeared to be the most important parameter governing attenuation.
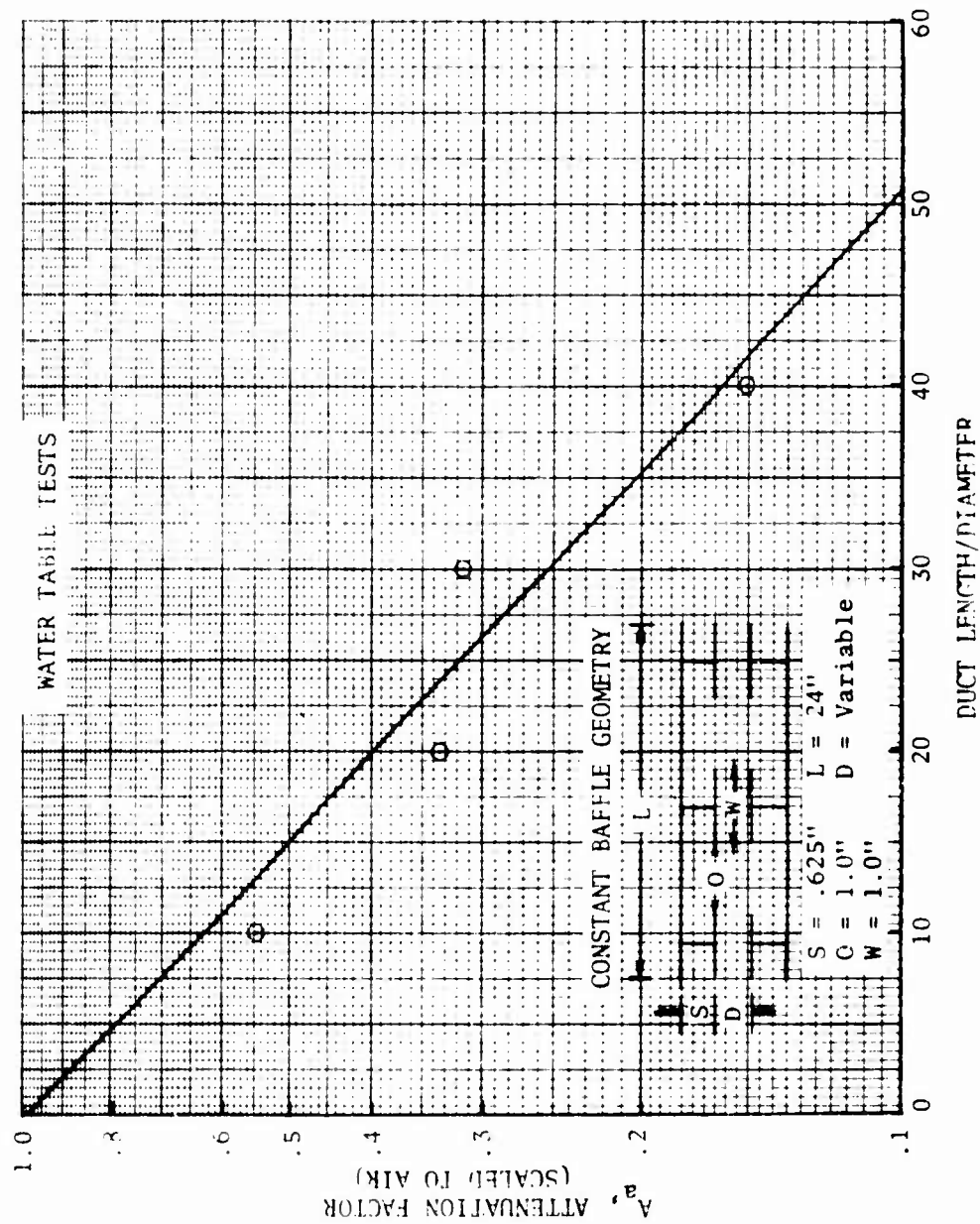
Figure 7. Effect of Suppressor Length on Wave Attenuation

Three water table tests were made to examine the effect of cavity depth on atten-
uation (Fig. 8). All parameters were held constant except cavity depth. The
data indicated that increased cavity depth resulted in increased attenuation. It
is thought that this resulted from the increased cavity volume and the resulting
increased time required for the secondary wave to travel in, and then out of, the
cavity. Consequently, it is desirable to use large suppressor cavity depths if
sufficient space is available.

WATER TABLE MODEL SUPPRESSOR PHOTOGRAPHY

Four photographs representative of the water table tests are shown in Fig. 9
through 12. The parameters significant to the suppressor model are listed with
the sketch below.
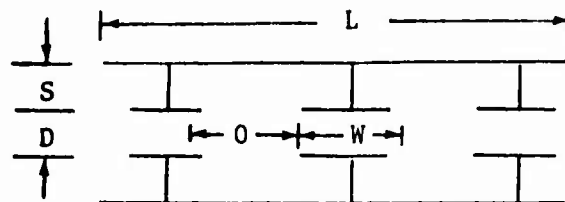
L/D = 20; O/D = 0.833; W/D = 0.833; S/D = 0.833; D = 1.2 inch

All four photographs show the water table analogous blast wave traveling down the
suppressor.

Figures 9 and 10 are photographs taken looking along the axis of the suppressor
from the exit end. The blast wave can be seen near the middle of the suppressor
in Fig. 9, and several diameters downstream of the suppressor in Fig. 10. The
exiting wave was observed to be considerably smaller than the entering wave.

Figures 11 and 12 are side-view photographs of the suppressor taken through a
transparent wall. The simulated blast wave can be seen in the baffle chambers.
Figure 11 shows the wave in the initial section of the suppressor where the front
is seen to be quite strong. The wave front was nearing the suppressor exit in
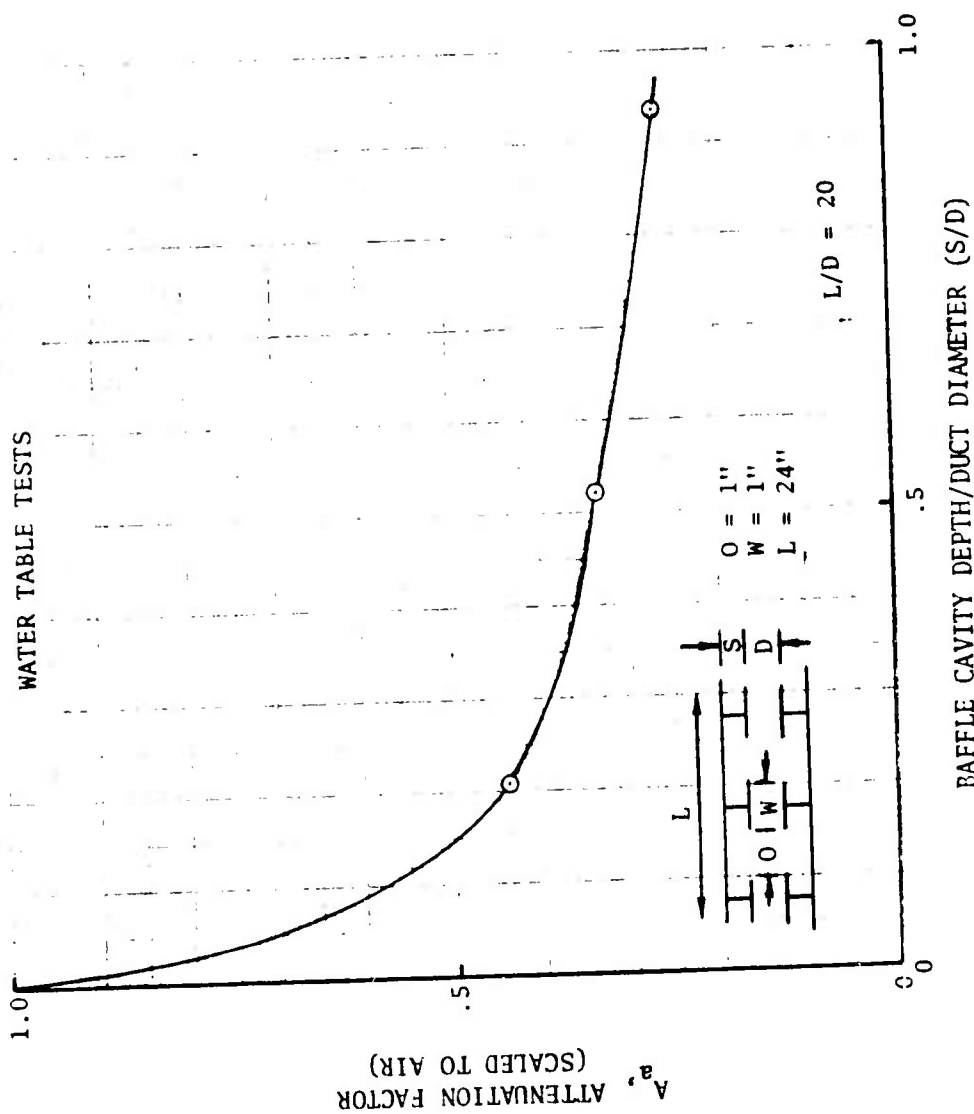
Figure 8. Effect of Suppressor Cavity Depth on Wave Suppression

WATER TABLE TESTS: BLAST WAVE PROPAGATION THROUGH SUPPRESSOR
(Model Represents Single Element of Multinozzle Suppressor with
L/D = 20, O/D = 1 in./1.2 in.)
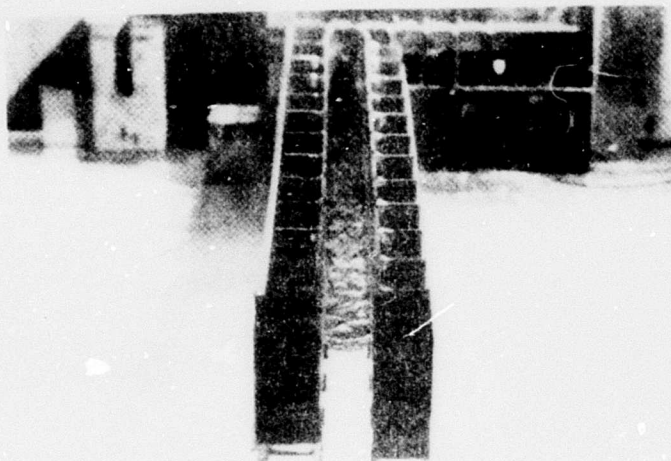
Figure 9.   End View of Model With Blast Wave 2/3 Distance Down
Suppressor

Figure 10. End View of Model With Blast Wave Several Diameters
Downstream of Suppressor Exit

R-9343
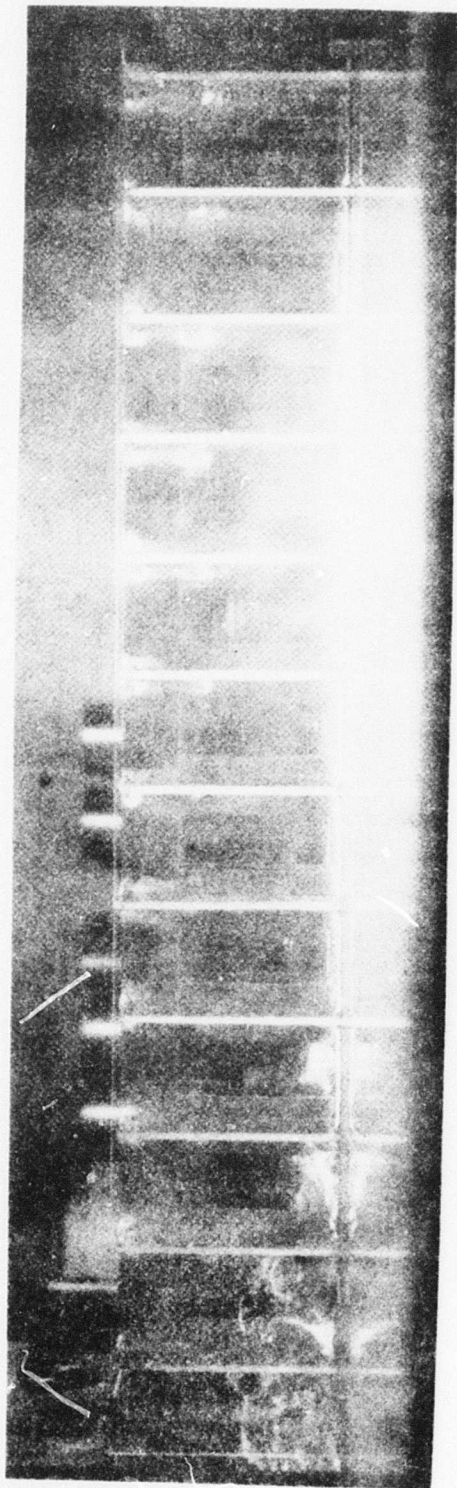
Figure 11. Side View of Model With Blast Wave Approximately 1/4 Distance Down Suppressor
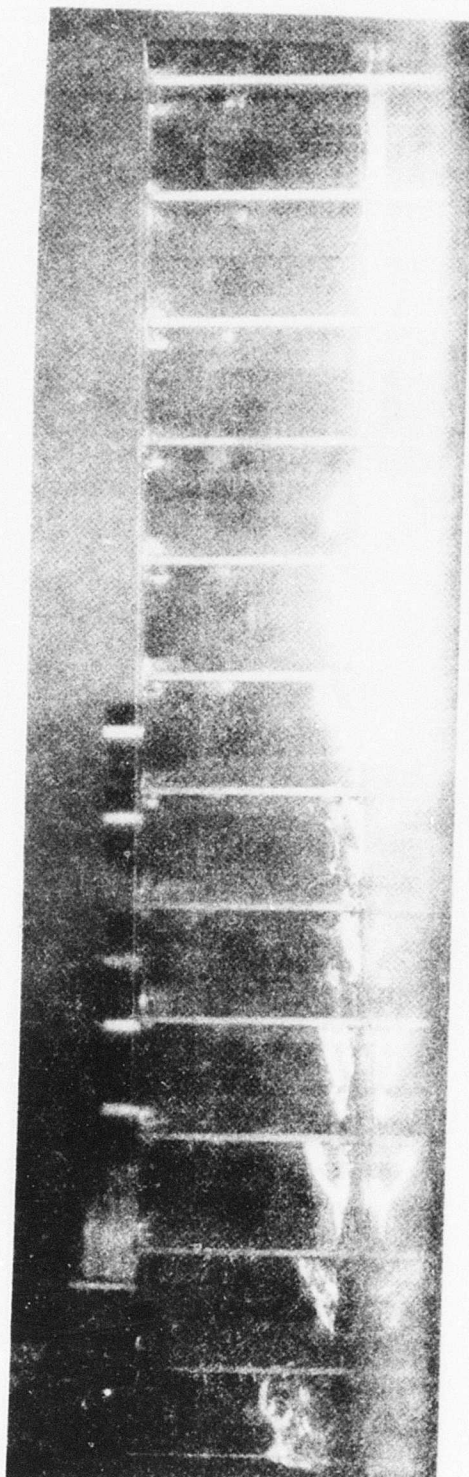
Figure 12. Side View of Model With Blast Wave Approximately 2/3 Distance Down Suppressor

Fig. 12. The front is considerably lower than that shown in Fig. 11, and wave decay can be observed behind the wave front. Water depth remains high near the suppressor entrance, indicating that the wave was quite strong as it passed this region.

MULTIPLE-NOZZLE SUPPRESSOR TESTS

A short water table study was made to compare the performance of a multiple-nozzle suppressor design with that of a similar single-nozzle suppressor. The multiple-nozzle concept is desirable because it allows a reduction in the physical length of the design without a reduction in L/D and, consequently (it was assumed), without much loss in wave attenuation. The tests described here were made to verify this assumption.

One single-nozzle suppressor and one multiple-nozzle suppressor were tested. Sketches of these designs are shown in Fig. 13 and 14. The multiple design used three nozzles and three suppressors. The physical baffle dimensions were the same for both suppressors, as were the ratios of length over diameter (L/D = 20). The suppressor "diameter" was 1.2 inches and 0.4 inch for the single and multiple suppressor, respectively. The total flow exit area of both designs was the same width, 1.2 inches. This provided equal simulated thrusts for the two designs and this dimension was used as the scaling parameter for the free-field reference distances required. In conjunction with this, the same initial simulated blast-wave strength was used in both cases.

Two free-field wave-strength measurements were made in both tests. The wave strength was measured in the free field because any wave combination effect involving the multiple design would not be observed at the nozzle exit. Because both designs had the same total flow exit area, the free-field wave height measurements for both tests were made at equal distances from the suppressor exit. The location of these measurements is shown in Fig. 13 and 14. The small size of the water table prevented measurements at greater distances for the single design and such measurements were, therefore, not useful for the multiple-suppressor test. The wave strengths recorded in these tests in terms of wave height divided by initial water depth are presented in Table 1. Actual depth measurements are included.
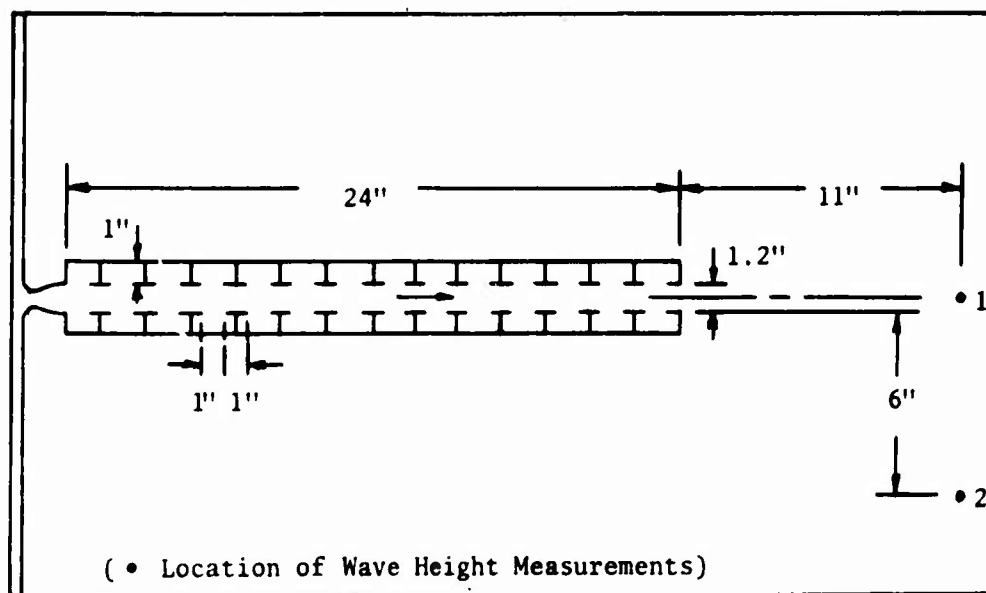
Figure 13. Single-Nozzle Suppressor Installed on Water Table Test Section
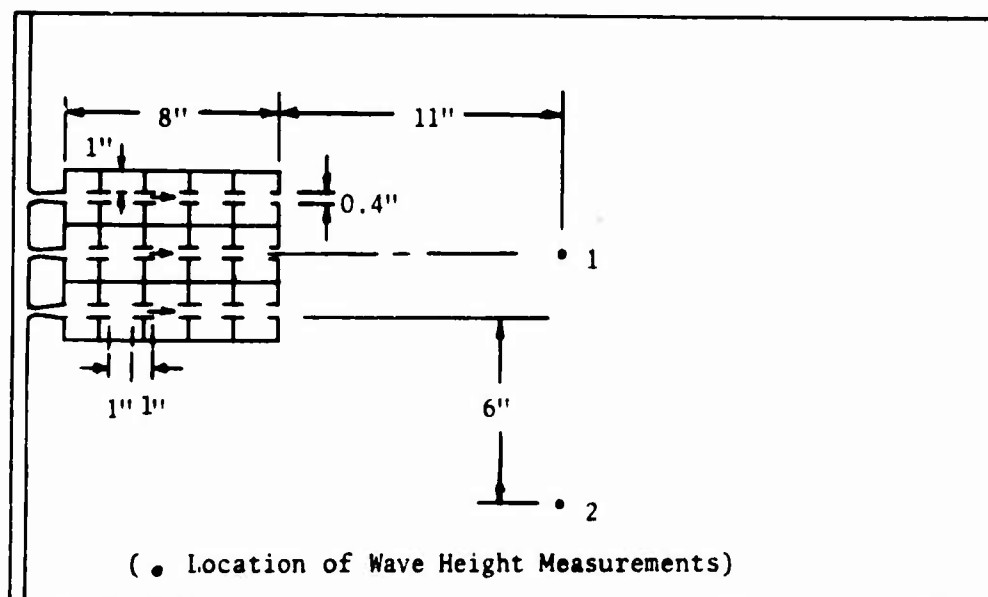
Figure 14. Multiple-Nozzle Suppressor Installed on Water Table Test Section

TABLE 1. COMPARISON OF SINGLE- AND MULTIPLE-
NOZZLE SUPPRESSOR RESULTS

| Parameter | Suppressor Design | | | |
| | Single | | Multiple | |
	Location 1	Location 2	Location 1	Location 2
Initial Water Depth, Y_a	0.09 in.	0.09 in.	0.094 in.	0.094 in.
Wave Height, Y_w	0.24 in.	0.18 in.	0.27 in.	0.21 in.
Wave Strength, Y_w/Y_a	2.7	2.0	2.9	2.2

Wave strength of the multiple design was slightly greater than that of the single design. However, this difference resulted from a 0.03-inch difference in water depth measurements, which was a smaller difference than the absolute accuracy of the measurements. Consequently, it was concluded that the degree of suppression of the two devices was essentially equal. Therefore, as long as the ratio of L/D is maintained, a multiple-nozzle suppressor is an effective method of reducing the physical length of a specific suppressor design.

It was noted that a more accurate water table test would have been desirable. However, due to the small size of the water table facility and the available method of measuring water depths, this was not considered feasible for the present study. The water depth was measured by observing the wave surface contact with a series of needle points suspended at various heights above the water table surface plate.

HELIUM SHOCK TUBE TEST PROGRAM

The shock tube testing program was conducted to simulate more closely the blast-wave effects from the full-scale recoilless rifle. A 1/6.86 scale model of the 105-mm recoilless rifle nozzle was fabricated to provide a performance comparison with other nozzle and suppressor devices. A series of model blast suppressors, or mufflers, was fabricated so that they could be attached to the single, 4:1 expansion area ratio nozzle (Fig. 15). A seven-nozzle cluster plate, with each small nozzle of area ratio = 4, and a seven-tube muffler also were fabricated and tested. The impulse obtained from the discharge of helium gas from the nozzle and muffler combinations was measured by suspending the apparatus to form a ballistic pendulum.

SHOCK TUBE HARDWARE

The suppressor assemblies for the single and multiple nozzles are shown in Fig. 16 through 19. The photographs show exploded views of the suppressors for the single nozzle. The first three inserts are made of stainless steel to provide strength in the cavities nearest the nozzle exit. The remainder of inserts are made of aluminum. The suppressor can be assembled with or without spacer rings, thus giving two values of baffle opening, O.
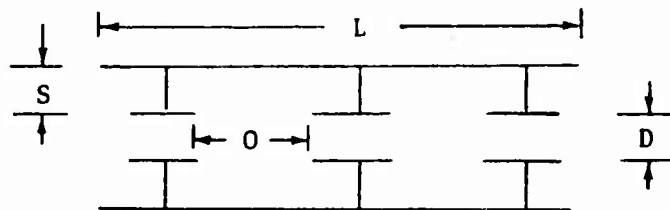
Figures 17 and 18 illustrate the longest suppressor, which is 32.75 inches from the nozzle exit plane to the suppressor exit plane. The spacers of Fig. 17 will give the suppressor a baffle opening of 1.0 inch and a cavity depth, S, of 0.5 inch. With the filler spacers shown in Fig. 18, the cavity depth will be 0.25 inch. The spacers also could be removed from the suppressor assembly to make baffle openings, O, as well as cavity depths, S, of 0.5 inch.

(2500 psi)

Figure 15. Shock Tube Model Assembly With 1/6.86 Scale Reference Nozzle and Suppressor

42 in.
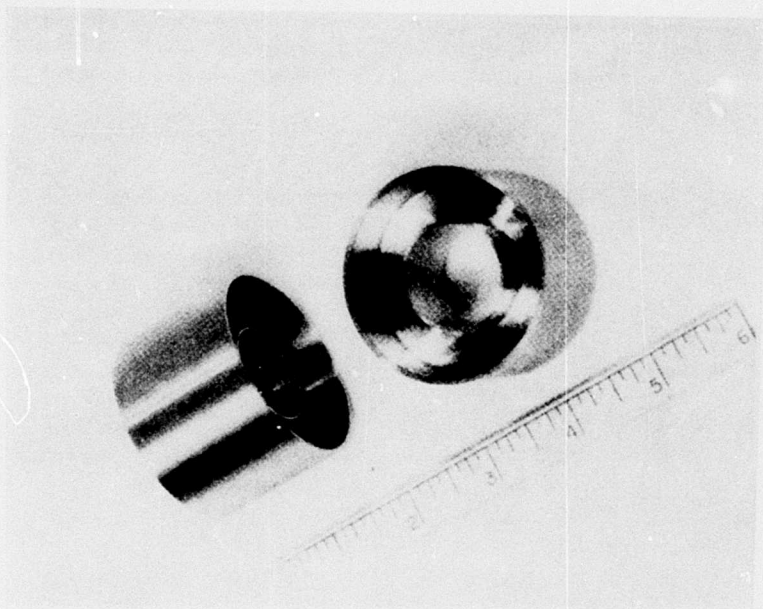
Figure 16. Shock-Tube Suppressor Inserts
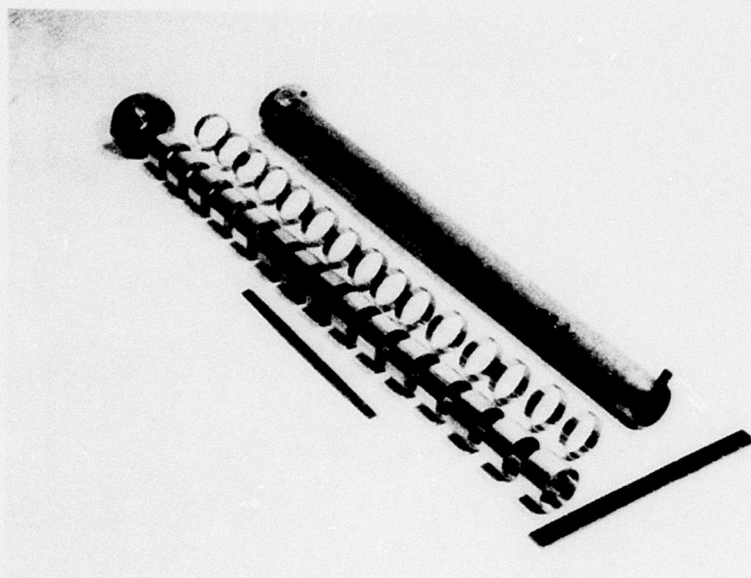
Figure 17. Shock-Tube Long Suppressor Assembly
Showing Inserts with 1/2-inch Cavity
Depth and Spacers for Making 1-inch
Baffle Openings

R-9343
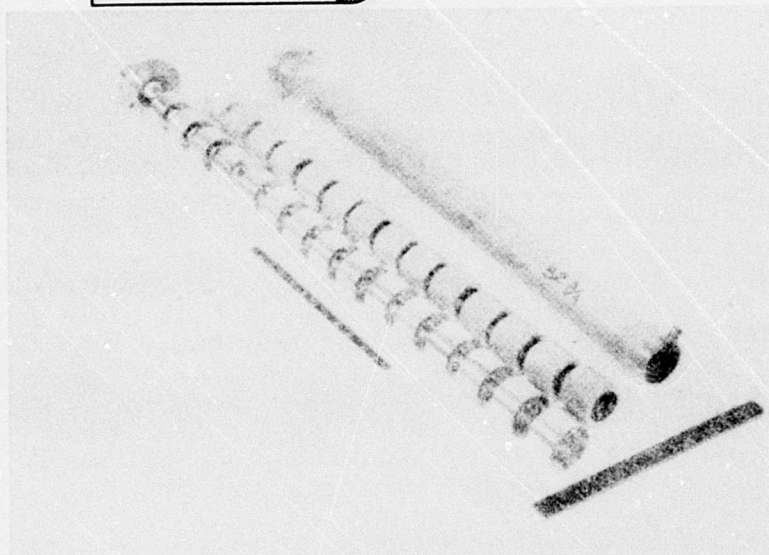
Figure 18. Shock-Tube Long Suppressor Assembly Showing
Inserts with Filler Spacers for Making 1/4-
inch Cavity Depth and 1-inch Baffle Openings
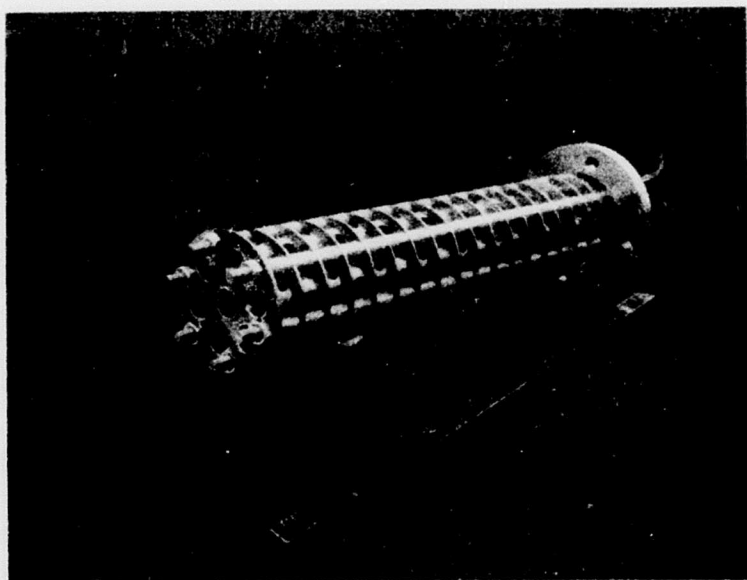
Figure 19. Multitube Suppressor Assembly for Shock Tube
Tests (Outer housing is removed to show
perforated tubes and baffle construction.)

Figure 19 shows a multiple-nozzle suppressor assembly, fabricated according to the sketch of Fig. 20. Seven 5/8-inch-diameter tubes were drilled with two 3/8-inch diameter in each of 18 cavities formed by the disks. The holes in the tubes were oriented so that they did not face each other.

SHOCK TUBE INSTALLATION

The shock tube and pendulum assembly were installed in an altitude-simulation cell as illustrated in Fig. 21. The blast wave-reflecting surface plate was installed with four 25-psi Kulite transducers located as shown on the lower floor plate of Fig. 22. When a muffler was installed on the nozzle, the floor plate was moved downstream so that the transducers were located the same distances from the muffler exit as they were from the nozzle exit.

A linear potentiometer was calibrated so that the deflection angle of the pendulum was recorded on a strip chart recorder.

In addition to the four reflecting-surface transducers, Kulite pressure transducers were located at the nozzle and muffler exits. Three dual-beam Tektronix oscilloscopes were used to record the six Kulite pressure transducers' output signals. Six Dynamics 6050-dc amplifiers were used to filter as well as amplify the transducer signals. The four Kulite transducers in the floor surface plate had a natural frequency of approximately 100 KHz, while the two Kulite transducers used on the model and suppressor had a natural frequency of approximately 200 KHz. Because of the difficulty of recording shock pressures at these ringing frequencies, filtering was necessary and the amplifier served this purpose conveniently. The measured attenuation curve for the 6050 Dynamics amplifier is shown in Fig. 23; the amplifier effectively filters out the signals above 40 KHz.

SHOCK TUBE MODEL CONFIGURATIONS

The series of model nozzles and mufflers shown in Table 2 was used for test. A total of 19 nozzle and muffler designs were tested for shock-wave pressure and impulse on a ballistic pendulum.

R-9343

27

Figure 20. Multiple-Nozzle Attenuator
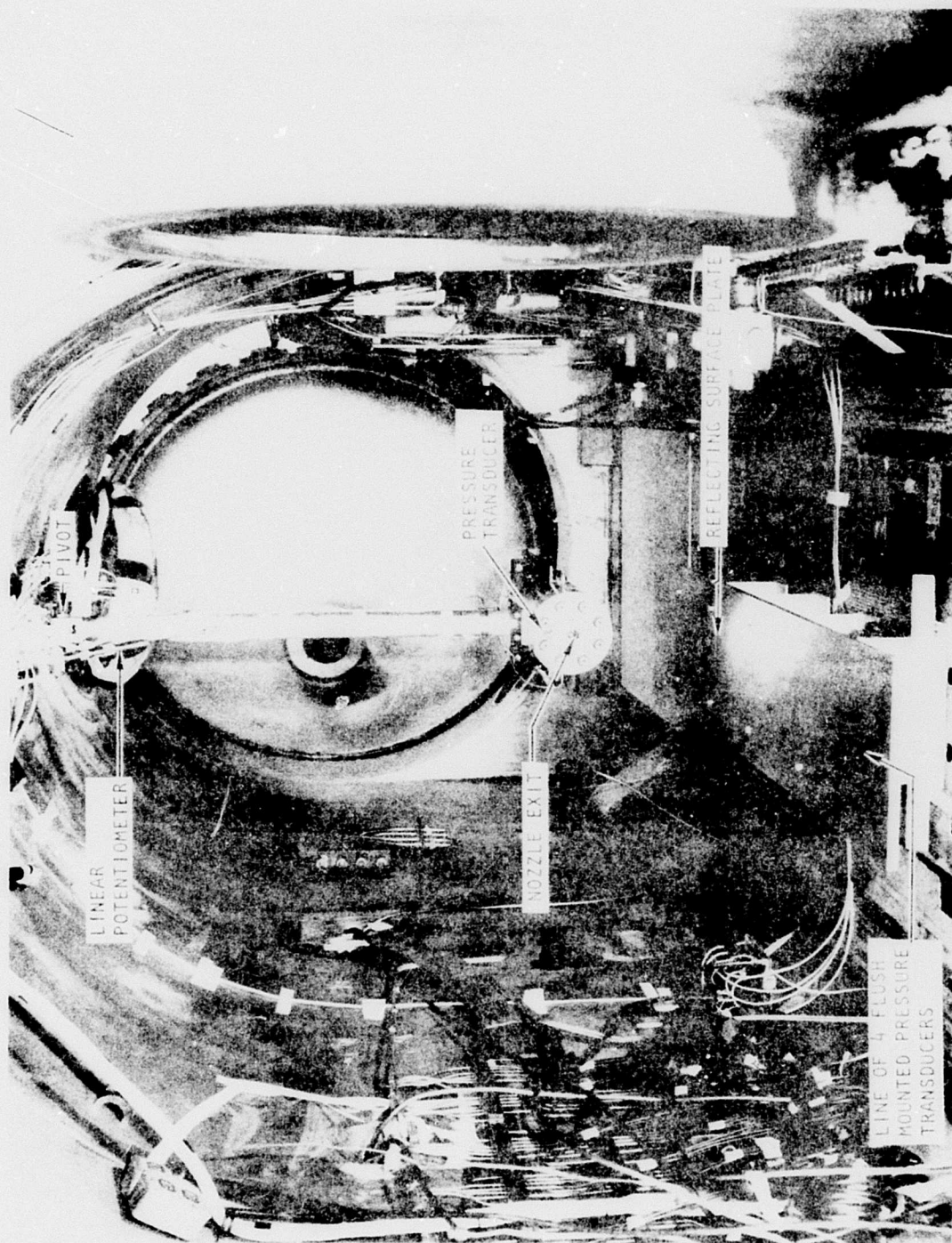
Figure 21. Installation of Shock Tube and Pendulum in Test Cell

PIVOT

PRESSURE TRANSDUCER

REFLECTING SURFACE PLATE

LINEAR POTENTIOMETER

NOZZLE EXIT

LINE OF 4 FLUSH MOUNTED PRESSURE TRANSDUCERS
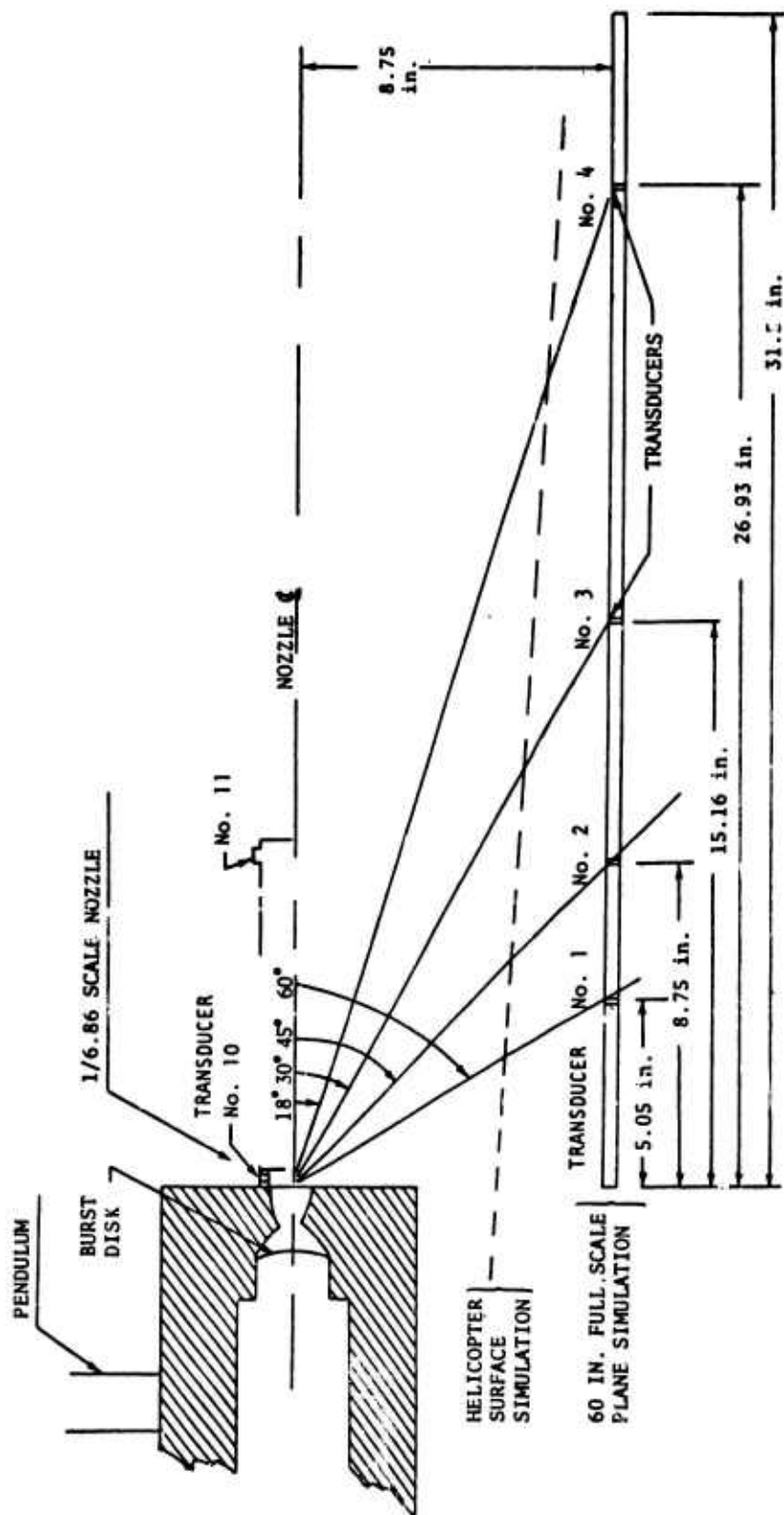
Figure 22. Location of Transducers on Blast-Wave Reflecting Surface
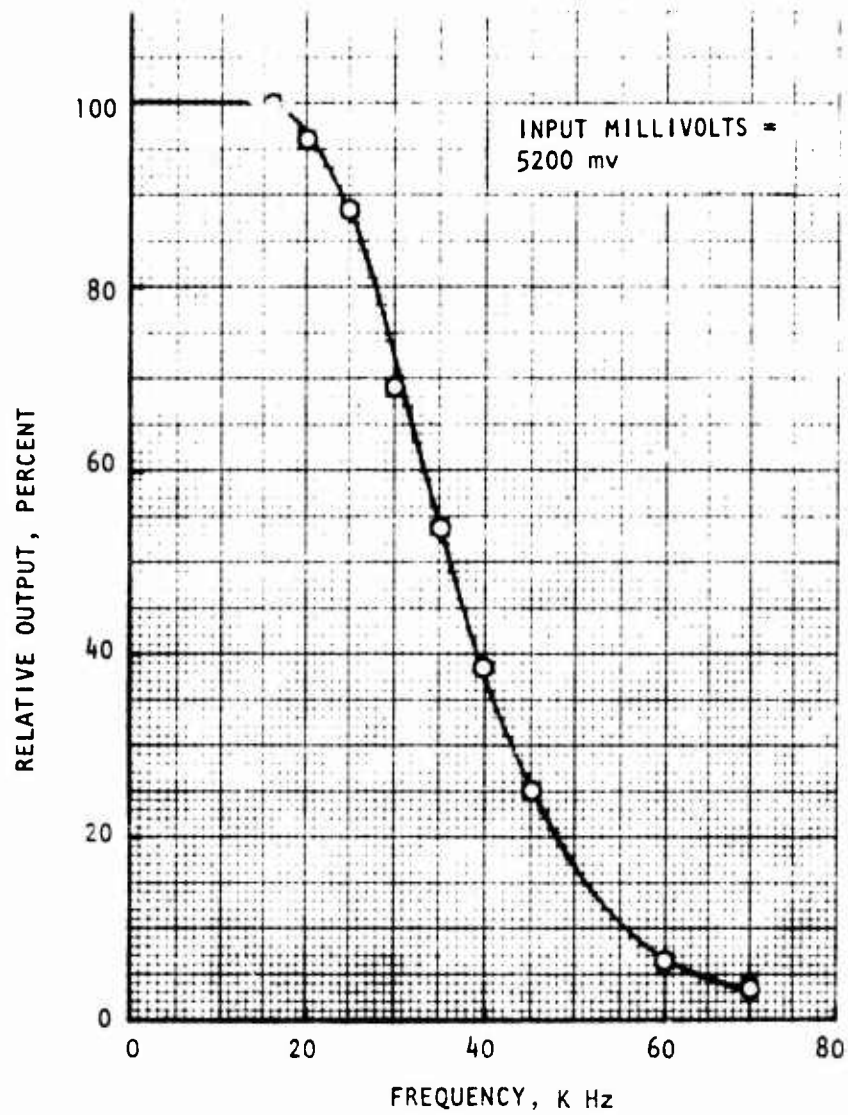
Figure 23. Signal Attenuation for a Range of Input
Frequencies - Dynamics 6050 Amplifier

R-9343

TABLE 2. SHOCK TUBE NOZZLE AND MUFFLER CONFIGURATIONS TESTED

Conf. No.	Nozzle Block	Spool Flange	Housing Length, (in.)	Number of:			Muffler L/D	Cavity Depth, (in)	Cavity Opening, (in.)	
				Spacers	Spacer rings	Filler Rings			Nom.	Next to Nozzle
001	Single Bell, ε = 4	On	0	0	0	0	0	--	--	
002		On	11	5	5	0	11.75	0.5	1.0	
003		Off	21.5	11	9	0	21.5	0.5	1.0	1/4 and 1/2 in.
004		Off	32	16	15	0	32.0	0.5	1.0	1/4 in.
006		Off	21.5	14	0	0	21.5	0.5	0.5	1/4 in.
007		On	11	5	5	5	11.75	0.25	1.0	
009		On	32	15	16	15	32.75	0.25	1.0	
010		On	11	6	2	0	11.75	0.5	0.5	1 in.
011		On	21.5	13	2	0	22.25	0.5	0.5	1 in.
012	Multi-nozzle	Off	0	--	--	--	0	--	--	
013		Off	11.75	--	--	--	23.5	0.25 or more	23% porosity	
030	Single Bell, ε = 4	Off	21.5	8	18	0	21.5	0.5	1.5	1.25 in.
031	Single Bell, ε = 4	Off	21.5	10	12	0,Steel Wool	21.5	0.5	1.0	1.25 in.

TABLE 2. (Concluded)

Conf. No.	Nozzle Block	Spool Flange	Housing Length, (in.)	Number of:		Filler Material	Muffler L/D	Cavity Depth, (in.)	Cavity Opening, (in.)	
				Washers- .15" Thick	Spacer Rings				Nom.	Next to Nozzle
041	Single Bell, ε = 4	Off	32	48	47(1/2") 1(1/4") 1(3/8")	0	32	0.5	0.5	5/8 in.
042		Off	32	29 Loose, Canted 15° + 2 Spools	2	8-Mesh Screen Tube + Copper Packing	32	0.5	0.75 (Approx.)	1-1/4 in.
043		Off	32	18 + 1 Spool	54(1/2") 1(1/4") 1(3/8")	28.5" Long Screen Tube	32	0.5	1.5	7/8 in.
044		Off	32	25	51(1/2") 1(1/4") 1(3/8")	28.5" Long Screen Tube	32	0.5	1.0	7/8 in.
045		Off	32	28	53(1/2") 1(1/4") 1(3/8")	0	32	0.5	1.0	1-1/8 in.
150	Multi-nozzle	Off	11.75	20(1/16") Baffles with 7 (5/8") Holes in Each	18 Cavities	0	18.8	1.8	0.56	9/16 in.

The first series of configurations for the single nozzle (configurations 1 through 11) was used to evaluate the spool type of insert, Fig. 16 (enclosed cavity). The second series of single-nozzle configurations (configurations 41 through 45) was used to evaluate the effect of cavities made up by a series of 2-1/8-inch-diameter washers with 1-inch holes (Fig. 24).

The procedure for testing the various nozzles and mufflers was to evacuate the altitude chamber to about 1/3 atmosphere, then to pressurize the shock-tube chamber with helium gas until the 2500-psi burst diaphragm ruptured.

SHOCK TUBE TEST RESULTS

The shock-tube data are shown in Table 3, where each test number represents a burst diaphragm used for the configuration noted. During some of the tests, the trigger signal for the oscilloscopes was unpredictable and pressure data were not recorded properly. By the end of the testing, four 200-psi Kulite transducers and one 25-psi Kulite transducer had been damaged. As a result, some of the nozzle, muffler, and surface plate pressures were not recorded late in the test program.

Blast-wave pressures as recorded on the oscilloscopes during a typical test are shown in Fig. 25. Oscilloscope sweeps were triggered by the wave-pressure signal from the nozzle exit transducer (No. 10) and delay times were measured from that event.

Test data for the reference single nozzle, without an attenuator, and for blast attenuators, made up of spool inserts forming 0.5-inch-depth cavities with 1.0-inch openings, are plotted in Fig. 26. The typical unattenuated pressure profile, with low amplitudes at transducer No. 1, high amplitudes at transducers No. 2 and 3, and decreasing amplitudes at greater distances downstream, is quite apparent. It is also noted that the unattenuated wave exhibited a second pressure peak of higher amplitude than the first one at transducer No. 4 (this second peak was eliminated by the blast attenuators). The spool-cavity attenuators' effectiveness is clearly

Figure 24. Muffler Model, Configuration 045, Showing Arrangement of 2-1/8-inch OD Washers and Spacer Rings in 32-inch Housing

R-9343

35

TABLE 3. SHOCK TUBE AND MUFFLER TEST DATA

Test No.	Config.	Chamber Pressure P_c	Ambient Pressure P_a	Nozzle No. 10 1st Peak	Nozzle No. 10 2nd Peak	Muffler No. 11 1st Peak	Muffler No. 11 2nd Peak	Transducer Pressure, psig — Surface Plate No. 1 1st Peak	No. 1 2nd Peak	No. 2 1st Peak	No. 2 2nd Peak	No. 3 1st Peak	No. 3 2nd Peak	No. 4 1st Peak	No. 4 2nd Peak
16	001	2631	2.88	103	110	--		4.5	3.0	10.0	3.0	7.0	0	4.7	6.2
17	001	2604	2.95	132	--	--									
18	↓	2871	2.97	170	161	--									
19	↓	2726	2.97	150	161	--									
20	↓	2438	2.95	130	125	--									
21	↓	2790	2.96	100	110	--		5.0	0	8.6	1.2	9.0	2.1	4.2	7.0
22	↓	2535	2.98	82	90	--		4.6		9.7		9.3	-0.5	4.0	5.0
23	↓	2728	3.0	90	96	--		5.5		9.8		> 8.0	2.0	4.3	6.5
24	002	2910	3.02	102	119	41	91	4.0		8.1		8.5		4.6	8.0
25	009	2400	2.90	--	--	--		3.1		4.4		6.8		4.6	
26	004	2880	2.97	100	110	30	52	--		--		6.2		3.5	
27	004	2864	2.93	105	117	32	60	--		--		--		--	
28	004	2456	2.92	100	100	--		2.8		3.8		5.1		2.7	
29	003	2388	2.88	113	123	--		4.0		5.3		4.8		2.0	

TABLE 3. (Concluded)

Test No.	Config.	Chamber Pressure P_c	Ambient Pressure P_a	Nozzle No. 10		Muffler No. 11		Transducer Pressure, psig — Surface Plate							
								No. 1		No. 2		No. 3		No. 4	
				1st Peak	2nd Peak	1st Peak	2nd Peak	1st Peak	2nd Peak	1st Peak	2nd Peak	1st Peak	2nd Peak	1st Peak	2nd Peak
30	006	2512	2.92	130	138	45	58	--		--		--		--	
31	006	2889	2.98	150	162	61	82	--		--		--		--	
32	006	2687	2.96	140	150	45	80	--		--		--		--	
33	006	2764	2.89	150	168	50	75	--		--		--		--	
34	006	2793	2.94	133	149	35	69	3.8		6.1		6.7		4.4	
35	013	2694	2.94	85	80	--						7.7	1.0	4.1	
36	013	2835	2.93	85	79	--		6.3		9.0		7.7		4.3	
37	012	2896	2.96	--	118	--		4.5		8.0		7.2		6.5	
38	001	2696	14.7	118	130	--								8.5	
39	030	2696	2.92	140	130	--						7.1		3.1	
40	031	2747	2.92	122	93	--		2.7		4.2		6.0		5.5	
41	042	2834	3.02	99	110	--		2.6		3.9		4.0		2.7	
42	041	2774	2.98	110	138	--		3.4		3.0		3.4		1.9	
43	043	2784	2.92	125	95	--		2.5		3.2		3.4		3.8	
44	044	2788	2.90	115		--		2.4		2.9		3.3		3.1	
45	045	2912	2.92	--		--		2.1		2.5		--		1.8	
46	150	2907	2.96	--		--		--		6.3		5.6		3.1	

TEST 44

CONFIGURATION 044

Muffler Length = 32 Inches

115 PSI   95 PSI

Transducer No. 10 →
Nozzle Exit

0

.1 ms

2.4 PSI   2.9 PSI

.1 ms
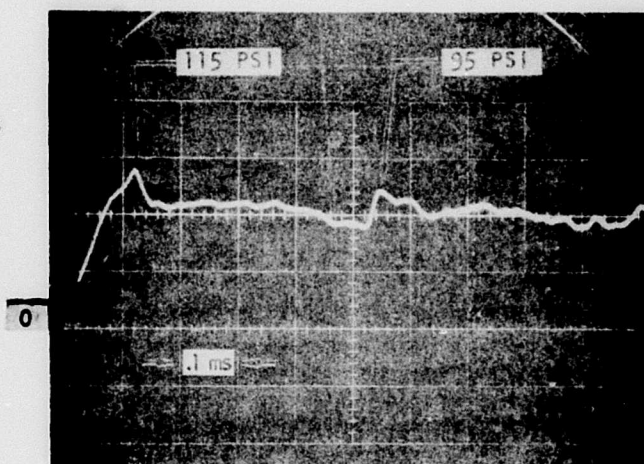
Transducer No. 1 →
Time Delay = 0.7 msec
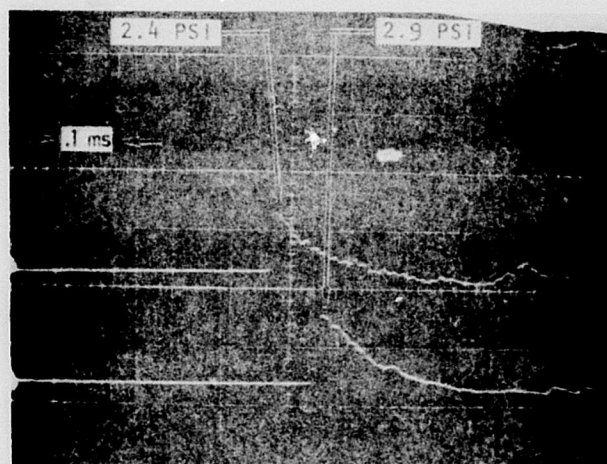
Transducer No. 2 →
Time Delay = 0.7 msec

3.3 PSI

2 ms
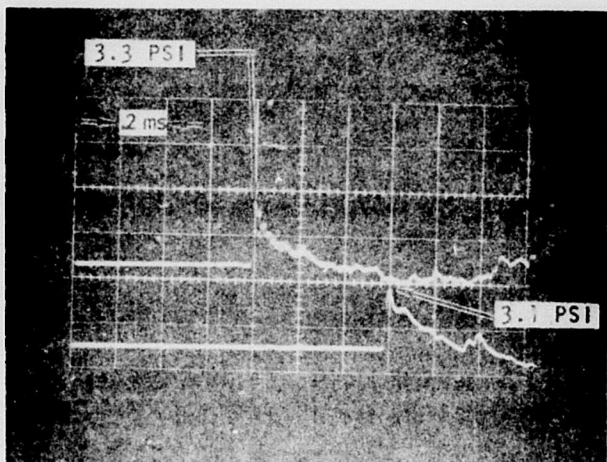
Transducer No. 3 →
Time Delay = 0.7 msec

Transducer No. 4 →
Time Delay = 0.7 msec

3.7 PSI

Figure 25. Blast Wave Pressure Traces for Single Nozzle Muffler With
0.5-Inch Cavity Depth and 1.0-Inch Cavity Opening, Using
Flat Washers and Screen Tube

R-9343/38
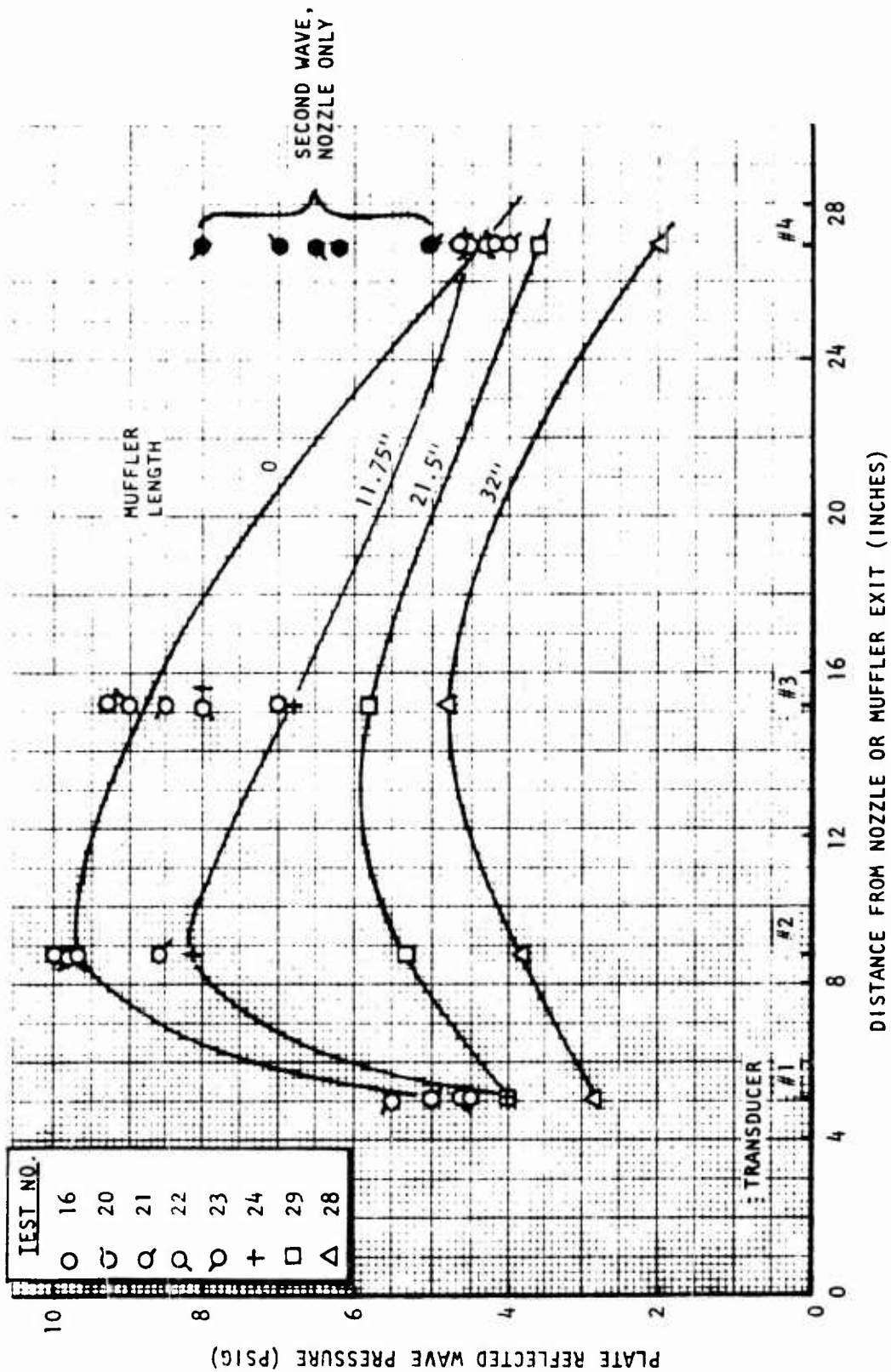
Figure 26. Shock Tube Test Data: Effect of Muffler Length on Blast Wave Pressure (Single Nozzle Mufflers Having 0.5-Inch Cavity Depths and 1.0-Inch Cavity Openings)

shown and apparently increases monotonically with increasing attenuator length. Although the greatest attenuation was of the highest-amplitude portion of the wave, the longer attenuators did effect significant amplitude reductions in the lower-amplitude regions as well.

A similar data plot for attenuators made up of washer-and-spacer cavities is shown in Fig. 27. Here, only 32-inch-long attenuators are represented; the various curves represent a variety of washer spacings and other related design variants. The curve labeled "Loose, Canted Washers" is from test No. 41 of configuration 042, wherein copper wool was packed between successive washers to hold them apart and successive washers were canted approximately ±15 degrees from perpendicular to the attenuator axis. This configuration neither gave as good blast suppression as did the fixed, uniformly spaced washer designs or withstood the blast pressure as well; the washers and packing were driven down the attenuator tube and were compressed from their original 32-inch-length column to about 6 inches. The other design variant, insertion of a cylinder of 8-mesh screen down the center of the washers, did not appear to offer appreciably greater attenuation than did the simple washer-and-spacer design.

To gain insight into the relative attenuation and L/D effects, data from transducers No. 2 and 3 of Fig. 26 and 27 are plotted in Fig. 28 on a reduced pressure amplitude versus attenuator L/D basis comparable to that used for water table data (Fig. 7). The spool-cavity data appear to substantiate the exponential decay of blast-wave amplitude with increasing attenuator L/D (i.e., the data plot as a straight line on semilog paper), but the rate of decay is considerably lower than was expected from the scaled water table data. Extrapolation suggests that on the order of $L/D \approx 100$ would be required to achieve blast-wave attenuation to the 10- to 15-percent level. The washer-and-spacer attenuator's suppression rate appears to be a stronger function of L/D, so that comparable attenuation might be attained with $L/D \approx 55$.

While the preceding paragraphs summarize the main results represented by the single-tube attenuator data in Table 3, some other aspects deserve comment. Comparison of tests using configurations 006 and 030 (with more and fewer spools to
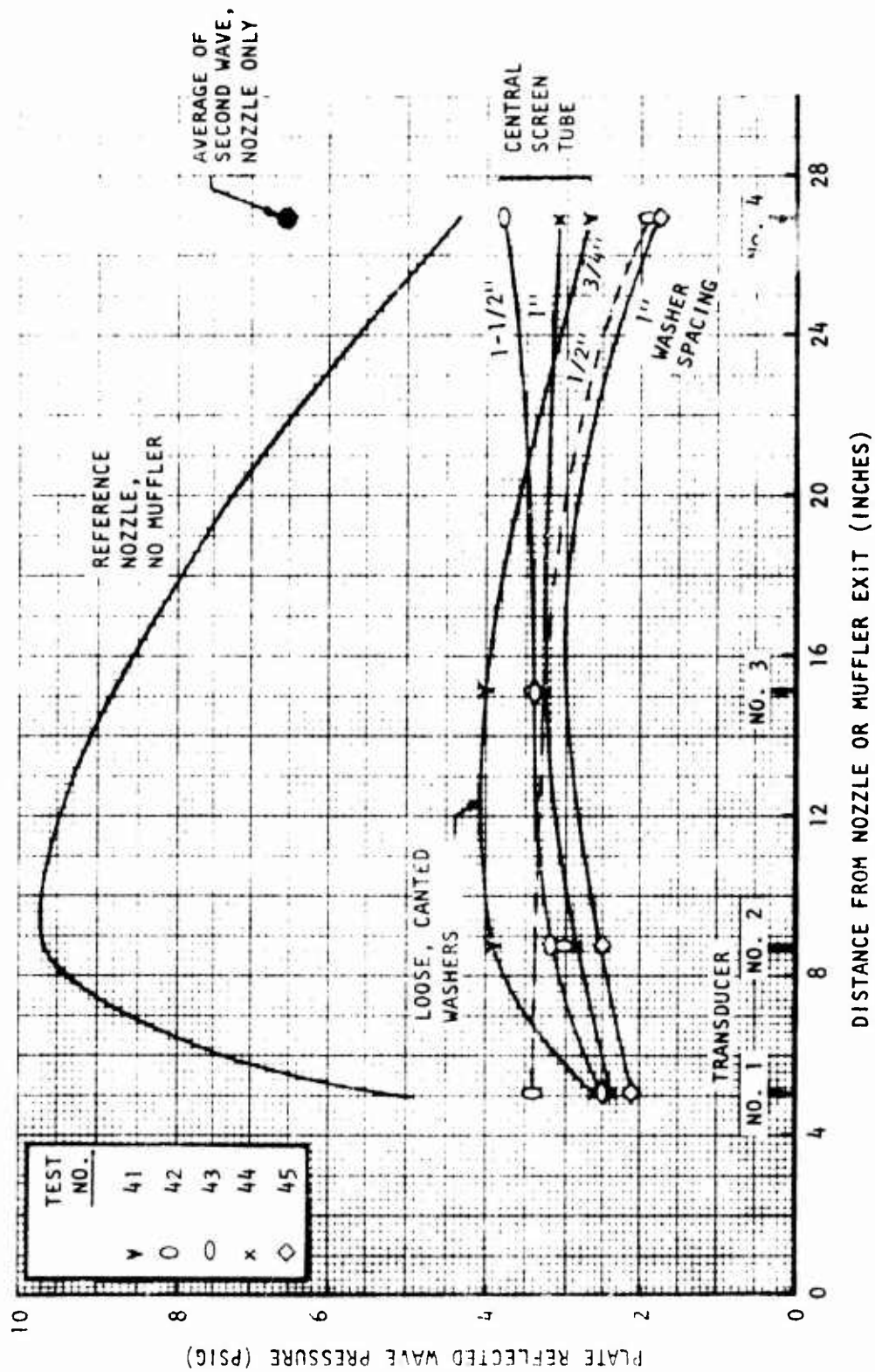
Figure 27. Shock Tube Test Data: Comparison of Blast Wave Reflected Pressures for 32-Inch Mufflers With Washers and the Reference Nozzle
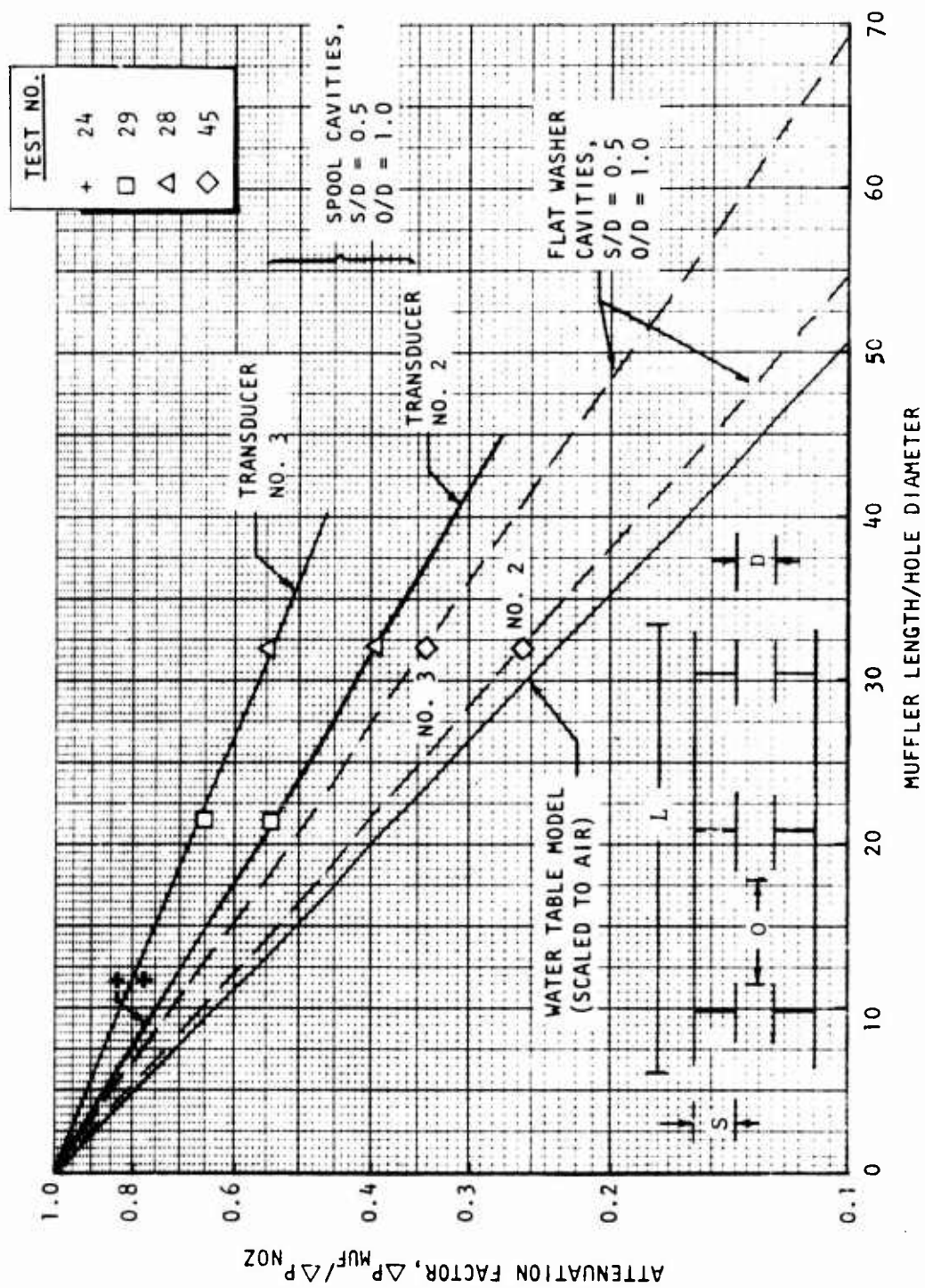
R-9343

41

Figure 28. Effect of Muffler Length on Blast Wave Attenuation

give narrower and wider cavity openings than the 003 configuration) indicated that little could be gained by attempting to optimize the spool cavity opening width. This was corroborated by the modest effect of washer spacing shown in Fig. 27 for the washer and spacer design. Also, the use of metal wools as absorbent materials filling the cavities did not appear to offer any benefit to either design.

Concerning the seven-nozzle/seven-tube muffler shown in Fig. 19 and 20, the test results were disappointing in that essentially no attenuation was measured. (The seven-nozzle plate alone gave approximately 12-percent attenuation.) Removal of the seven perforated tubes from the model (configuration 150) resulted in attenuation essentially comparable with the $L/D \approx 21.5$ single-tube attenuator. Thus, direct evidence was not obtained in the shock-tube testing to support the assumption that a number of short, small-diameter attenuators can be as effective as a long, single attenuator having the same L/D.

BALLISTIC PENDULUM IMPULSE MEASUREMENTS

Pendulum Operation

The 140-pound pendulum shown in Fig. 21 was suspended from a rail at the ceiling of the altitude test cell. A clevis joint with a Delrin bushing and Teflon spacers was used to pivot the pendulum, which had an arm length of 42 inches from the center of the pivot to the center of the nozzle (Fig. 15).

A 50,000-ohm, variable-resistance, linear potentiometer was attached from the rail to the pendulum arm. Its output was recorded on a Honeywell recorder at a rate of 1 inch per second. A Clinometer was used to calibrate the pendulum deflection angle. The pendulum was deflected in 2-degree increments up to 13 degrees, using the center region of the linear potentiometer.

The horizontal surface of the nozzle assembly was adjusted for each test configuration by adding counterweights until the bubble-leveling gage indicated a horizontal position. In a given test, the peak of the first cycle, recorded immediately after the diaphragm burst, was measured and used as the deflection angle, φ,

listed in Table 4 for the various tests. The period, T, was measured as the interval, in seconds, between peaks of the second and third cycles. Each muffler, with its counterweight, was weighed separately and added to the basic mass to arrive at the total weight, W.

The theoretical derivation of the equation used for calculating the gas impulse is presented in Appendix A.

Impulse Data Correlation

Measurements of the impulse obtained from the gas discharge from the shock tube are shown in Table 4. A surprising effect was obtained. The impulses from the muffler configurations did not differ from those of the reference nozzle, configuration 001, by more than ±10 percent.

The impulse data from the single-tube blast suppressors are plotted versus the helium gas chamber pressure when the diaphragm burst (Fig. 29). (Some of the burst diaphragms did not split completely into four full tabs, so the data for tests No. 16, 17, 18, 20, 25, 29, and 38 were omitted from this correlation.)

The trend of the reference nozzle impulse is to increase approximately with the square root of the chamber pressure. There was not a consistent loss in impulse with the blast suppressor attachments (L/D = 11.75, 21.5, 32); in fact, the data for the longest attenuator seem to be within the scatter of the reference nozzle data. There may even be a reverse trend, with higher impulse loss effects with shorter attenuators. This might be caused by the expanding gas being colder than the ambient temperature hardware so that it would pick up more heat, and thus regain some lost energy and momentum on passing through a longer attenuator.

The unusually high impulse of the L/D = 21.5 spool suppressor packed with 1 ounce of fine steel wool may be partially due to the high-speed ejection of the steel wool during the test blowdown.

TABLE 4. BALLISTIC PENDULUM IMPULSE MEASUREMENTS

Test No.	Config. No.	P_c/P_a	Weight Total, lb	Impulse Defl., deg.	Period, sec	Impulse, $\dfrac{W \phi T}{360}$
			W	ϕ	T	lb-sec
15	001	1017	147.6	11.1	2.02	9.19
16	001	914	141.9	11.1	2.02	8.84
17	001	883	141.9	11.38	2.02	9.06
18	001	967	141.9	11.38	2.02	9.06
19	001	918	141.9	12.88	2.02	10.26
20	001	826	141.9	12.16	2.02	9.68
21	001	942	142.6	12.47	2.02	9.98
22	001	851	142.6	12.06	2.02	9.65
23	001	909	142.6	12.44	2.02	9.95
24	002	964	143.6	12.18	2.02	9.81
25	009	828	165.2	9.6	2.06	9.07
26	004	970	154.0	11.93	2.06	10.51
27	004	977	154.0	12.0	2.05	10.52
28	004	841	154.0	10.56	2.07	9.35
29	003	829	149.1	10.5	2.06	8.96
30	006	860	149.8	10.88	2.05	9.28
31	006	969	149.8	12.12	2.03	10.24
32	006	908	149.8	11.46	2.03	9.68
33	006	956	149.8	11.8	2.04	10.02
34	006	950	149.8	11.8	2.03	9.97
35	013	916	146.9	11.33	2.03	9.39

R-9343

TABLE 4. (Concluded)

| Test No.	Config. No.	P_c/P_a	Weight Total, lb	Impulse Defl., deg.	Period, sec	Impulse, $\frac{W \, \varphi \, T}{360}$
			W	φ	T	lb-sec
36	013	968	146.9	11.6	2.02	9.56
37	012	978	144.9	13.2	2.0	10.63
38	001	183	142.6	11.13	2.01	8.86
39	030	923	149.4	11.2	2.02	9.39
40	031	940	149.2	13.05	2.05	11.09
41	042	938	158.2	11.9	2.05	10.72
42	041	930	168.1	10.9	2.05	10.43
43	043	953	159.8	10.8	2.07	9.92
44	044	96:	160.7	10.94	2.08	10.16
45	045	997	160.6	11.2	2.07	10.34
46	150	982	143.7	11.3	2.01	9.07
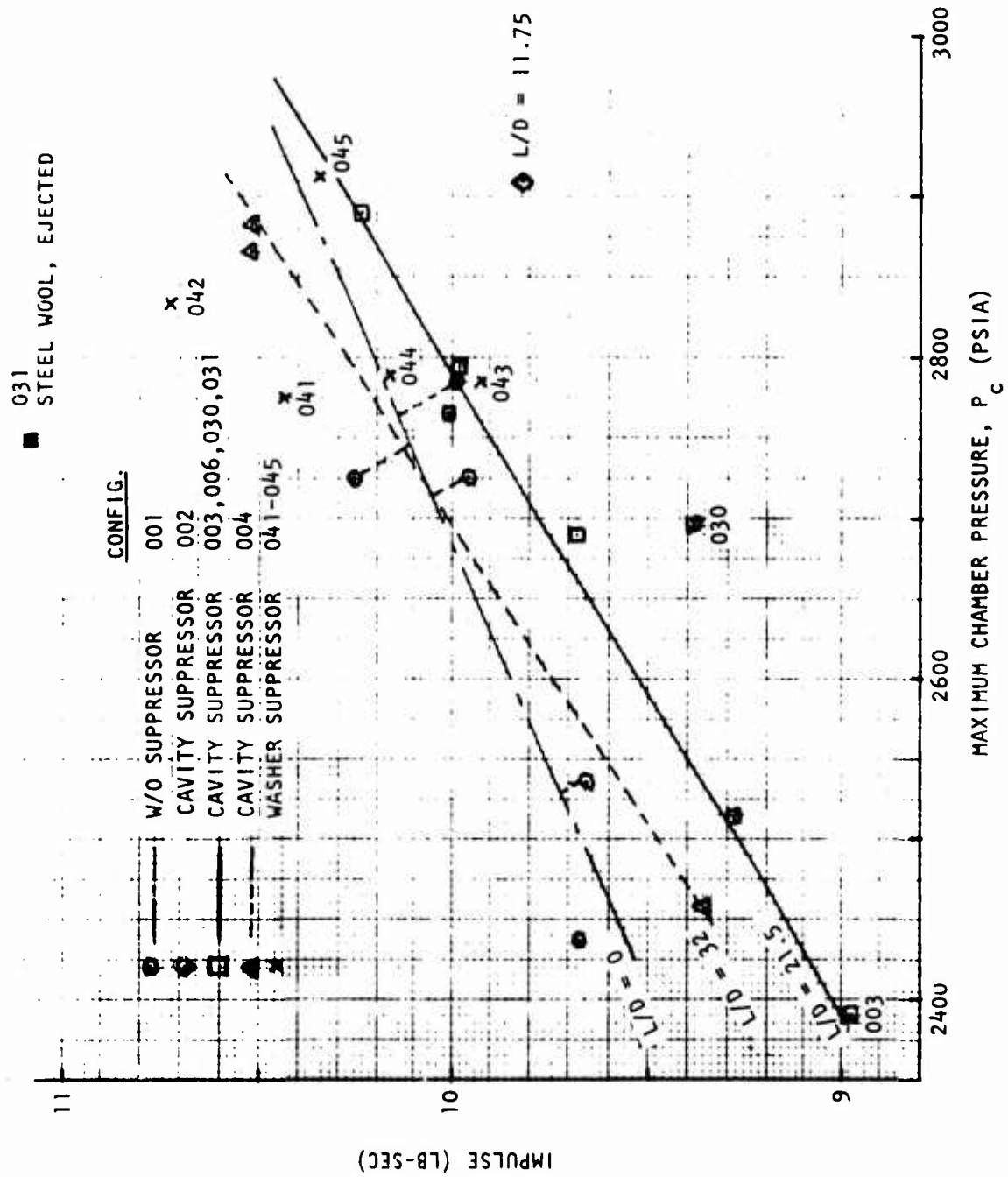
Figure 29. Cold Flow Shock Tube Test Impulse Measurements for Single Tube Suppressors

FULL-SCALE SUPPRESSOR DESIGN CONCEPT

AERODYNAMIC BASIS OF DESIGN SELECTION

Test Data

An overall review was made of the preceding water table and shock-tube test results to determine a full-scale, recoilless rifle blast-wave suppressor design concept. The shock-tube data were given primary significance as this test series most closely represented the actual rifle blast. These data indicated less attenuation from the suppressor designs than expected from water table tests. Because the design sketched below yielded the best suppression (attenuation factor of 0.26 with an L/D of 32), it was selected for the actual rifle suppressor design.

```
     |   |   |   |   |   |   |   |   |
  1 IN.                                   2 IN.
     |   |   |   |   |   |   |   |   |
         |--1"--|
```
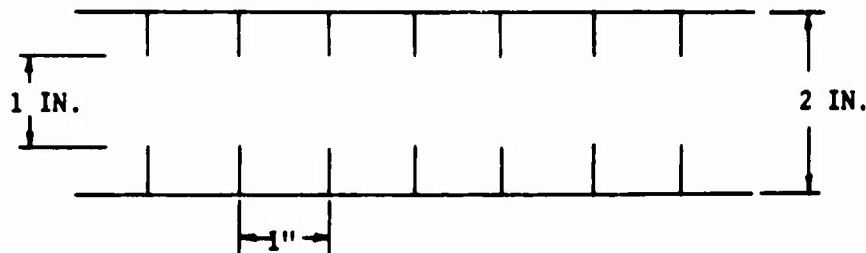
This design also produced essentially no impulse loss in the cold-flow helium tests. Consideration of this thrust data indicated that suppressor designs with increased baffle blockage or longer lengths would yield only small thrust losses. As a result, it was considered quite feasible from a thrust standpoint to increase the L/D of the rifle suppressor design.

Required Suppressor L/D

Since none of the shock-tube suppressors yielded sufficient attenuation, it was necessary to design the rifle suppressor somewhat differently than those tested. Both water table and shock-tube data indicated that suppressor performance can be increased by increasing suppressor L/D, and this was the approach taken. Parametric L/D data were not available for the selected baffle configuration; however,

attenuation factor versus L/D curves were generally straight lines on a semilog plot and passed through the point 0, 1 by definition. Consequently, to determine the attenuation of the selected baffle design as a function of L/D, a straight line was drawn through the 0, 1 point and the single data point at an L/D of 32. In this manner, the attenuation factor was extrapolated to smaller attenuation factor levels at greater values of L/D. It was noted that this was a considerable extrapolation and could result in some performance uncertainty for the rifle suppressor.

The required attenuation for the rifle suppressor was determined from Army test data. These data indicated maximum gun blast overpressures on a simulated helicopter surface of 20 psig at gun chamber pressures of 6000 psia. Other Army test data have indicated that blast overpressure is proportional to gun chamber pressure. Consequently, for the 12,000-psia chamber pressures considered here, the maximum unsuppressed wave strength was taken to be 40 psig. This approach was considered to be conservative as theoretical shock tube relationships indicate the maximum wave strength at a chamber pressure of 12,000 psia to be less than 1.5 times greater than the value at 6000 psia.

The rifle suppressor is required to reduce blast wave overpressures to less than 5 psig at the helicopter surface. Thus, the required attenuation factor at the helicopter surface is between 0.125 and 0.167. These factors were determined by dividing the maximum allowed surface overpressure (5 psig) by the maximum expected unsuppressed values (30 to 40 psig) and, for the baffle configuration selected, the attenuation factor decreases to the lower of these values at an L/D of approximately 62.5 (Fig. 28).

Multiple-Nozzle Design

Considering the uncertainty of the data extrapolation, the rifle suppressor was chosen to have an L/D of 75. Because the length (L) was restricted*, the hole

---

*Because the overall weapon length must not exceed 170 inches, the existing rifle length of 149 inches allowed only 21 inches additional length for the suppressor design. Replacing the single nozzle (Fig. 1) with a multinozzle plate increased the total allowable length for the current design to 26.5 inches.

diameter was required to be quite small to provide an L/D of 75. (The "hole diameter" referred to here is equivalent to the rifle nozzle exit diameter.) Thus, small nozzle exit diameters are necessary to yield large L/D ratios. To achieve a small nozzle exit diameter and maintain the required total nozzle throat area, a multiple-nozzle configuration was necessitated; many small nozzles were designed to replace the single large nozzle. In this manner, a large L/D can be achieved for each individual nozzle suppressor within a specified overall length.

Little thrust loss would be expected by going to a multiple-nozzle design. It was also considered likely that the attenuation of a multiple nozzle-tube suppressor is nearly the same as that of a single-tube suppressor of the same L/D.

Basic Suppressor Design

As a result of the above considerations, the basic suppressor design was set to be a multiple nozzle-suppressor with an L/D of 75 and an overall length of 26.5 inches. The multiple nozzle plate of this design required 3.5 inches of this length, leaving 23 inches available for the actual suppressor. The inside diameter for the open port through each attenuator tube was thus determined to be: $D_{tube} = (23.0)/75 = 0.3066$ inch (hole diameter).

As stated previously, the diameter in the expression L/D is equivalent to the nozzle exit diameter. This nozzle exit diameter and the nozzle area ratio (ϵ) yield the nozzle throat diameter and area.

$$D_{throat} = \frac{D_{tube}}{\sqrt{\epsilon}} = \frac{0.3066}{\sqrt{2}} = 0.2167 \text{ in.}$$

for $\epsilon = 2$, and

$$A_{throat} = \pi \left(\frac{d}{2}\right)^2 = \frac{\pi (0.217)^2}{4} = 0.0369 \text{ in.}^2$$

R-9343

51

The individual nozzle throat area and the original single-nozzle overall throat area provide the number of small nozzles required.

$$\text{Number of Nozzles} = \frac{A_{\text{throat (total)}}}{A_{\text{throat (tube)}}} = \frac{9.3 \text{ in.}^2}{0.0368 \text{ in.}^2} = 253 \text{ nozzles}$$

Therefore, 253 nozzles and suppressors were estimated to be required to provide the needed attenuation within the allowed length.

A nozzle area ratio of 2 was used in the above calculation. The original nozzle area ratio was 4. A review of the procedure used to determine the required number of tubes indicates that the number of multiple nozzles and tubes required is proportional to the nozzle area ratio. Therefore, from a complexity standpoint, it was quite desirable to reduce the nozzle area ratio as much as possible. The primary effect of this area ratio reduction is a loss of thrust. However, a check of nozzle thrust coefficient data indicated that a reduction of rifle nozzle area ratio from 4 to 2 would yield a theoretical thrust loss of only 8 percent. This small sacrifice of thrust resulted in a decrease, by a factor of 2, of the required number of tubes, and a considerable reduction in the overall suppressor diameter. For this rifle suppressor design, therefore, a short secondary conical nozzle (Fig. 30) was added at the end of each suppressor tube to take advantage of the available area the design provides, as a result of the baffles, between each nozzle. It is expected that this secondary nozzle, which provides an overall area ratio of 12, will recover most of the thrust lost by reducing the primary nozzle area ratio.
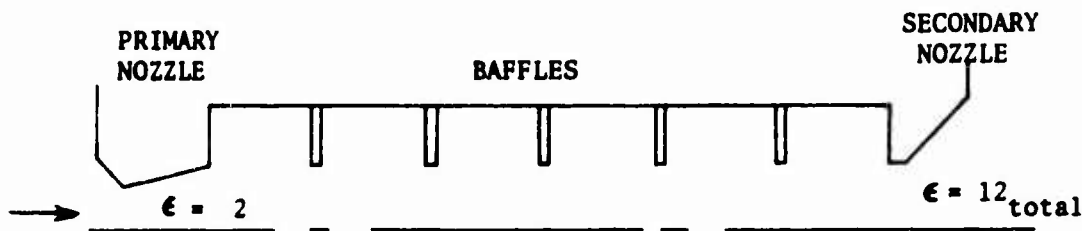

Figure 30. Primary Nozzle, Baffles, and Secondary Nozzle

These nozzle area ratio changes are a variation to those tested in the shock tube tests. Theoretical and experimental experience pertaining to the effects of multiple nozzles, nozzle extensions, and area ratio changes on thrust suggest that

these changes will result in only small thrust loss.s. The effects of the
reduced area ratio on attenuation are less well known, but it is likely that this
reduction, with the accompanying increase in mass velocity, would, if anything,
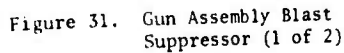tend to improve attenuation.

SUPPRESSOR HARDWARE

Based on the basic constraints and sizes discussed in the preceding section,
full-scale nozzle and suppressor hardware were designed (Fig. 31). The aerody-
namics of the design were given primary consideration within conservative con-
straints set by heat transfer and stress limits. For this embodiment of the
design concept, less consideration was given to suppressor weight than to
durability.

Subsonic Section

The initial section of the multiple-nozzle suppressor unit was designed to dis-
tribute the exhaust gases from the combustion chamber to the nozzles. The quasi-
steady-state flow here is subsonic and reaches a pressure near or equal to the
full rifle chamber pressure, which may be up to 12,000 psia. Consequently, the
walls were designed quite thick (see Fig. 31 for dimensions) in this region.
This section was made quite short to enable all length possible to be used for
blast-wave suppression.

Nozzle Adapter

The nozzle adapter will screw into the existing 10-inch OD housing with 8.250-12
UN-2 threads. A combustion chamber pressure of 12,000 psi was assumed and a load
of 633,000 pounds was used to calculate the shear stress in the threads. Results
of the calculations indicate that only three threads will take the load at a shear
stress of 150,000 psi. Because approximately 20 threads are used and the 4130
steel will be heat treated to 180,000 psi ultimate tensile stress, the threads
should have a sufficient factor of safety.

Figure 31. Gun Assembly Blast
Suppressor (1 of 2)

R-9343

54

Figure 31. Gun Assembly Blast
Suppressor (2 of 2)

The adapter body also was designed to withstand 12,000-psi internal pressure. The body was treated as the end plate of a boiler, with a resulting thickness of 1.5 inches. The resulting stress is slightly higher than the 180,000 psi ultimate. However, because helium shock-tube suppressor pressure measurements indicate lower internal pressures than assumed here, the 1.5-inch-thick adapter should provide sufficient support.

Multiple Nozzles

The next section within the suppressor is the nozzle plate. This plate is to be constructed of copper to provide adequate heat transfer within the high heat load regions of the nozzle entrance and, particularly, the nozzle throat. Each individual nozzle is of a converging (45-degree half-angle)-diverging (15-degree half-angle) conical design. The simple, double-conical design enables inexpensive construction, and the 15-degree half-angle of the diverging section should provide good thrust efficiency. The nozzle throat area was increased 5 percent to account for the low discharge coefficients of these sharp throat nozzles.

A pressure of 1000 psi was assumed to exist on the back of the 1/4-inch-thick plate with 253 countersunk holes. The load was taken up by 50 1/4-inch screws resulting in a tensile stress of 102,775 psi on the screws, which should be specified to withstand 165,000-psi minimum ultimate tensile stress.

A 2.00-inch-thick steel plate immediately follows the copper nozzle plate. This 16.372-inch-diameter steel plate was designed to support the high chamber pressures acting on the copper nozzle plate, which is bolted to it. Its distortion should be very low because only 37,000-psi bending stress is caused by the 2.2 million pound pressure load. Since this plate was quite thick and, therefore, costly in terms of suppressor length, the initial section of the suppressor was designed as an integral part of it.

This plate screws into the subsonic section of the suppressor. The special threads used to screw the backup plate into the nozzle adapter (16.250-8 UN-2) were assumed to take the 2.2-million-pound load. At a 180,000-psi stress level,

only four threads would be required. Because there are approximately 12 threads provided, the shear stress reduces to 23,000 psi or a safety factor of 4.26.

Suppressor Tubes

For each nozzle, a steel tube approximately 20 inches in length is extended downstream of the steel nozzle backup plate. These tubes house the actual suppression devices which are a series of baffles. Each baffle is a washer with an inside hole diameter equal to the exit diameter of the nozzles (0.307 inch) and is constructed of beryllium-copper for strength and good heat transfer. These baffles are separated by steel tubular spacers whose lengths are one baffle ID (0.307 inch). The baffle cavity ID is 0.62 inch, or just over twice the baffle hole diameter. These baffle washers and spacers combine to provide a suppressor geometrically similar to the best geometry tested in the shock-tube experiment.*

The 0.065-inch-thick washers were shown in Fig. 31 to have a 0.749-inch OD. This diameter has been revised downward to 0.740-inch OD to allow sufficient clearance in the 7/8-inch-diameter steel tubes. Assuming a pressure differential load of 7000 psi or 1552 pounds, the maximum bending stress was 99,500 psi. The beryllium-copper alloy was specified here to take the temperature and the stress.

Secondary Nozzles

The suppressor tubes are supported at the exhaust gas exit by another thick steel plate. The design is such that this plate shares the chamber pressure load felt by the nozzle support plate. As with the nozzle support plate, the end of the suppressor was designed as an integral part of this plate to take advantage of all available length for attenuation. A secondary nozzle for each tube was

---

*In view of the results of gun propellant tests (described later) of a seven-tube suppressor resembling a section of the 253-tube, full-scale suppressor design, the ends of the tubes are subject to leakage and erosion and should be sealed. Several methods are available: (1) attach a 0.030-inch copper gasket to the steel plate adjacent to the tubes, (2) use a 1/32-inch-diameter metallic O-ring at the end of each tube, (3) countersink each hold for the tube and bend the tube; conical copper washers can then be used to enhance the sealing, and (4) the entire tube assembly can be furnace-brazed, if the previous methods are not effective.

designed into the exit side of this plate. This total area ratio 12, 50-degree half-angle, conical nozzle was added at little increase in cost to take advantage of the available base area of the suppressor design and is expected to recover the thrust lost by reducing the primary nozzle area ratio to 2.

Outer Housing

A cylindrical tube 20 inches long and 16 inches in diameter houses the suppressor tube bundle and attaches the exit plate to the nozzle support plate. This tube, which is welded to these plates, provides a rigid support between them and allows the two plates to share the chamber pressure loads. The 1/4-inch housing thickness is twice that required to withhold the pressure load if stressed in tension to the 180,000 ultimate tensile strength.

Weight

It was realized that weight would be of considerable significance in a flight design. However, for these initial tests, primary significance was given to blast-wave suppression and durability of the suppressor. As a result, this design is purposely very conservative. However, it is considered that the use of more production-oriented techniques would reduce the suppressor weight by close to a factor of 2. These techniques would include use of the tube bundle to support the nozzle plate. Also, the baffle washer thickness can be reduced considerably as distance increases from the nozzle throat as a result of the reduced blast-wave strength with this distance. It may also be possible to eliminate the 16-inch-diameter outer tube. Also, conservative estimates of the internal pressures were made. Based on shock tube test data, these estimates can be refined and most likely reduced, thus decreasing the required structure thicknesses. Consideration of all these factors would be expected to reduce the overall suppressor weight to significantly less than 30 percent of the present weight. Strain gage test data would be very beneficial.

Alternate Designs

The recoilless rifle blast-wave suppressor discussed above was designed to reduce rifle overpressure effects on a simulated helicopter surface to less than 5 psig. However, substantial extrapolation was involved in this design and, as a result, uncertainty in suppressor performance exists. It is possible that some reduction in rifle chamber pressure may be required to meet the 5-psig constraint. The use of rocket-assisted projectiles to compensate for reduced chamber pressure is discussed in Appendix C.

On the other hand, the design described above was developed as a result of the highest recorded rifle unsuppressed blast-wave data, and later rifle data indicated somewhat lower wave overpressures. Also, the L/D of this design was approximately 15 percent greater than that indicated by the most optimistic shock-tube data extrapolations. If this "safety factor" were eliminated and the lower overpressure rifle firing data were considered, the L/D of the suppressor design could be reduced to as low as 53. This would reduce the required number of nozzles and suppressor tubes to 125 or one-half of the number in the present design. This would result in a considerable reduction in cost and weight of the suppressor. However, due to the extrapolations of the shock tube data and some data scatter in the rifle firing data, the foregoing more conservative approach was recommended for fabrication and test on the full-scale, 105-mm recoilless rifle.

SUPPRESSOR HEAT TRANSFER ANALYSIS

A heat transfer analysis of the full-scale, multitube suppressor was made, and is reported in Appendix B. The critical areas for overheating were in the multinozzle plate and the washers. For protection against short-duration, transient heat fluxes as high as 160 Btu/in.^{2}-sec, a removable nozzle plate section of pure copper was found to be adequate. The heat transfer to the washers was found to be sufficiently high to require the use of a special high-conductivity, high-strength, beryllium-copper alloy.

Slight erosion of the steel aft discharge nozzle plate and the attach screws for the copper nozzle plate was predicted.

RECOMMENDED TEST PROCEDURE

It was recommended that the rifle test procedure for the proposed suppression device be basically the same as the procedure used for previous arsenal tests. This approach would enable direct comparisons of the Rocketdyne device with other suppressors tested and with the reference firing cases.

Test Firings

A minimum of five firings of the rifle with the Rocketdyne suppressor was recommended. Chamber pressures of 3000, 6000, and 8000 psia were suggested for the first three tests in order of increasing chamber pressure. The remaining two tests should be made at the most interesting chamber pressure levels indicated by the first three firings. This might include firings up to 12,000 psia, depending on the suppression device effectiveness and condition.

Test Instrumentation

Two additional chamber pressure transducers and three strain gages were suggested for the firings of the Rocketdyne suppressor. The pressure transducers would be used to observe the pressure at the multiple nozzle entrance manifold (PA) and initial field pressure (PB) (Fig. 32).
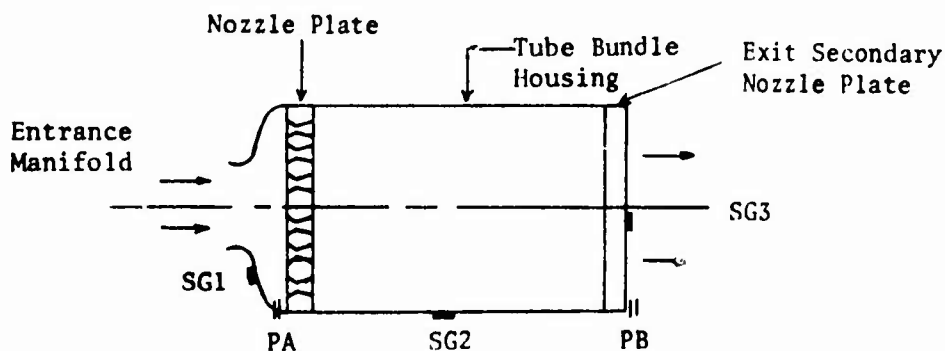

Figure 32. Additional Suppressor Instrumentation

The three strain gages would be used to gain an understanding of the stresses experienced by the device. These gages should be installed on the outer surfaces of the nozzle entrance manifold, tube bundle housing, and exit secondary nozzle plate as shown in Fig. 32. This degree of instrumentation is considered an adequate minimum for initial testing. However, upon success of this test program, future tests with a substantial number of suppressor strain and internal pressure measurements are recommended. These measurements would refine the understanding of the loads experienced by the suppressor and form the basis for future significant decreases in structure weight and simplified cavity geometry.

GUN PROPELLANT TEST PROGRAM

A third experimental test program was conducted to obtain data that might more directly support the foregoing full-scale attenuator design than did the shock tube tests. Specifically sought were: further corroboration of the effects of L/D ratio, including data at a value of 75; confirmation that multiple, short, small-diameter suppressors are as effective as a large, single-tube attenuator of the same L/D; and an assessment of hardware durability, i.e., whether the full-scale attenuator might be used for several rounds without erosion or distortion problems. To attain the latter goal, and also to better simulate recoilless rifle back-blast conditions, this test series was made with gun propellant charges fired in subscale test hardware.

The gun propellant test program was undertaken late in the contract and under a very modest budget. Therefore, to the extent possible, existing apparatus was used and the test sequence was designed to provide answers even if a set of hardware was damaged before its intended testing was completed. Gun propellant charges were loaded in the former helium pressure chamber which was modified to provide for propellant ignition and for measuring the chamber pressure. Burst disks ~1000 psi were used to promote rapid propellant burning and reduce the quantity of unburned propellant discharged through the nozzle.

The test sequence chosen is detailed in Table 5. The 4:1 expansion area ratio nozzle and its attendant 32-inch-long, single-tube washer-and-spacer suppressor were the existing 1:6.86 scale model components tested in the prior helium/air shock-tube tests. These gun propellant tests were intended to provide reference unattenuated blast data, new attenuation data for comparison with the helium/air shock results, an indication of blast amplitude variation with chamber pressure, and information on durability of these all-steel components.

TABLE 5. HOT-GAS MODEL SUPPRESSOR TEST PARAMETERS

Test Series	Nozzle Type	Suppressor L/D	Peak Peak Chamber Pressure, psia	Scheduled No. of Tests
1	Single $\epsilon = 4:1$	None	6000	2
2	Single $\epsilon = 4:1$	32	3000/6000	2 (1 each)
3	Multinozzle $\epsilon = 2:1$	75	3000 6000 9000	1 - 3 1 - 3 1 - 2

The multinozzle suppressor was a new device that essentially duplicated a seven-nozzle, seven-tube attenuator cluster out of the 253-tube, full-scale design of the preceding section. (Minor dimensional changes were made so the subscale data could be compared directly with the subscale single-nozzle data.) This device was an important key to answering the topics discussed in the first paragraph of this section. The tests were scheduled for one at each pressure level, progressing from lowest to highest, before making any duplicate tests. Ultimately, the number of replicate tests would depend on the hardware condition as testing proceeded.

SEVEN-NOZZLE AND -TUBE SUPPRESSOR

To compare the blast-wave pressures from a single nozzle to that from a nozzle and suppressor combination, a seven-nozzle cluster model was designed with the total throat area equal to that of the single nozzle. The diameter of each throat in the seven-nozzle cluster was 0.189 inch. Each nozzle exit diameter was 0.267 inch (area ratio = 2.0), and this was equal to the orifice diameter in the washers. Figure 33 shows the design of the seven-nozzle plate and the seven-tube suppressor. To minimize erosion by the hot gases, the nozzle plate and washers in the tubes were made of copper. This apparatus is shown in Fig. 34.
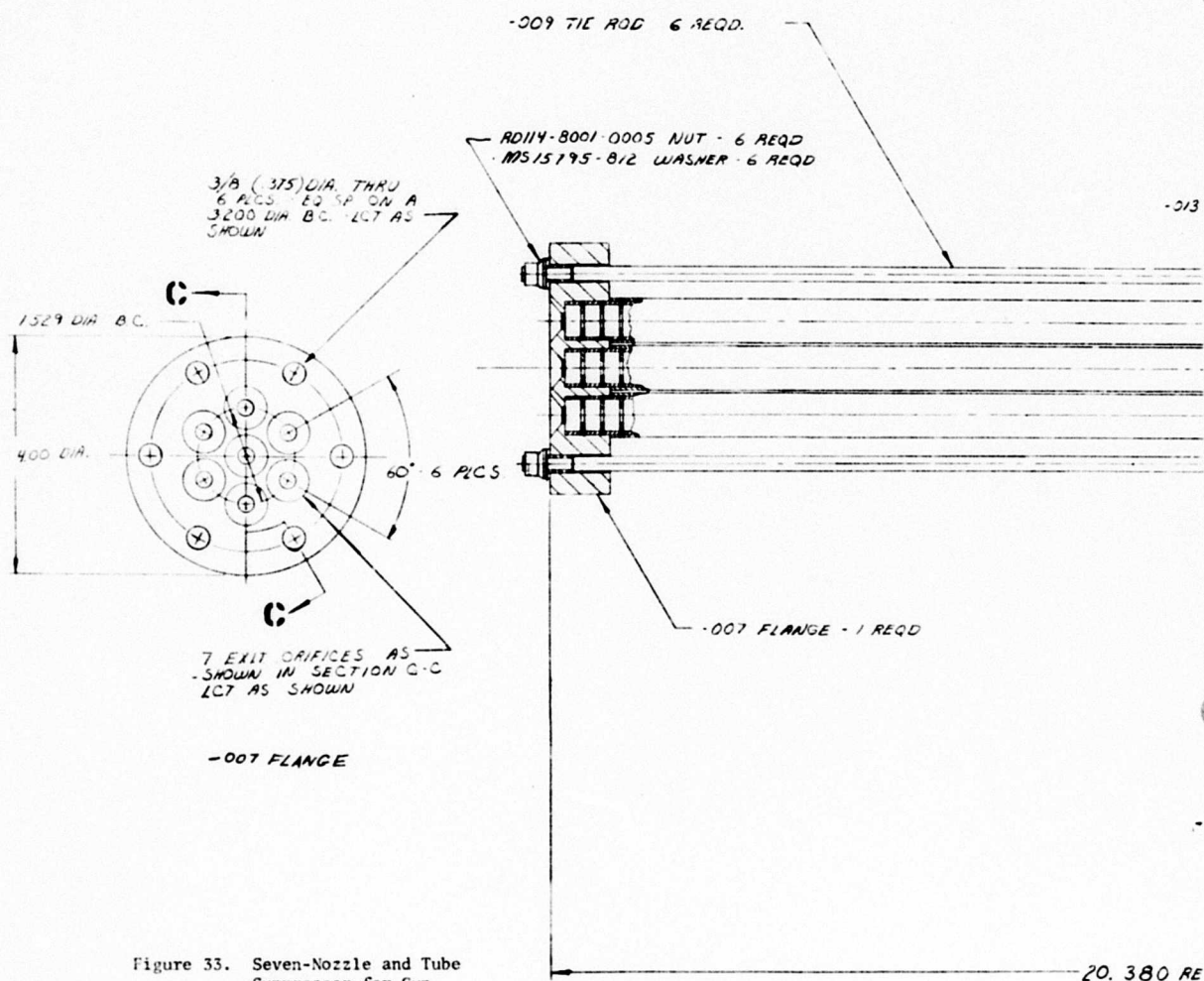
-009 TIE ROD 6 REQD.

AD114-8001-0005 NUT - 6 REQD
MS15795-812 WASHER - 6 REQD

-013

3/8 (.375) DIA. THRU
6 PLCS EQ SP ON A
.3200 DIA. B.C. LCT AS
SHOWN

1.529 DIA. B.C.

4.00 DIA.

C

60° 6 PLCS

C

7 EXIT ORIFICES AS
SHOWN IN SECTION C-C
LCT AS SHOWN

-007 FLANGE

-007 FLANGE - 1 REQD

20.380 RE

Figure 33. Seven-Nozzle and Tube
Suppressor for Gun
Propellant Tests (1 of 2)

R-9343

66

RUPTURE DISK · REF.

·017 WASHER · 420 REQD.

·015 SPACER · 420 REQD.

MS29513 · 233 1 REQD.

MS29513 · 229
1 REQD

AP · 72 · 407 RING · REF.

TUBE · 7 REQD

RD111 · 4014 · 4073 BOLT · 8 REQD.
RD153 · 5004 · 0010 WASHER · 8 REQD.

003 MULTIPLE NOZZLE PLATE · 1 REQD.

·005 FLANGE PLATE · 1 REQD.
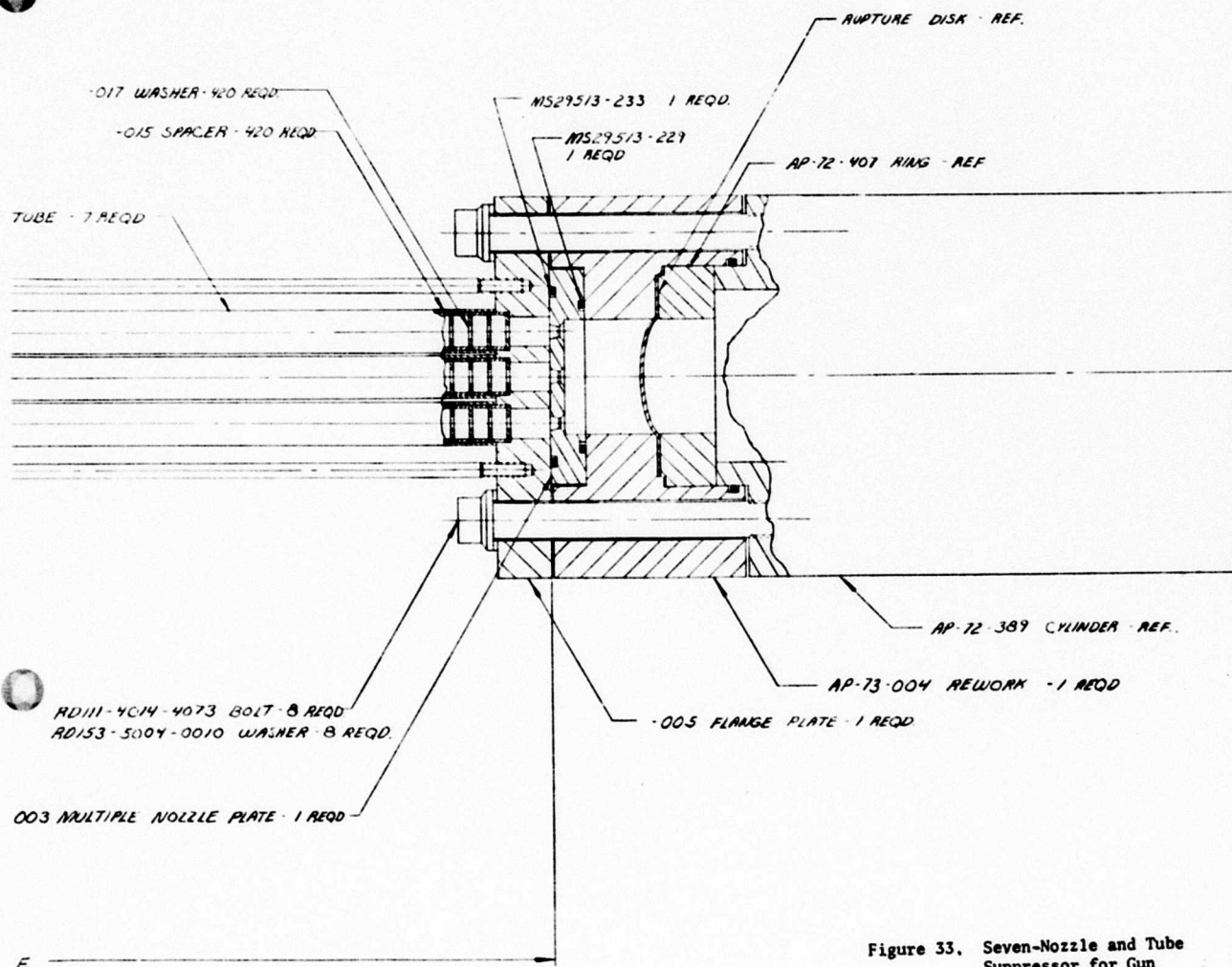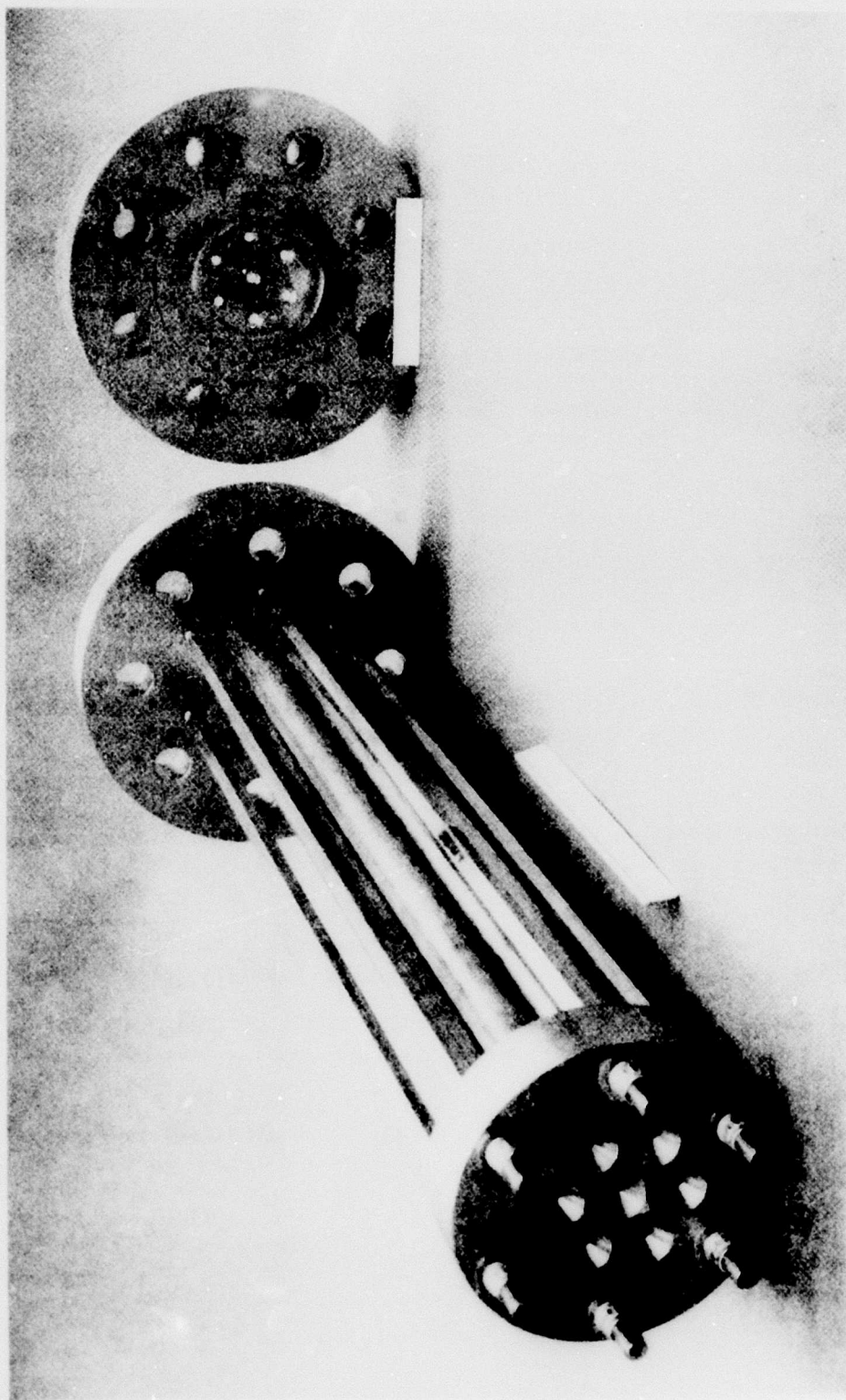
AP · 73 · 004 REWORK · 1 REQD.

AP · 72 · 389 CYLINDER · REF.

F.

Figure 33. Seven-Nozzle and Tube
Suppressor for Gun
Propellant Tests (2 of 2)

R-9343
67/68

Figure 34. Seven-Tube Blast Suppressor and Multinozzle Plate Before Firing

DESCRIPTION OF TESTS

Testing was performed essentially as detailed in Table 5, with some changes in the peak chamber pressures. The apparatus previously used for helium/air shock formation and attenuation experiments was modifed to permit testing of blasts generated by gun propellant charges. Accurately weighed charges of M-2, single-perforated, 37-mm gun propellant were confined* in the closed-volume pressure section, separated from the discharge nozzle(s) by a burst diaphragm. Charge ignition led to smooth pressurization of the chamber. While the pressure was still rising, rupture of the burst diaphragm permitted flow of gases (and burning propellant) out of the exhaust nozzle(s). The impulsive initiation of flow through the nozzle(s) formed a steep-fronted blast wave which, if discharged directly without an attenuator, had substantially higher pressure amplitude than any waves or pressure perturbations formed later in the propellant-combustion, chamber-pressurization, flow-discharge process. The main objective of the gun propellant shots was to determine experimentally the reduction of amplitude of the frontal blast wave achieved by the subscale attenuators.

Test Apparatus

The basic test apparatus has been described in previous sections. Three discharge configurations were tested: a single 4:1 expansion area ratio nozzle; the same nozzle fitted with a tube-and-washer attenuator having a length 32 times the nozzle exit diameter (L/D = 32), Fig. 24; and a seven-nozzle discharge plate fitted with a seven-tube, L/D = 75, tube-and-washer attenuator (Fig. 33 and 34). The seven-tube apparatus is a full-scale embodiment of the central seven tubes of the 253-tube attenuator detailed in the Design Concept section. The cross-sectional throat area of each of the nozzles was equal to 1/7 of the scale-model single-nozzle throat area, so that a fixed charge weight would give equivalent pressure-time histories for both discharge configurations.

---

*A lightweight, circular, cardboard disk was used to hold the propellant charge against the upstream end of the cylinder. Individual grain dimensions were: 0.067-inch OD by 0.0082-inch ID by 0.258-inch long.

Test Setup and Instrumentation. The test setup used is illustrated in Fig. 35 and 36. The single-nozzle exit diameter of 1.00 inch was 1/6.86 of the full-scale recoilless rifle's nozzle discharge; therefore, the reflection plate with pressure transducers was positioned 7.00 inches from, and parallel to, the nozzle axis, modeling the 48-inch, full-scale helicopter simulation plane.

The reflecting plate which contains transducers K-2 through K-3 was repositioned for each attenuator configuration to maintain the same geometric relationship with respect to its discharge end as to the nozzle discharge.

Four Kistler pressure transducers were used to measure the blast pressures produced. Their types, locations (Fig. 35) and nominal calibrations were as follows:

No.	Type	Location Designation	Nominal Calibration psi/volt recorded
K-1	607L	Chamber Pressure	5000
K-2	603A	Reflection Plate, 45 degrees Off-Axis	10
K-3	603A	Reflection Plate, 30 degrees Off-Axis	10
K-4	603A	Reflection Plate, 18 degrees Off-Axis	10

The charge amplifiers for the three Model 603A transducers were set (spanned) for measuring pressures in the lower 2 percent of this model's useful range. Because that is below the region where the voltage output versus pressure is linear, these transducers were statically calibrated to obtain correction factors to apply to their linear, factory-supplied calibrations.

The pressure data were recorded on a 14-channel Sangamo high-speed tape recorder at 120 in./sec tape speed (Fig. 37). The recording system has flat response to 40 KHz. Data were retrieved by playback of the tapes into a dual-channel oscilloscope and/or into a multichannel Statos-3 strip chart recorder.
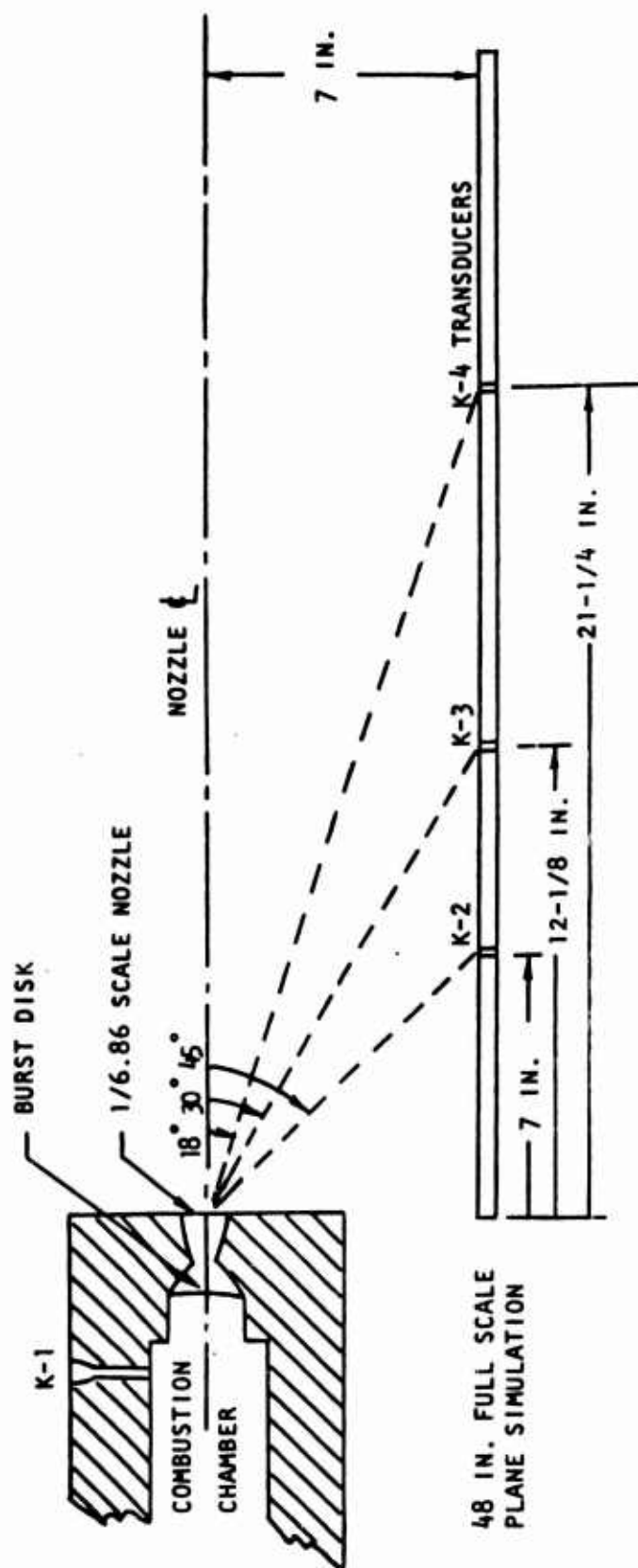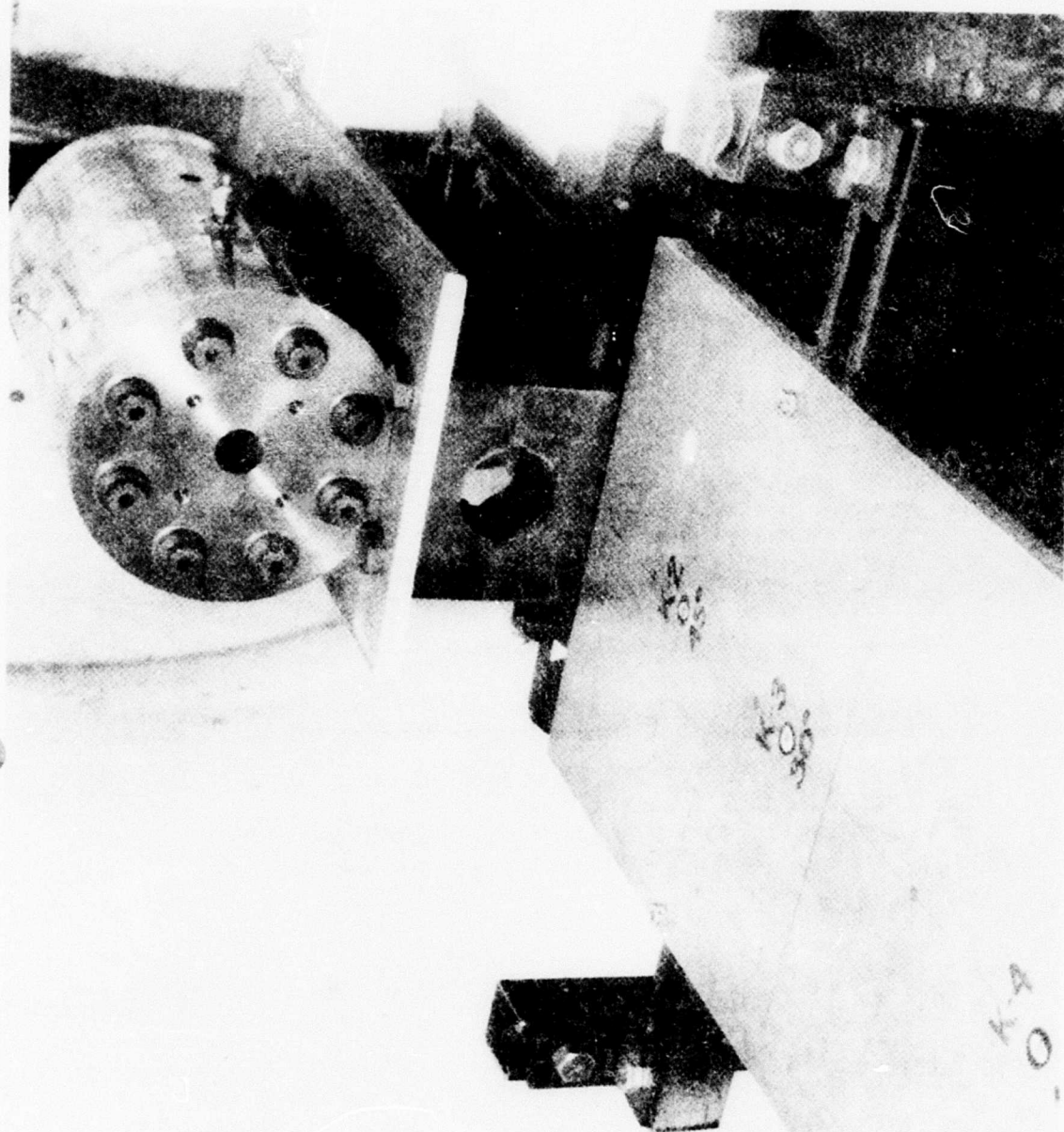
Figure 35. Gun Propellant Blast-Wave Test Setup and Location of Thermocouples on Blast-Wave Reflecting Surface

Figure 36. Installation of Shock-Tube Cylinder in Gun Firing Range Tunnel (transducer positions are indicated on surface plate)

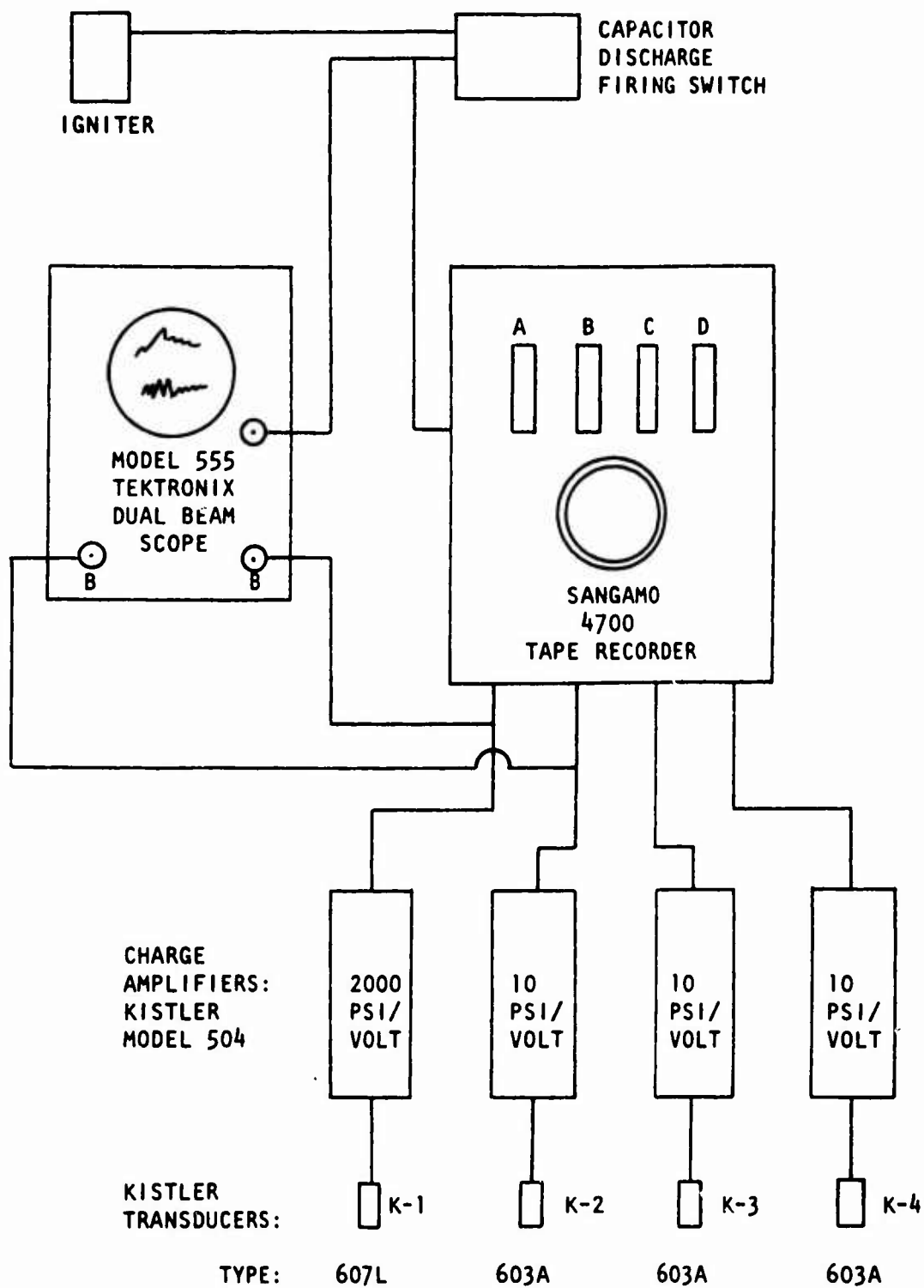5A024-7/6/73-S1B

R-9343

73

Figure 37. Schematic Drawing of Electrical Circuit for Measuring Chamber and Blast-Wave Pressures Using Gun Propellants

R-9343

Propellant-Charge Weights. Although it was desired to burn propellant-charge weights that would produce peak combustion chamber pressures of 3000, 6000, and 9000 psi, exploratory shots with the no-attenuator, single-nozzle configuration yielded the following:

Charge Weight, grams	Peak P_c, psi
55.00	4000
70.00	6000
85.00	8000

Rather than expending additional shots to determine charge weights for the 3000- and 9000-psi peak pressure levels, it was decided to proceed with the attenuator tests using these three charge weights.

Burst Diaphragms. Burst diaphragms used in the previous helium/air shock tunnel testing were designed to rupture at 2500 psi. For the gun propellant shots, burst pressures on the order of 1000 to 1500 psi were thought to be more representative of the recoilless rifle firing behavior. It was discovered that the supplier who had given 3-week delivery time on the 2500-psi diaphragms was no longer in business. No other supplier was found that could make the required diaphragms without causing at least a month's delay in testing. Therefore, diaphragms were designed and machined in-house. Initially, two diaphragms were made and tested in shots No. 1 and 2. These burst diaphragms were made from 0.060-inch stainless steel recessed to 0.040-inch thickness in which a cross with a minimum thickness of 0.020 inch was grooved. When these proved to be nominally satisfactory, a second batch of 12 diaphragms was made for tests 3 to 14, but with lowered resistance to breakage.

RESULTS OF PRELIMINARY TESTS

Two preliminary tests were conducted to determine the amount of M-2 gun propellant
needed to attain a chamber pressure of 6000 psi. Results of the tests are as
follows:

Shot No.	1	2
Charge Weight, grams	55.00	70.00
Peak Pressure, K-1, psia	4100	6238
Burst Disk Rupture Pressure, psia	1580	2500
Peak Blast Pressure, K-2, psia	17.1	19.2
Peak Blast Pressure, K-3, psia	23.2	29.4
Peak Blast Pressure, K-4, psia	10.9	18.0

Figure 58 illustrates the chamber pressure histories from these tests. Chamber
pressure peaked in 10 to 13 milliseconds, which is considerably longer than the
full-scale 105-mm rifle rise time of 3 to 4 milliseconds. This resulted from a
combination of factors, e.g., absence of a projectile, lower propellant specific
burning rate, and higher chamber volume-to-nozzle throat area ratio. It was
decided to proceed with the attenuator testing, rather than devoting more of the
limited number of total tests possible to better match of the rifle's pressure
history. That decision was augmented by the observation that the initiation and
highest amplitude of the back blast propagated into the atmosphere corresponded
to rupture of the burst diaphragm and not to the peak chamber pressure.

TEST RESULTS

Results from the gun propellant firing tests may be subdivided into principal
categories of blast-wave attenuation, as determined from pressure data, and atten-
uator durability, as indicated by the posttest condition of the apparatus. Addi-
tionally, some test bed recoil data were obtained which permitted a preliminary
assessment of how an effective attenuator might affect weapon recoillessness.
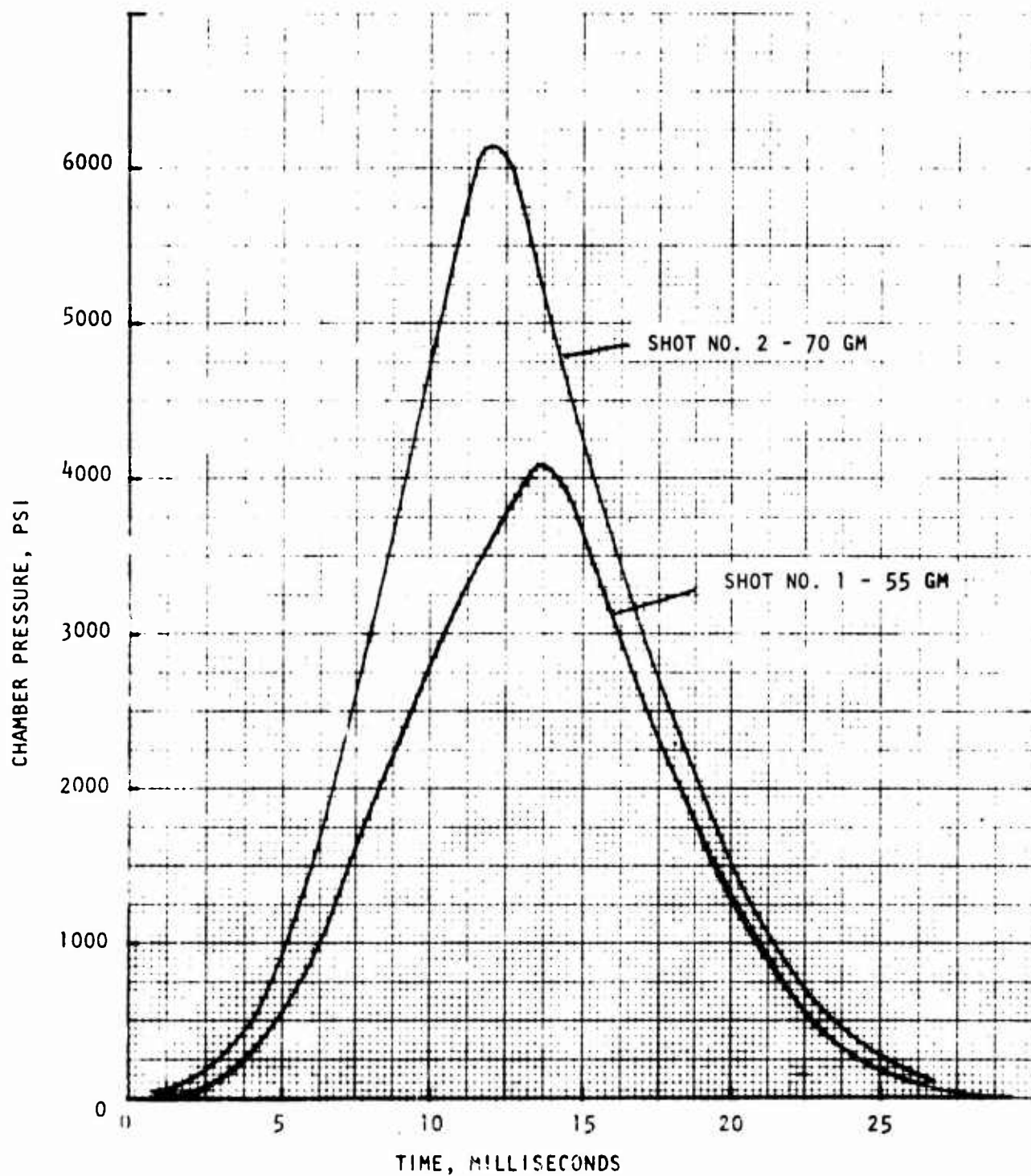
Figure 38.   Pressure-Time Histories of the Model Reference Nozzle Fired
With Two Different Gun Propellant Charges

Blast-Wave Attenuation

Pressure data recorded during the 14 gun propellant shots were reduced from Polaroid photographs obtained by playback from the magnetic tapes into a dual-beam oscilloscope. As shown in Table 6, these data are subdivided into series corresponding to the three test configurations and, within each series, are grouped by chamber pressure level. Included are peak chamber pressure, whose reading was straightforward; chamber pressure just before the diaphragm ruptured, which showed as a distinct interruption of the trace in some tests but could only be discerned by examination through a low-power microscope in others; and blast-wave initial peak pressures at the three reflection-plane transducer positions. Particularly, with the L/D = 75 seven-tube attenuator, the times of initial wave arrival were not apparent because no disturbances in the pressure traces, attributable to diaphragm rupture, could be seen. Because the noise level on the recording systems was estimated to be no more than 1 psi, those pressures are tabulated simply as "less than 1 psi"; they certainly may have been lower.

For better visualization of the relationships among all the pressure records and of pressure-field behavior for substantial times after the initial blast, the tape records were also played back into a Statos-3 multichannel strip chart recorder. Three of these charts, one for each of the test configurations at a peak chamber pressure of about 5830 psi, are reproduced in Fig. 39 through 41, at a paper speed that displays the entire shot. On these figures, there are three separate channels which show chamber pressure; the upper one was recorded at a different gain setting than the others and its calibration signal was later found to be in error so it should be neglected; the lower one is an amplified signal of the upper one and was run to aid in identifying the burst diaphragm rupture; the other trace, unfortunately, exhibited a lot of noise on this playback equipment (which was not present on the original tape recording). Calibration factors are shown for the various traces; although they generally gave chamber pressure and shock wave amplitudes that agreed with those in Table 6, they were believed to be less accurate than those from the oscilloscope. It will be seen that these factors remain unchanged in Figures 41 through 43, so that direct visual comparisons are possible.
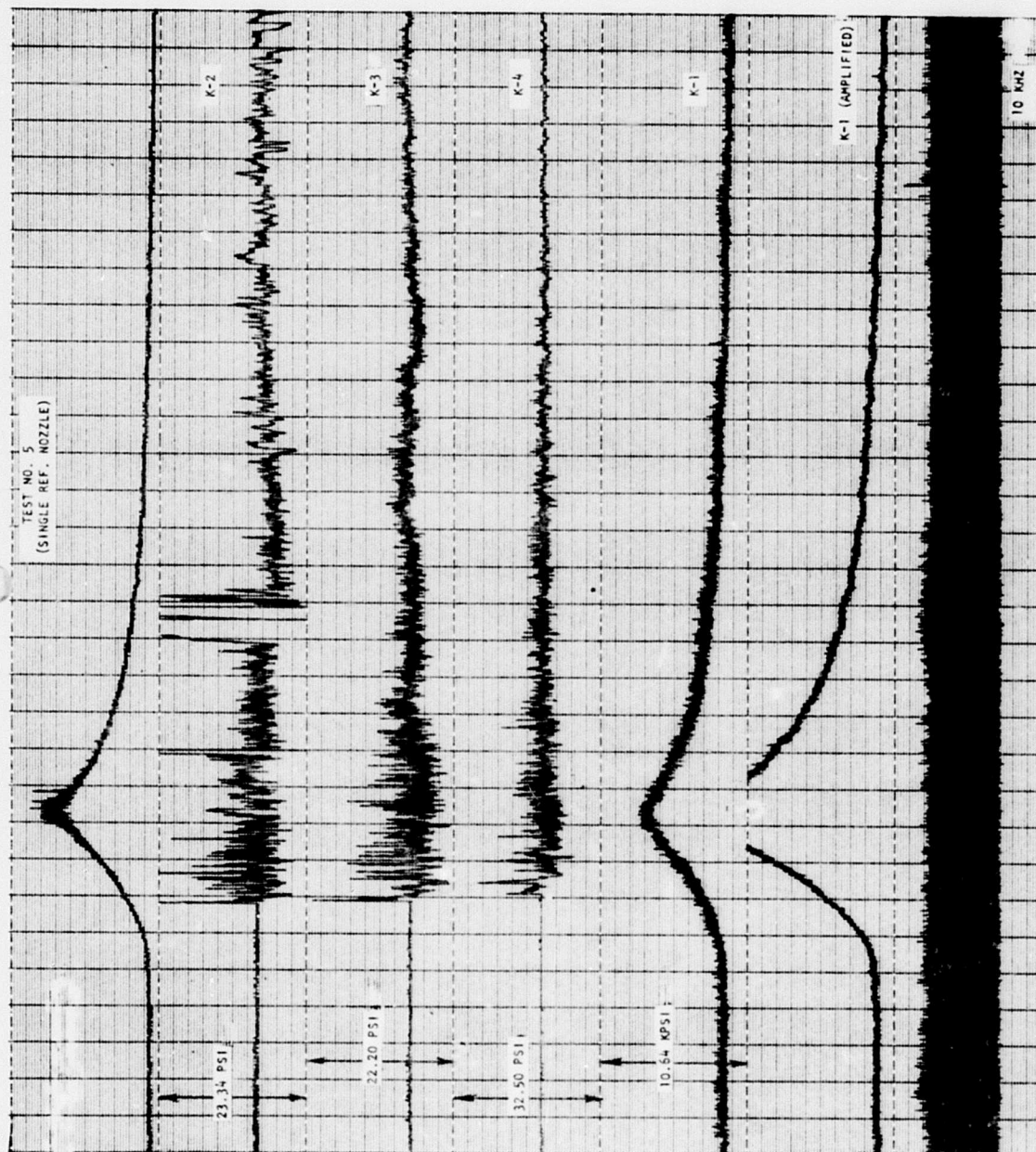
Figure 39. Tape Records of Transducer Readings Made During Gun Propellant Tests, Test No. 5
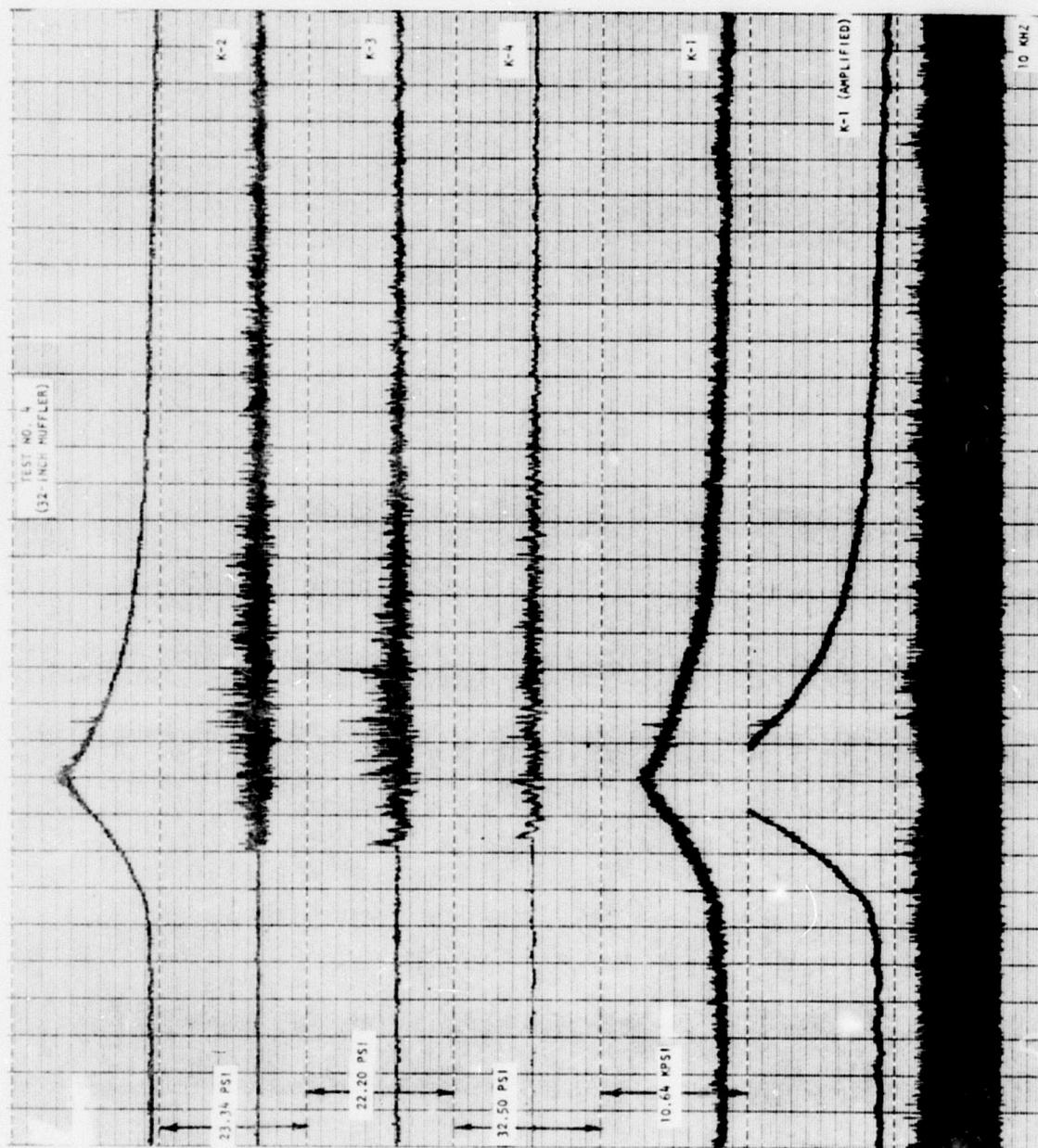
Figure 40. Tape Records of Transducer Readings Made During Gun Propellant Tests, Test No. 4
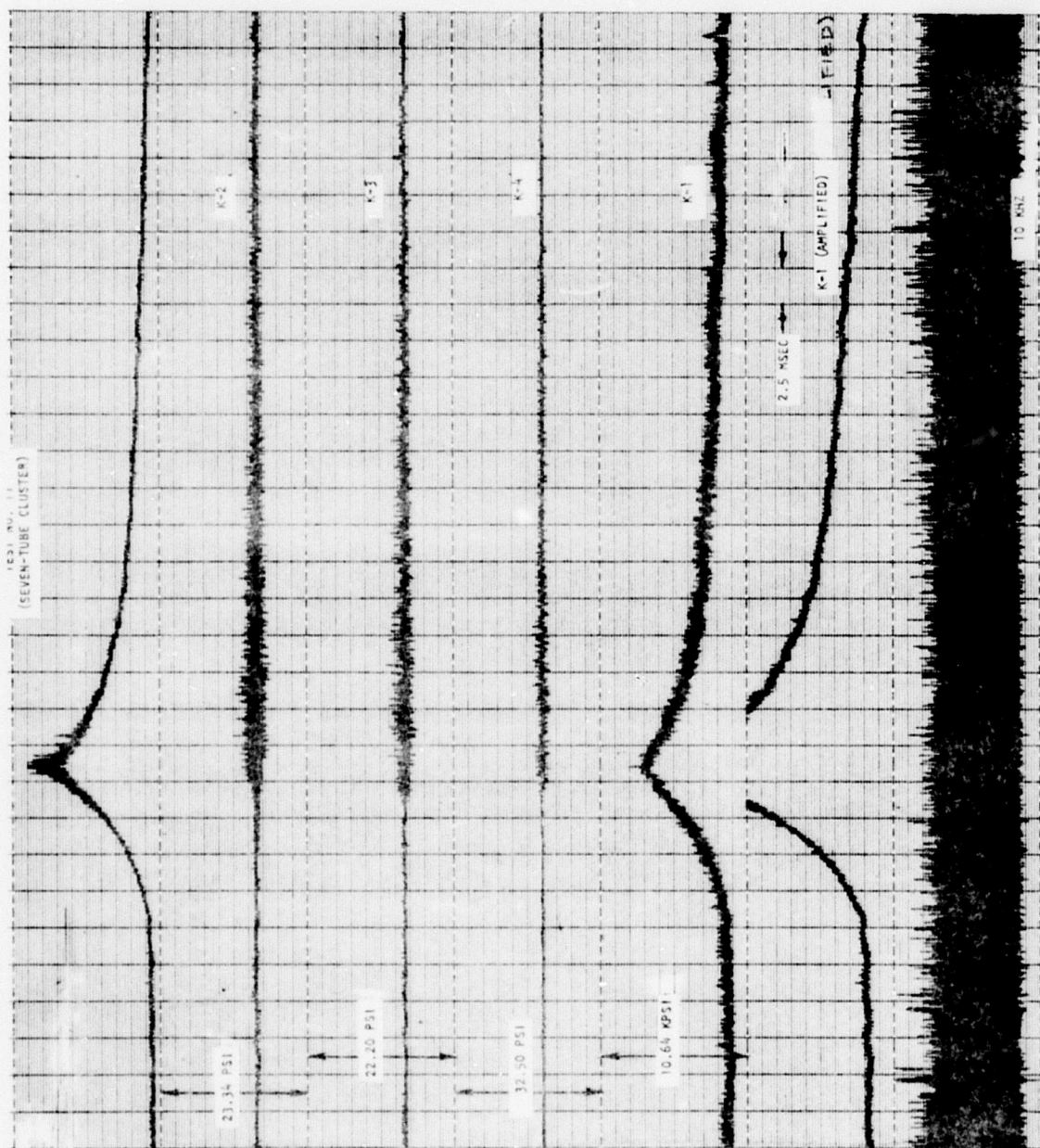
Figure 41. Tape Records of Transducer Readings Made During Gun Propellant Tests, Test No. 11

TABLE 6.   SUMMARY OF BLAST DATA FROM SUBSCALE GUN PROPELLANT SHOTS

Shot No.	Peak Pressure, psig	Diaphragm Burst Pressure, psig	Shock Pressure, psig		
			K-2	K-3	K-4
Series I: Single Nozzle, No Attenuator					
1	4100	1580	17.1	23.2	10.9
2	6238	2500	19.2	29.4	18.0
5	5838	1375	15.4	14.7	7.8
6	7790	1250	14.0	16.0	7.5
Series II: Single Nozzle, L/D = 32 Attenuator					
3	3925	1125	4.6	3.3	3.2
4	5825	1200	2.1	4.9	4.2
Series III: Seven-Nozzle, L/D = 75 Attenuator					
7	3875	875	< 1.0	< 1.0	< 1.0
10	3825	925	↓	↓	↓
13	3625	750			
8	5425	950			
11	5842	800			
14	5700	950			
9	7512	950	↓	↓	↓
12	7788	975	< 1.0	< 1.0	< 1.0

Such a comparison of Fig. 39 with Fig. 40 and 41 shows dramatically the reduced blast pressure field amplitudes at the reflection plate (K-1 through K-2) affected by the blast attenuators. (As noted later, aural sound level observations were in agreement with these results.)

To show the complicated nature of the noise in the pressure field, time-base expanded sections from these same three runs are reproduced in Fig. 42 through 44.

The following observations may be drawn from the data presented.

Peak Pressures. For a given charge size, repeatability of peak pressure is within approximately ±5 percent. No effective difference between the single-nozzle and the seven-nozzle configurations is apparent.

Diaphragm Burst Pressures. The estimated chamber pressures at diaphragm rupture appear to depend on the nozzle configuration. Except for shots 1 and 2, whose diaphragms were made separately from the main batch of 12, the single-nozzle values are approximately 1250 psi ±10 percent. The seven nozzle values are significantly lower, having a mean value of about 900 psi and somewhat wider scatter.

The batch of 12 burst diaphragms used for shots 3 through 14 was made from 0.060-inch-thick 347 CRES stock, machined to a 0.038-inch thickness within a 2.22-inch diameter. A grooved cross was cut to a 0.020-inch minimum thickness. The breaking of the diaphragms was consistently clean but differed between the single- and multiple-nozzle configurations. The multinozzle diaphragm opened up to a full 2-inch diameter when broken, whereas the single-nozzle diaphragm could open only to a 45-degree half-angle cone.

Blast Overpressures at the Reflection Plate. Tabulated data for K-1, K-2, and K-3 refer to the blast wave's initial frontal shock amplitude. A cursory inspection immediately suggests that: (1) shock amplitudes are definitely dependent on diaphragm rupture pressure and, perhaps, on peak chamber pressure; (2) the single-tube L/D = 32 attenuator effected substantial reductions in amplitude,
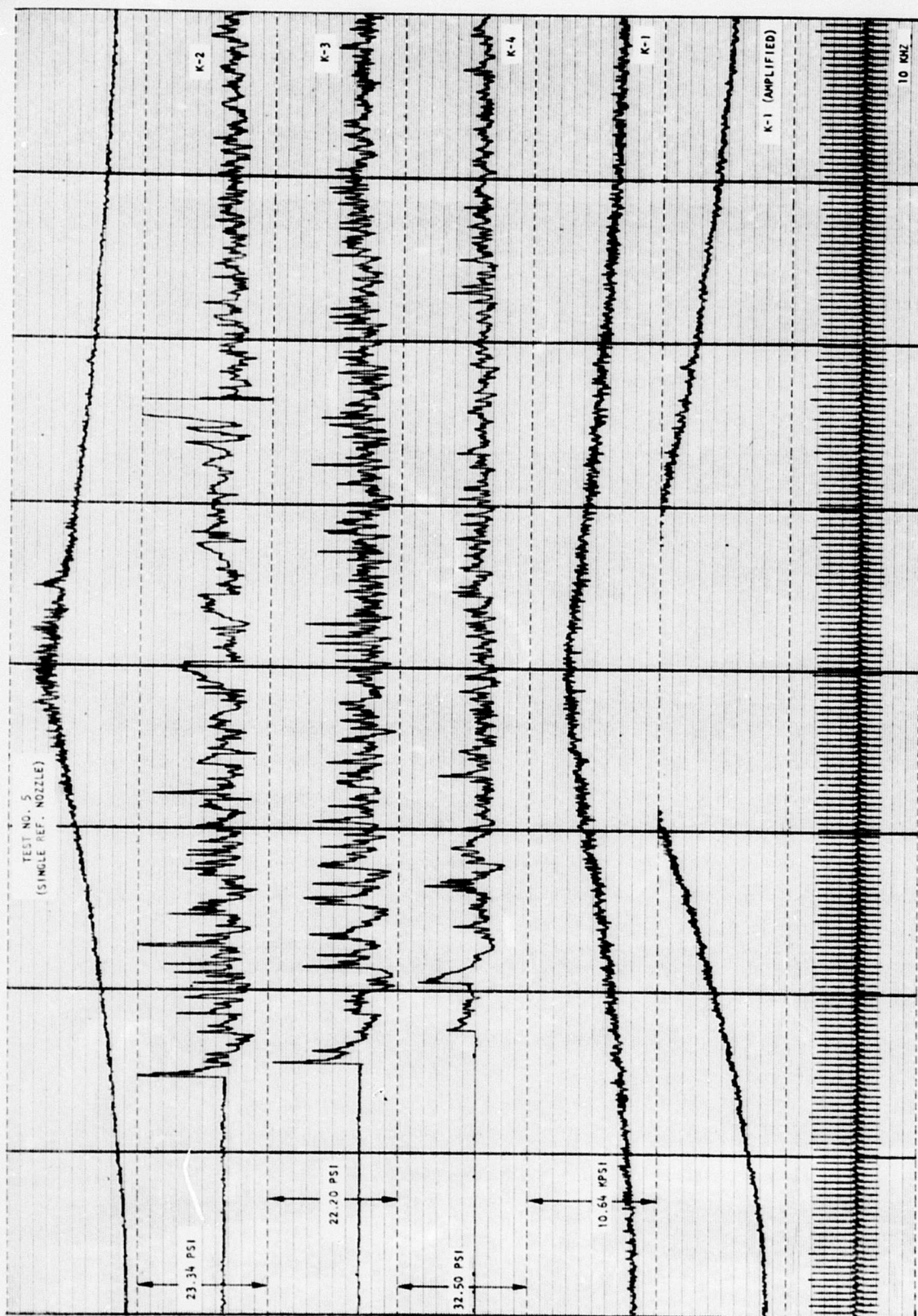
Figure 42. Tape Records of Transducer Readings Made During Gun Propellant Tests With Time Base Expansion, Test No. 5
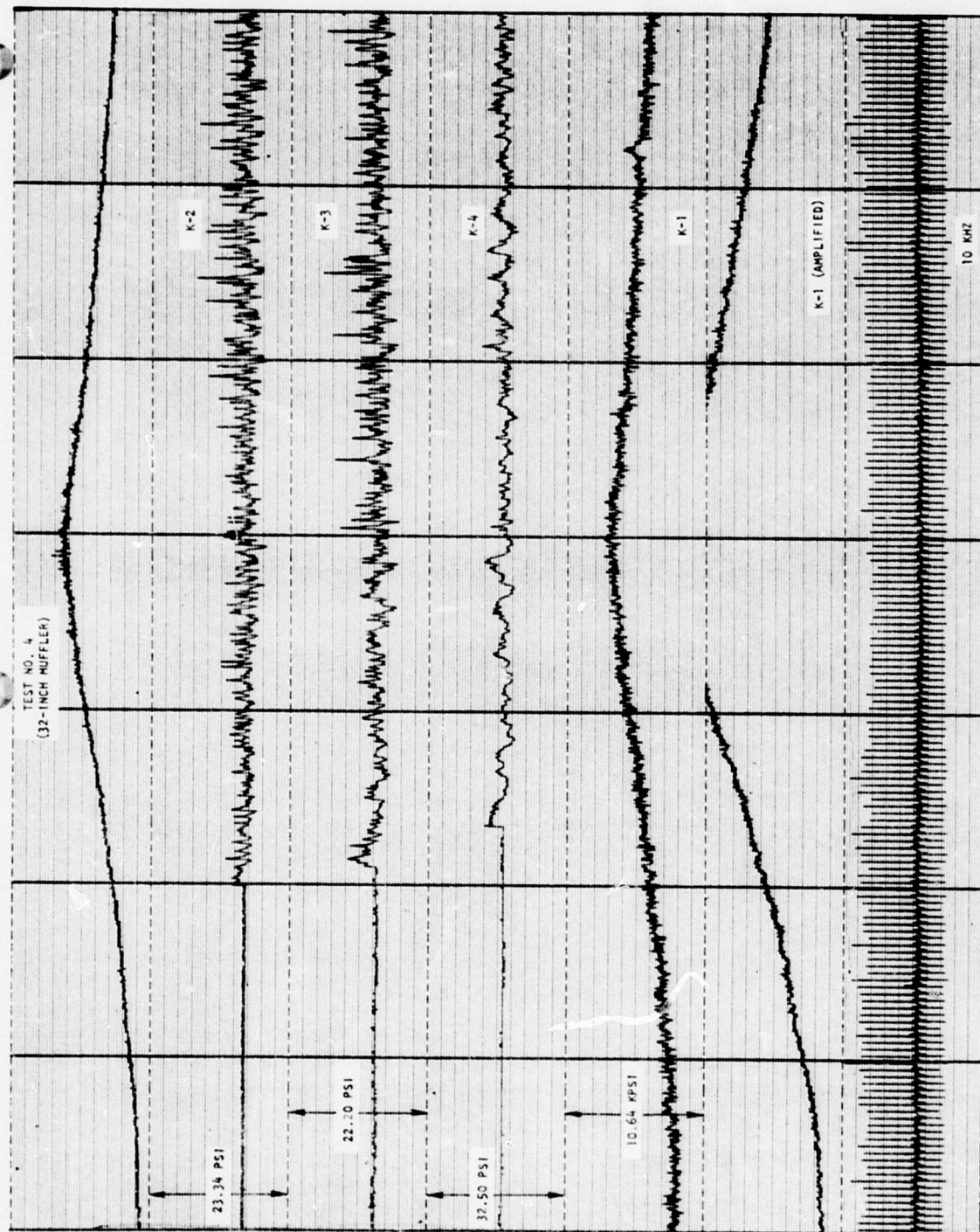
Figure 43. Tape Records of Transducer Readings Made During Gun Propellant Tests With Time Base Expansion, Test No. 4
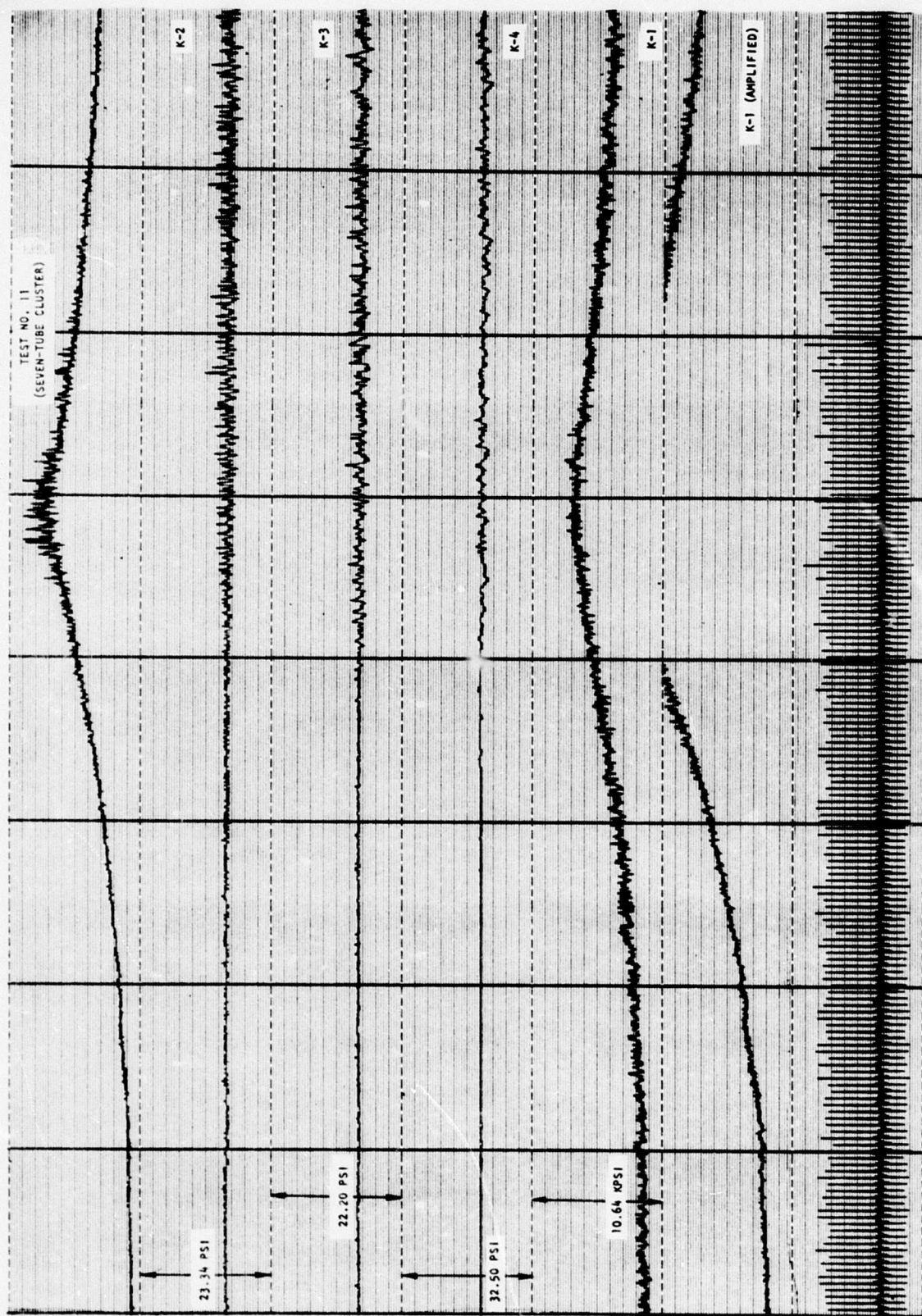
R-9343

85

Figure 44. Tape Records of Transducer Readings Made During Gun Propellant Tests With Time Base Expansion, Test No. 11

(3) the seven-tube L/D = 75 attenuator effectively eliminated the shock front, with initial disturbances being indistinguishable from the background noise in the recording system.

The reflection plate pressure data are plotted versus peak pressure in Fig. 45 and versus diaphragm burst pressure in Fig. 46 . Examination of Fig. 45 shows no apparent correlation between peak chamber pressure and the shock overpressures. Conversely, Fig. 46 shows that, with the unattenuated single nozzle, the over-pressures recorded at a given transducer location varied approximately linearly with diaphragm burst pressure. Because of this strong effect, it appears inappropriate to make quantitative run-by-run comparisons among the three configurations. Rather, it is recommended that attenuator data be compared with unattenuated, single-nozzle pressure values read from the correlating lines. Thus, using mean values for the L/D = 32 single attenuator at an 1175 mean burst pressure, the attenuation factors for the three transducers may be approximated as:

$$K\text{-}2: \quad A = (4.6 + 2.1)/(13.0)(2) = 0.26$$
$$K\text{-}3: \quad A = (3.3 + 4.9)/(14.6)(2) = 0.28$$
$$K\text{-}4: \quad A = (3.2 + 4.2)/(8.0)(2) = 0.46$$

Similarly, using mean values at a 900-psi burst pressure and assuming a value of 1.0 psi for all reflection-plate pressures, indicates approximate values for the seven-tube attenuator of:

$$K\text{-}2: \quad A \cong 1/10 \cong 0.1$$
$$K\text{-}3: \quad A \cong 1/11.2 \cong 0.09$$
$$K\text{-}4: \quad A \cong 1/6.2 \cong 0.016$$

A major goal of this program was to develop an attenuator design capable of reducing reflected blast amplitudes at the simulated helicopter surface to below 5 psi. This represents a value of $A \cong 0.125$. The foregoing data offer direct support that this goal can be achieved with the 253-tube attenuator design desribed earlier. In fact, the seven-tube model data suggest that the design is
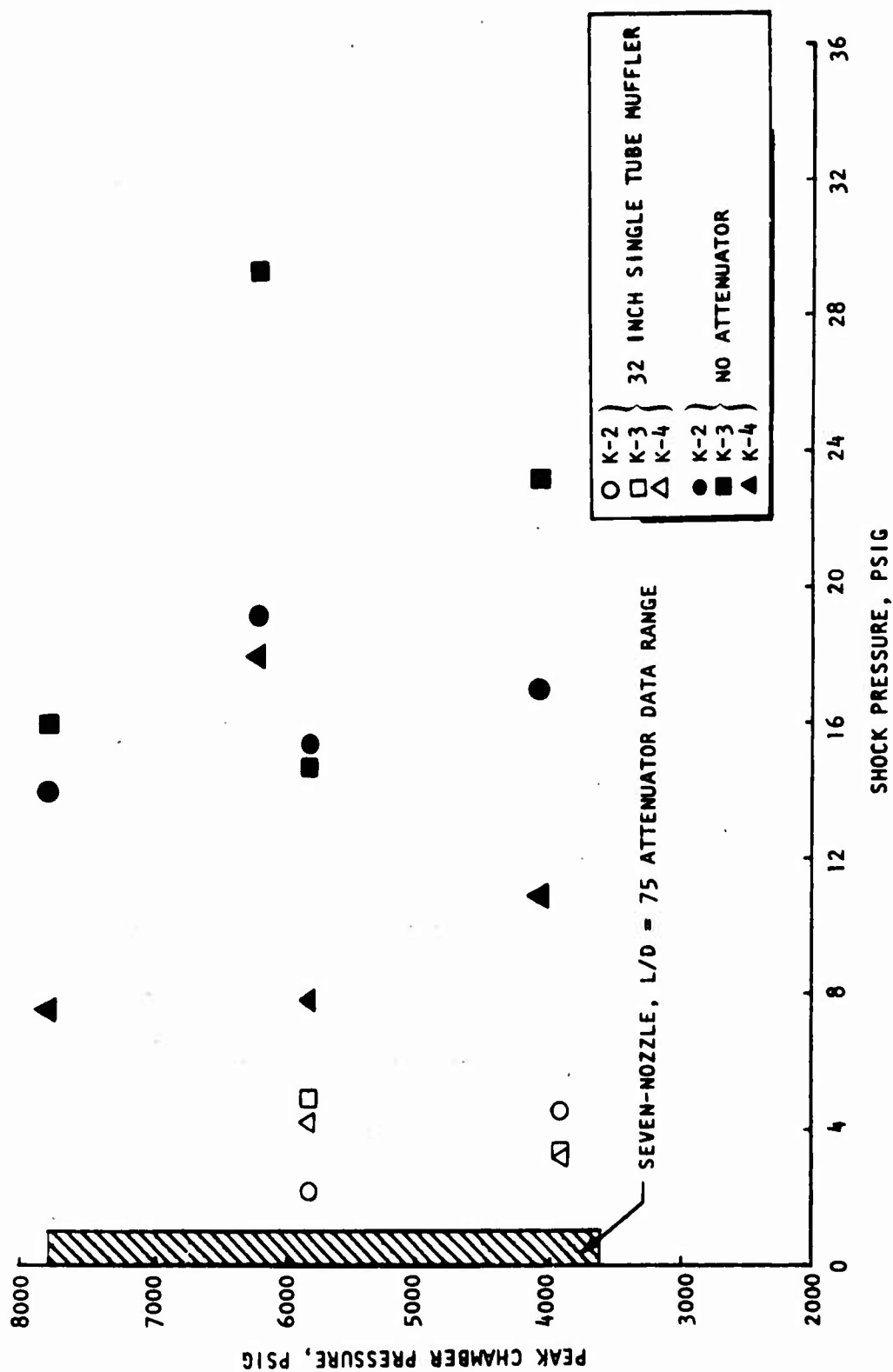
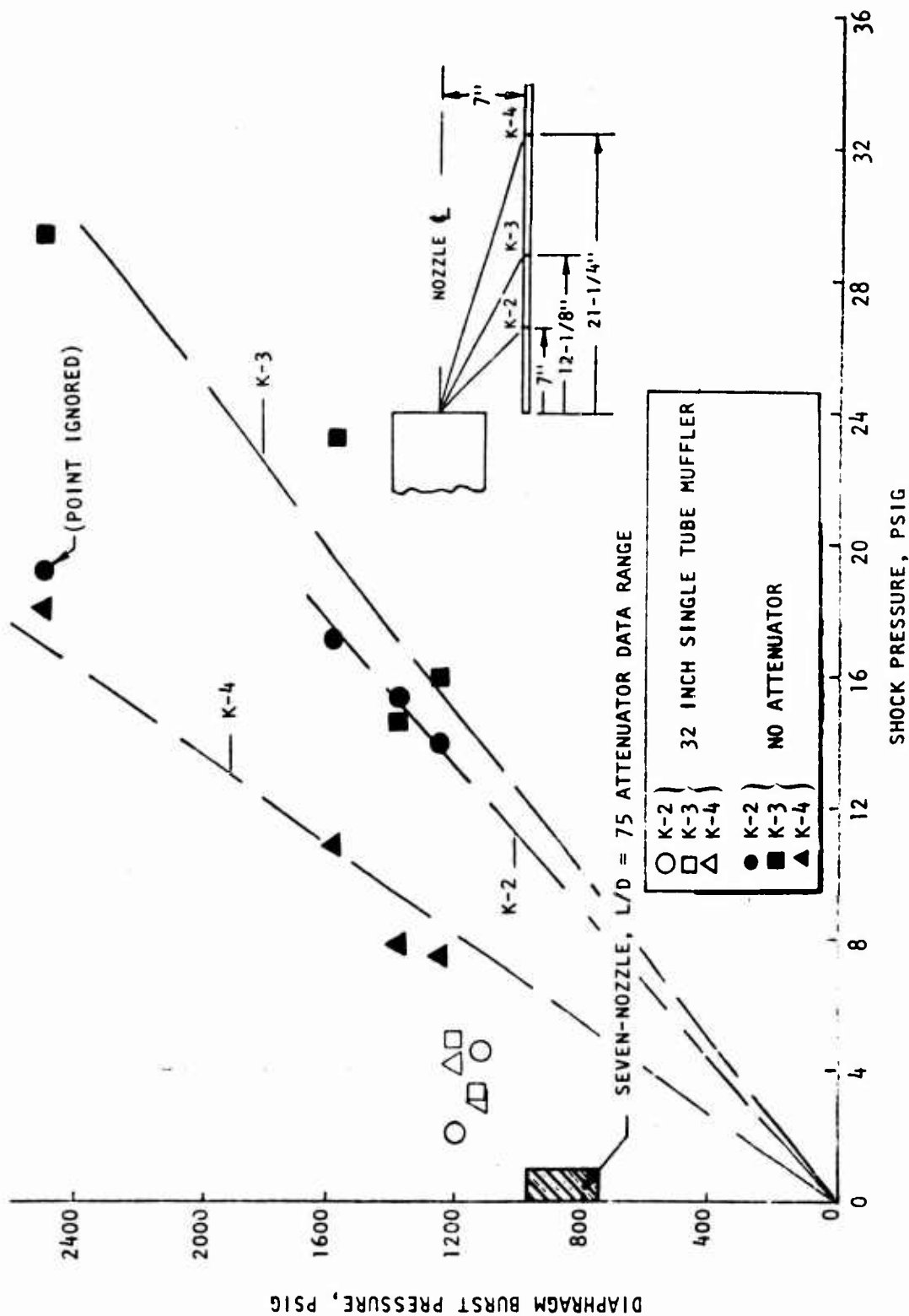Figure 45. Recoilless Rifle - Backblast Attenuation Peak Chamber Pressure vs Shock Pressure

Figure 46. Recoilless Rifle - Backblast Attenuation, Diaphragm
Burst Pressure vs Shock Pressure

R-9343

89

probably conservative and that the requisite attenuation can be obtained with a lower L/D ratio (i.e., within the length constraint, a smaller number of larger tubes could be used). Also, further attenuator simplfication might be achieved by careful selection and control of the rifle's rupture disk burst behavior.

POSTTEST INSPECTION OF HARDWARE

Visual inspection of the nozzle and suppressor hardware was made after every firing test with gun propellants. The single nozzle, without a suppressor, produced a definite blast sound and discharged a flame approximately 3-feet long and 3 inches in diameter during the firing. Solid-grain particles were discharged with the exhaust jet, as evidenced by the penetration of solid-grain particles through a paper barrier 6 feet downstream. The single nozzle was not eroded or affected by these reference nozzle firings.

Inspection of the 32-inch suppressor showed no effects of the firing except for the slight tarnishing of the washers. The flame from this suppressor during test was shorter and narrower than the reference nozzle firing. A definite blast noise was produced, but not as loud as the reference nozzle. The multinozzle and seven-tube suppressor firing did not produce a blast noise. The sound resembled a hiss of gas gradually discharging from a pipe. There was no visible flame issuing from the multitube suppressor.

Five tests were made with the multitube suppressor at peak chamber pressures from 4000 to 8000 psi; inspection of the passage through the washers and at the tubes showed no damage. However, on the sixth test, at a peak pressure of approximately 8000 psi (test No. 12), an axial flash of fire was noticed externally along the entire length of the suppressor tubes. The tube assembly was inspected from both ends and a slight blackening was noted near the upstream tube joint. Because the washer passage appeared clear, and the leak appeared to be minor, tests were continued with the same hardware after tightening all assembly bolts. On the next two tests, flashes of flame along the length of tubes were again noted.

R-9343
90

The multitube hardware was disassembled as shown in Fig. 47 and 48. In each tube, the copper washer nearest the nozzle plate was deflected or dished to a maximum of 0.035 inch from its original flat configuration. The spacers and remaining washers were not eroded or dished.

The leakage path of gun propellant gases from the tubes can be seen in Fig. 47 and 48. Erosion of four tubes occurred to a maximum depth of 0.050 inch at the nozzle end. The copper nozzle plate was tarnished but not eroded.

IMPULSE MEASUREMENTS

When the models were fired with gun propellants, the combustion products were exhausted only through the backflow nozzle so the model and mounting assembly would recoil from the force of the blast. The mounting structure was fixed to a movable plate in a channel and was restrained by two automobile shock absorbers, one on each side of the plate. Measurements of the recoil distance were made after each test with a steel rule. These data were incidental to the program and no calibration of the equipment was made. However, to approximate and compare the impulse from the suppressors with the nozzle alone, the recoil distances were used in an analysis of the probable impulse. Table 7 tabulates the recoil distances for every test made with gun propellants.

The data of Table 7 (with the single nozzle, no attenuator) were used to establish a calibration curve by plotting the measured recoil distance versus a calculated total impulse (Fig. 49). The impulse for the single nozzle without attenuator could be determined from the variation of chamber pressure, P_c, versus time: $\int F_1 \, dt = C_F A_t \int P_c \, dt$ where C_F ($\simeq 1.58$) is the thrust coefficient, $F/(A_t P_c)$ for a 4:1 area ratio nozzle using helium gas, and $A_t = \frac{\pi}{4}(0.5)^2$ is the nozzle throat area. The calibration curve determined in this way (Fig. 49) shows a variation of the recoil distance with the 2/3 power of the impulse. It was found by analysis that this relationship could be satisfied if the resistance force exerted by the shock absorbers would follow the law:

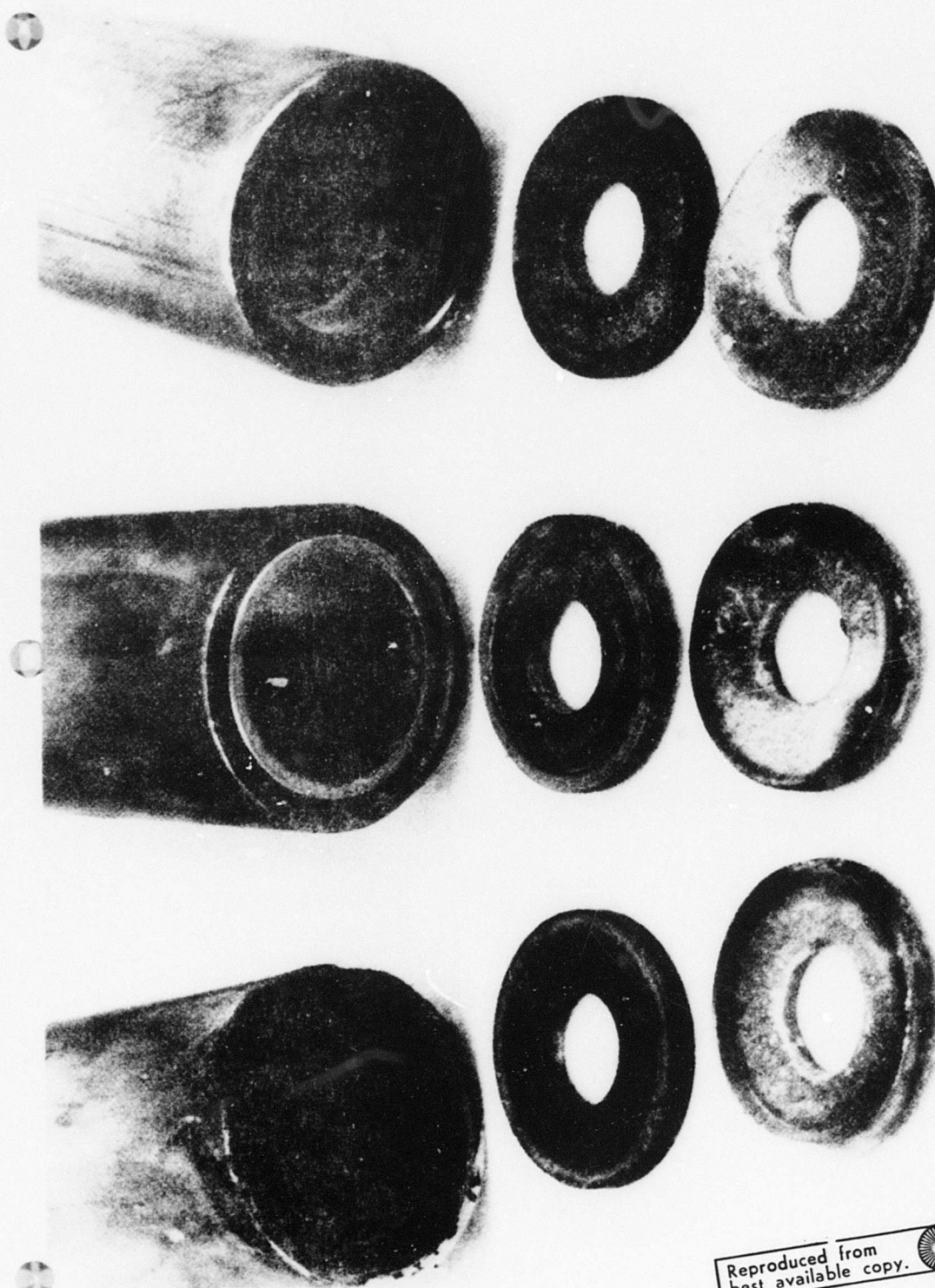$$F_2 = kxV^{4/3}$$

Figure 17. Photograph of Seven-Tube Suppressor After Firing with Gun Propellants (three tubes are removed showing first washer and spac exposed to multinozzle jet discharge)

5A036-7/20/73-C1C

Figure 48. Photograph of Seven-Tube Suppressor Tubes After Firing with Gun Propellants (first washers exposed to nozzle jet blast are shown in foreground)

5A036-7/20/73-C1E

R-9343

93

TABLE 7. SUMMARY OF IMPULSE DATA FROM SUBSCALE GUN PROPELLANT SHOTS

Shot No.	Peak Pressure, psig	Weight of Shock Tube + Attenuator + Sliding Mount, pounds	Recoil Distance, inches	Total Impulse, lb/sec
Series I: Single Nozzle, No Attenuator				
1	4100	195	1.0	12.8
2	6238		1-1/4	18.8
5	5838		1-1/4	19.3
6	7790	↓	1-7/16	22.9
Series II: Single Nozzle, L/D = 32 Attenuator				
3	3925	206	3/4	8.4
4	5825	↓	15/16	11.5
Series III: Seven-Nozzle, L/D = 75 Attenuator				
7	3875	217.5	3/8	3.0
10	3825		3/8	3.C
13	3625		7/16	3.6
8	5425		1/2	4.4
11	5842		5/8	6.3
14	5700		11/16	7.1
9	7512		3/4	8.2
12	7788	↓	13/16	9.0

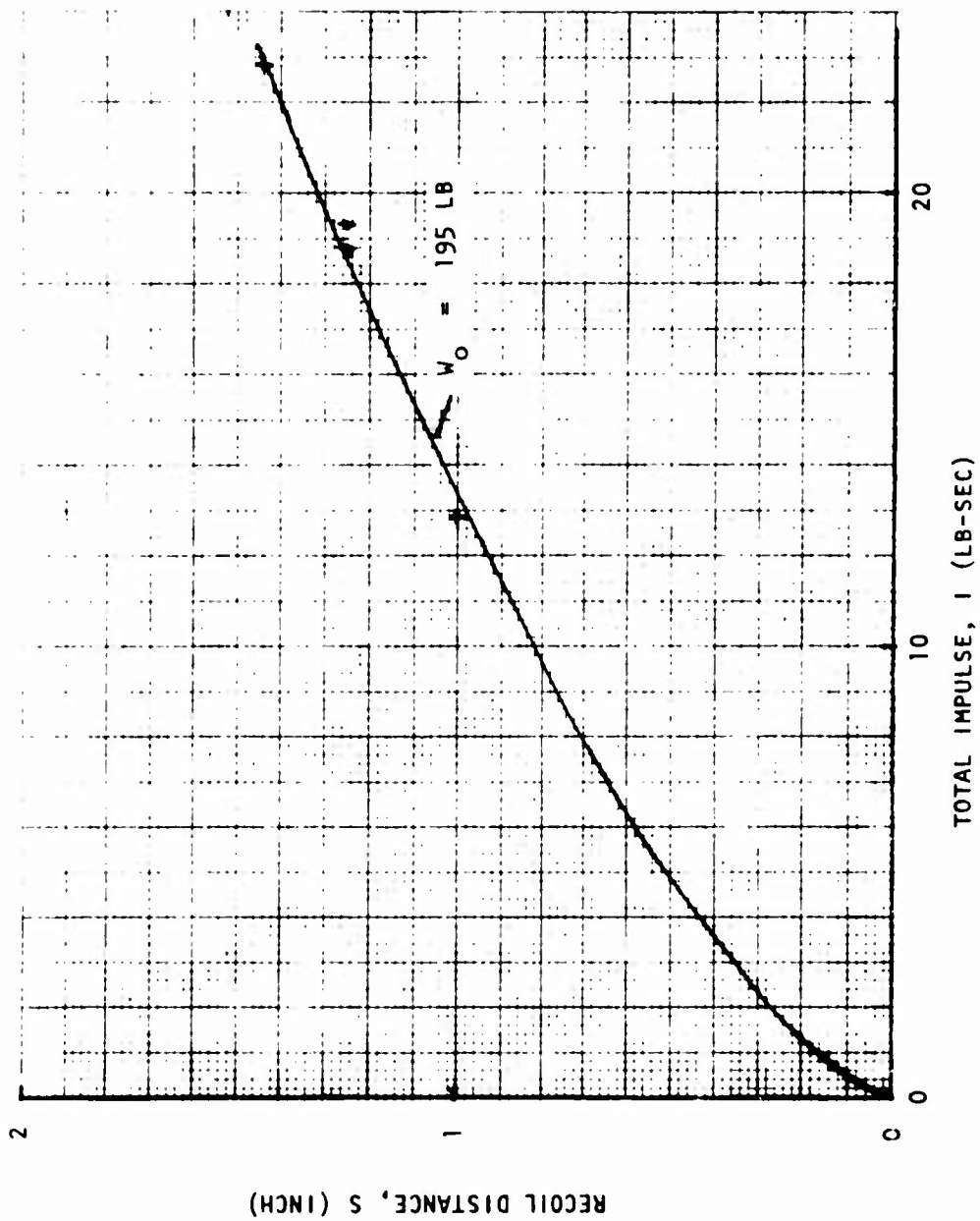TOTAL IMPULSE, I (LB-SEC)

RECOIL DISTANCE, S (INCH)

W_o = 195 LB

Figure 49. Shock Absorber Calibration Curve

where V is the velocity of the movable mounting structure and model. In that case, the total impulse associated with a given recoil distance would also be affected by the total mass of the moving parts:

$$I \quad \alpha \quad \frac{S^{3/2}}{\sqrt{W/g}}$$

and this was taken into account in determining the total impulse for the tests with the attenuators.

A plot of the total impulse versus peak chamber pressure for the reference nozzle and the two back-blast attenuators is shown in Fig. 50. The curves indicate a definite loss in impulse due to the attenuator. The L/D = 75 suppressor is shown to lose 2/3 of its original impulse. These results are not consistent with those of the helium shock-tube tests. Here again, however, heat transfer from the gases to the suppressor may provide at least a partial explanation of the observed results. Whereas it was conceived from the shock-tube tests that heat transfer from the attenuator to the gases might produce a lower loss in impulse as L/D is increased, cooling of the gases by the hardware would conceivably acentuate impulse losses by further declerating the gases, and this effect should increase monotonically with increasing L/D.

These data were correlated at the very end of the program so that it was not possible to analyze them further. The results presented certainly emphasize the importance of including thrust measurement (as a function of time) in any future back-blast attenuator experiments. A fluid dynamic analysis, including thermal effects, of the transient flow through an attenuator would also be desirable.
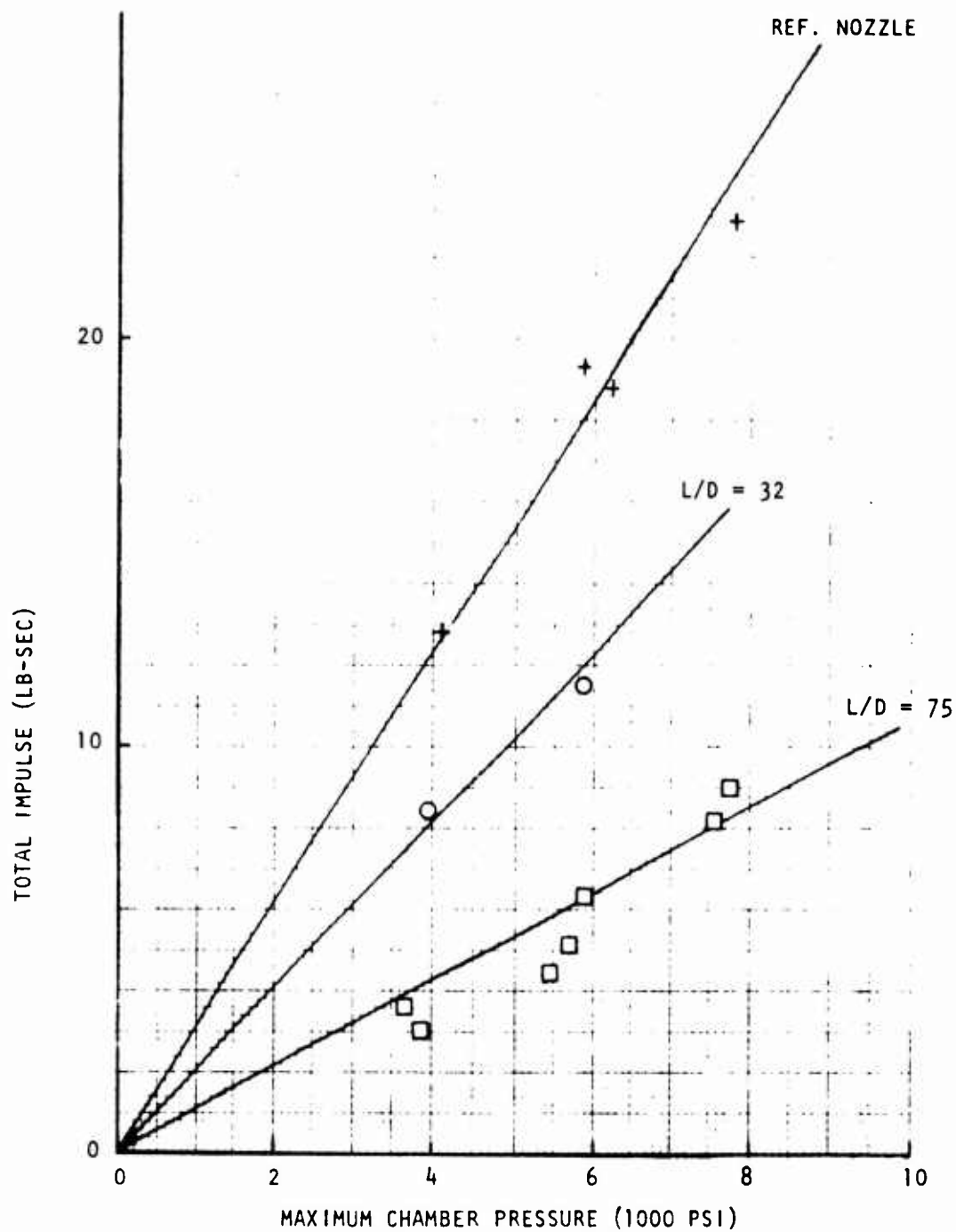
Figure 50. Comparison of Total Impulse From Reference Nozzle
and Blast Wave Suppressors

CONCLUSIONS AND RECOMMENDATIONS

A systematic series of laboratory tests, including the use of the water table, the shock tube with helium in an evacuated altitude test chamber, and the shock tube with gun propellants at the atmospheric gun firing range tunnel has been conducted for the Department of the Army, Watervliet Arsenal. The purpose of these tests was to develop a design concept that would attenuate the original nozzle blast wave-reflected pressure from the firing of a 105-mm recoilless rifle on a helicopter surface down to 5 psig, or approximately 0.15 of the original pressure.

Results and conclusions are summarized below:

1. Analysis of the shock wave pressures indicates that simulation of the full-scale blast wave can be made by using helium gas in a chamber with a burst diaphragm. Correlation of water table data indicates that preliminary trends in model performance can be observed.

2. Water table tests showed that the best suppression of the blast wave from a nozzle was obtained with a multibaffle, enclosed duct attached to the nozzle exit. It was shown that sufficient attenuation would not be obtained unless a long L/D ratio (suppressor length to hole diameter) was used.

3. The results of 30 tests with 16 different suppressor configurations on a 1/6.86 scale model of the 105-mm rifle chamber and nozzle with helium showed that the best suppressor configuration consisted of a series of baffled chambers in a closed tube in which the baffles are spaced 1 hole diameter (= nozzle exit diameter) apart, and the cavity depth is one-half the hole diameter. Extrapolation of L/D data from 32:1 indicated that L/D ratios of 60:1 or higher were needed to acquire attenuations as low as 12.5 to 15 percent of the original blast pressure.

4. A suppressor design concept was evolved from the laboratory tests and the recommended design for the full-scale rifle consisted of a 16-inch diameter shell, 23.5 inches long enclosing 253 steel tubes, 7/8 inch in diameter, each packed with a series of 60 copper washers and spacers. The baffled tubes had a length-to-hole diameter ratio of 75:1.

R-9343

5. A cluster of 7 tubes out of the 253 tube full-scale suppresor design was fabricated and tested with gun propellants at chamber pressures up to 7800 psi. The suppressor was successful in eliminating the blast wave and reducing the pressure levels to 0.15 or less of the original reference nozzle-reflected blast-wave pressure.

6. Inspection of the seven-tube suppressor hardware after eight gun propellant tests showed all hardware intact, except for minor leakage at the ends of the tubes and dishing of the first copper washers in each tube.

7. Examination of gun propellant blast-wave pressure test data showed no correlation between peak chamber pressure and blast-wave pressure. However, the wave pressure strength was dependent on the diaphragm burst pressure.

8. The impulse measurements from the helium shock tube tests showed little or no loss due to the suppressors. In the gun propellant tests, the 75:1 L/D ratio, seven-tube cluster, showed impulse losses, so that only one-third of the original nozzle impulse was obtained.

9. It is recommended that the full-scale design concept for the blast suppressor be built and evaluated experimentally, with the following design changes:

   a. Shorten the L/D from 75 to 60 to reduce the number of nozzle and tubes

   b. Reinforce the washers closest to the exhaust nozzles

   c. Seal the leakage path to the outside of the tubes

   d. Eliminate the outer shell surrounding the attenuator tubes

10. Subscale tests are recommended for investigating further the effect of burst diaphragm rupture pressure on the blast wave initial shock amplitude

11. Subscale tests are recommended to determine, by force-time measurements, the loss in impulse of suppressors with gun propellants.

REFERENCES

1. Alpher, R. A. and D. R. White: "Flow in Shock Tubes With Area Change at the Diaphragm Section," J. of Fluid Mech., Vol. 3, February 1958, p. 457.

2. AF Technical Report No. 5985, Studies on the Validity of the Hydraulic Analogy to Supersonic Flow, MIT.

3. Skochko, L. W. and H. A. Greveris: Report R-1896, Addendum I, Silencers, 9 mm P38 Walther Piston With Silencer (U), Ammunition Development and Engineering Laboratories, August 1968.

4. Skochko, L. W. and H. A. Greveris: Report R-1896, Silencers, Frankford Arsenal, August 1968.

APPENDIX A

BALLISTIC PENDULUM IMPULSE MEASUREMENT THEORY

The ballistic pendulum, as shown in Fig. A-1 provides a simple method of measuring the impulse from the gas discharging from the nozzle and/or muffler. The theory and operation are described below.

PENDULUM THEORY

The pendulum used for the shock tube investigation was analyzed as a compound pendulum because the mass was not concentrated below the pivoted arm, but was distributed in the vertical arm, the main chamber, the forward nozzle and suppressor and the rear counterweights.

The impulse from the gas discharge, $\int F_1 \, dt$, causes a reaction force F_2 on the pivot and a change in momentum of the center of gravity,

$$\int F_1 \, dt - \int F_2 \, dt = m \dot{x} \tag{A-1}$$

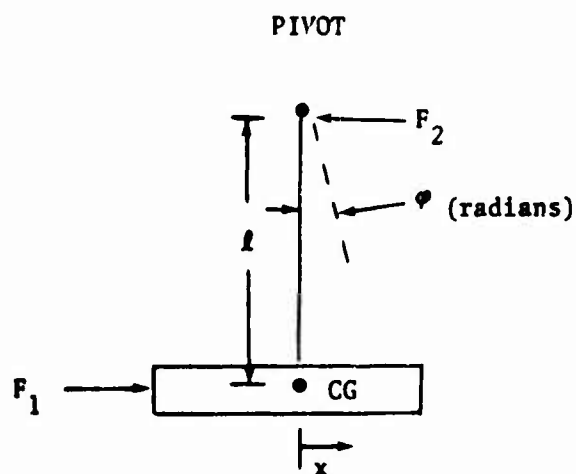where $\dot{x}$ is the horizontal velocity:

PIVOT

Figure A-1. Compound Pendulum

R-9343

A-1

$$\ell \int F_2 \, dt = I_{CG} \, \dot{\varphi} \tag{A-2}$$

where I_{CG} is the moment of inertia about the center of gravity, and $\dot{\varphi}$ is the angular velocity.

$$\int F_1 \, dt = m \dot{x} + \frac{I_{CG} \dot{\varphi}}{\ell} \tag{A-3}$$

Substituting $\dot{\varphi} = \dfrac{\dot{x}}{\ell}$ \hfill (A-4)

$$\int F_1 \, dt = m \dot{x} \, \frac{m + I_{CG}/\ell^2}{m} \tag{A-5}$$

From the conservation of energy principle, the kinetic energy is transferred to potential energy:

$$\frac{m \dot{x}^2}{2} + I_{CG} \frac{\dot{\varphi}^2}{2} = m g h \tag{A-6}$$

where h is the height to which the center of gravity is raised.

$$\frac{\dot{x}^2}{2} \left[m + \frac{I_{CG}}{\ell^2} \right] = m g h \tag{A-7}$$

$$\dot{x} = \sqrt{2 g h} \, \sqrt{\frac{m}{m + \dfrac{I_{CG}}{\ell^2}}} \tag{A-8}$$

From Eq. (5) and (8),

$$\int F_1 \, dt = m \sqrt{2 g h} \, \sqrt{\frac{m + I_{CG}/\ell^2}{m}} \tag{A-9}$$

Using the circular frequency of the pendulum, $\omega = \dfrac{2\pi}{T} = 2\pi f$ \hfill (A-10)

where T is the period and f the frequency,

$$\dot{x} = \omega x \tag{A-11}$$

$$h = \ell(1 - \cos \varphi) \approx \ell \frac{\varphi^2}{2} \approx \ell \frac{x^2}{2\ell^2} \approx \frac{x^2}{2\ell} \tag{A-12}$$

Using Eq. (8),

$$\omega x = \sqrt{2g\frac{x^2}{2\ell}} \sqrt{\frac{m}{m + \frac{I_{CG}}{\ell^2}}} \tag{A-13}$$

$$\omega x = x \sqrt{\frac{g}{\ell}} \sqrt{\frac{m}{m + \frac{I_{CG}}{\ell^2}}} \tag{A-14}$$

$$\omega = \sqrt{\frac{g}{\ell}} \sqrt{\frac{m}{m + \frac{I_{CG}}{\ell^2}}} \tag{A-15}$$

From Eq. (9) and (15)

$$\int F_1 \, dt = m \sqrt{2gh} \frac{\sqrt{g/\ell}}{\omega} \tag{A-16}$$

or, from Eq. (12), where $h = \frac{\varphi^2}{2} \ell$

$$\int F_1 \, dt = m \sqrt{2g\ell} \frac{\varphi}{\sqrt{2}} \frac{\sqrt{g/\ell}}{\omega} \tag{A-17}$$

$$\int F_1 \, dt = m g \frac{\varphi}{\omega} \tag{A-18}$$

$$\int F_1 \, dt = \frac{W \frac{\varphi \text{ (deg.)}}{180} \pi}{\frac{2\pi}{T}} \tag{A-19}$$

$$\int F_1 \, dt = \frac{W \, T \, \varphi}{360} \qquad \text{lb-sec} \qquad (A-20)$$

where the pendulum weight, W, is in pounds, T is the period of the pendulum in seconds, and φ is the angular deflection in degrees.

APPENDIX B

SUPPRESSOR HEAT TRANSFER ANALYSIS

Suppressor Thermal Analysis

Review of the thermal environment in the suppressor was made based on the design shown in Fig. B-1. The most critical areas in the suppressor are the individual throat sections of the suppressor nozzles where the heat transfer coefficients are the highest. For provision against a high heat transfer rate, a removable throat plate section of pure copper is to be used.

Throat Section

Based on a thermal analysis of the throat section a heat transfer coefficient may be approximately determined as follows:

$$N_{ST_B} \, N_{PR_B}^{2/3} = \frac{0.0296}{Re_x^{0.2}}$$

where Re_x is a surface distance Reynolds number based on a throat stagnation pressure average of 7000 psia (12,000 psia peak) and an effective episode time of 14 milliseconds. This is based on the Fig. B-1 operating pressure history. The following properties were used for analysis:

$\rho_\infty \, V_\infty$ (1b/in^2-sec)	40.8
N_{PR_∞}	0.82
C_{P_∞} (Btu/1b/R)	0.6
μ (1b/in-sec)	4.5×10^{-6}
x (in.)	0.095
$\overline{T}_{AW}$ (F)	4000

A heat transfer coefficient (h_g) value of 0.0535 Btu/in^2-sec-R was calculated corresponding to a heat flux of 160 Btu/in^2-sec at a time-averaged wall temperature of 1000 F.
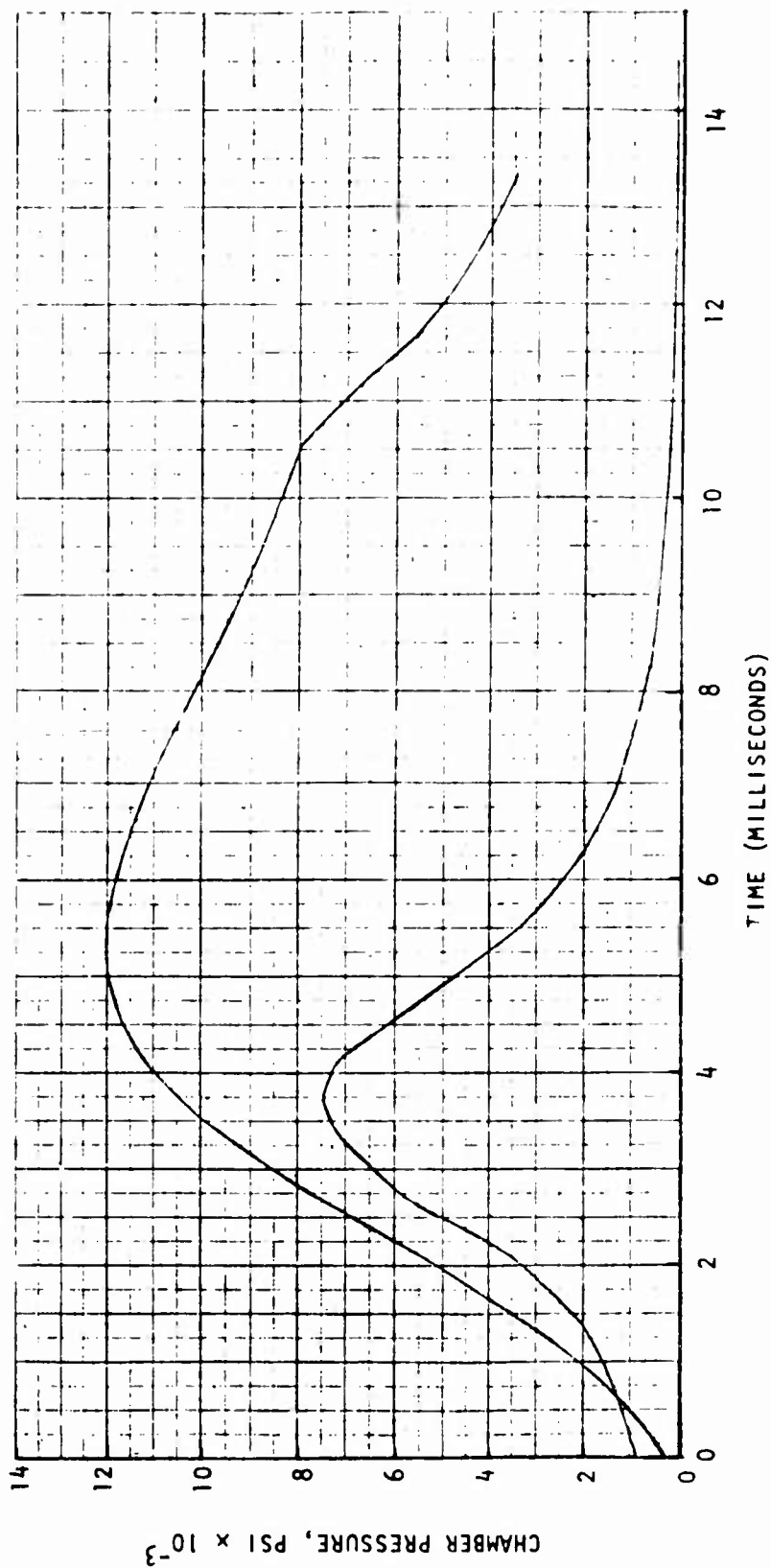
Figure B-1. Chamber Pressure History vs Time (105-mm Recoilless Rifle)

R-9343

A determination of the allowable heat transfer coefficient to the melting point of the copper throat can be defined from the infinite slab solution for a short thermal transient. For this approach the solution becomes:

$$\frac{h_g \sqrt{\alpha \tau}}{K} = f\left(\frac{\overline{T}_{AW} - T_W}{T_{AW} - T_i}\right)$$

where the right-hand side above becomes a function of initial ($T_i = 60$ F), adiabatic wall ($T_{AW} = 4000$ F) and maximum wall temperature of 1980 F (melting point). For a melting point level, f becomes:

$$f\left(\frac{\overline{T}_{AW} - T_i}{T_W - T_i}\right) = 0.71$$

The copper properties used were

α (ft^2/hr)	4.0
K (Btu/hr-ft-R)	200

Figure B-2 illustrates the throat heat transfer coefficient allowable vs time (τ). Comparing the allowable heat transfer coefficient (0.072) and the time averaged calculated value (0.0535), it is seen that a melting condition should not occur for the throat section.

Washer Section

Analyses indicate a reduced heat transfer coefficient for the beryllium copper washer section as a result of lowered pressure level. The upstream edge of the washer should however be the rounded edge to avoid a sharp edge condition. Based on a carryover of the free jet from the nozzle throat section to the first washer, an estimated heat transfer coefficient of $h_g = 0.027$ Btu/in.^{2}-sec-R
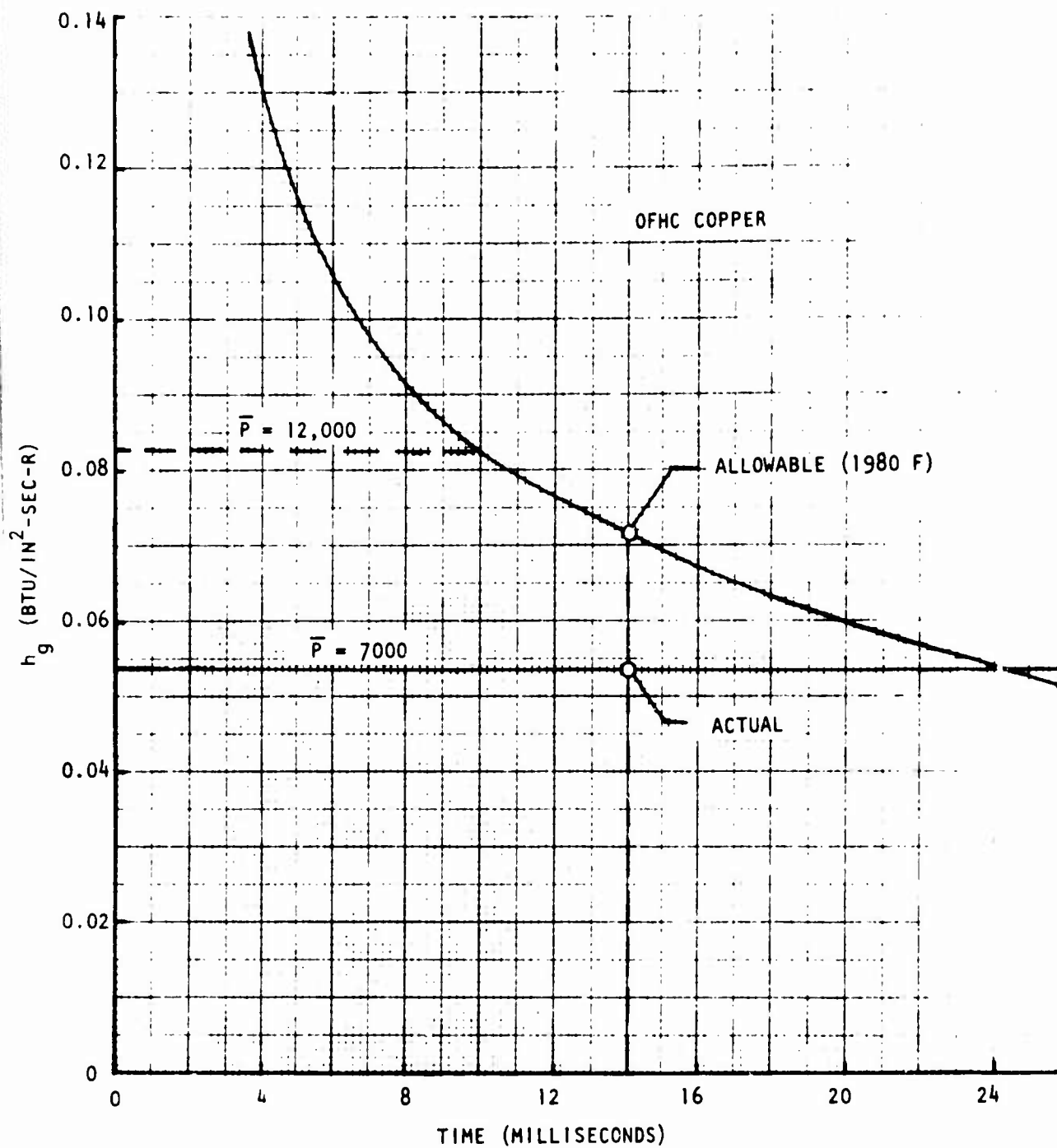
Figure B-2. Breech Blast Suppressor Throat Heat Transfer Coefficient vs Episode Time

should be imposed on the washer surface. A high-conductivity Be-Cu alloy should be chosen for the washers (70-100 percent of copper conductivity). The Be copper washers at a heat transfer coefficient mentioned should be satisfactory.

Aft Plate Section

The aft discharge nozzle plate of the suppressor is proposed to be manufactured of 4130 steel. Based on the thermal diffusivity (α) and thermal conductivity (K) values, the allowable heat transfer coefficient may be calculated as before. The assumptions made were:

$\overline{T}_{AW}$ (F)	3500
$T_{W\ MAX}$ (F)	2600
α (ft^2/hr)	0.452
K (Btu/hr-ft-R)	25
f (T)	1.91

The resulting heat transfer coefficient allowable vs time is shown in Fig. B-3 compared to the actual. It is noted that the actual exceeds the theoretical limit and some erosion may take place with 4130 steel at this point.

An estimate of erosion of the surface may be made by a determination of the thermal penetration distance ($x_{penet.}$). For a Fourier (N_{FO}) number:

$$N_{FO} \approx \frac{2}{\pi}$$

where $\quad N_{FO} = \dfrac{\alpha \tau}{x^2_{penet.}}$
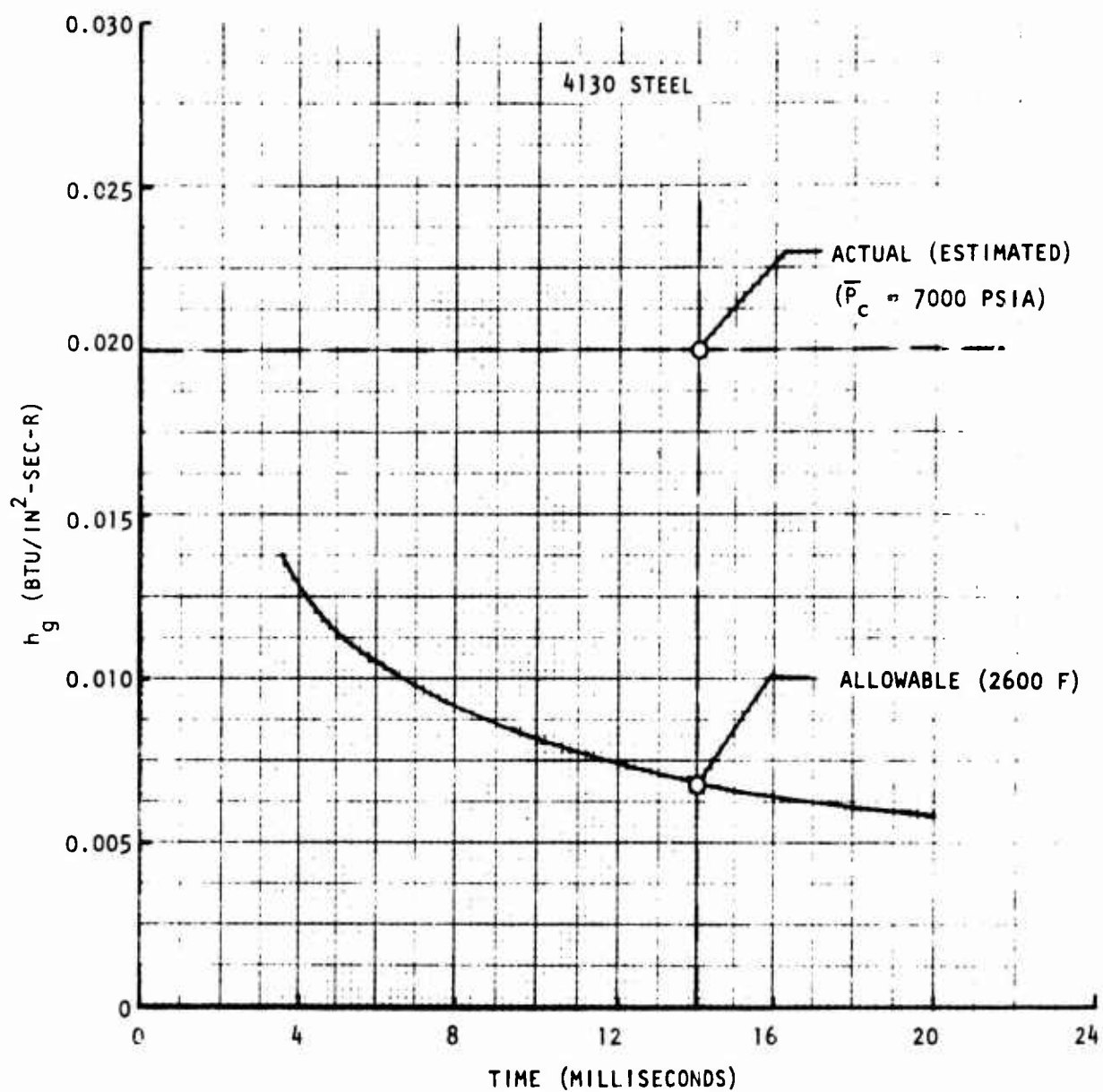
$$x = 0.94 \sqrt{\alpha \tau}$$

Figure B-3. Breech Blast Suppressor Exit Plate Heat Transfer
Coefficient vs Episode Time

For a 14-millisecond period the maximum erosion would be 0.015 inch. Actual erosion will be substantially less (≈ 0.003 inch) due to thermal blockage in the boundary layer resulting from 4130 metal melting and vaporization.

An alternate approach for a fully durable aft section would be to provide a copper nozzle aft plate bolted to the tubular suppressor assembly instead of the integral rear nozzle section.

Copper Nozzle Attach Screws

Review of the copper nozzle throat plate section attach screws was made. Heat transfer coefficients at these stagnation points was determined to be of the order of 0.03 Btu/in^2-sec. At this rate, some erosion on the screw head may take place as for the aft steel nozzle. However impingement of hot-gas particles on the stagnation areas may leave a thermally insulating residue to prevent further erosion. If substantial erosion is noted, replacement with Be-Cu high strength screws is proposed.

Thermal Result Summary

In summary, for short-term operation, the copper nozzle plate and copper suppressor washers should prevent major erosion with only slight erosion to be expected on the front plate screws and aft nozzle plate section.

APPENDIX C

ROCKET-ASSISTED PROJECTILE DESIGN CONSIDERATIONS

Based on the Rocketdyne suppressor performance projected for a rifle application with a 12,000 psia pressure, the 5-psi overpressure requirement would appear to be met. If, during full-scale testing of the device at 12,000 psia, the overpressure is greater than that allowed, a reduction in chamber pressure should afford a reduced overpressure at the expense of a reduced muzzle velocity.

Current arsenal testing with the 105-mm gun has indicated an overpressure (ΔP_o) directly proportional to the peak chamber pressure (P_c). As a result, the relationship below may be expressed;

$$\frac{(\Delta P_o)_1}{(\Delta P_o)_2} = \frac{(P_c)_1}{(P_c)_2}$$

Consequently, reducing chamber pressure to make up for any excess overpressure on the helicopter surface can be accomplished.

Evaluation of the 105-mm muzzle velocity testing has shown a reduced velocity over that anticipated for a given chamber peak pressure. As shown in Fig. C-1 the obtained muzzle velocity of 835 ft/sec at 8300-psia pressure is short of the required muzzle velocity of 1600 ft/sec. A comparison with the theoretical prediction is shown in Fig. C-1. At a 12,000-psia pressure condition, a muzzle velocity of 1200 ft/sec would be projected based on experimental results; this compares to 1800 ft/sec for a theoretical prediction. Adjustment of the grain burning rate is apparently necessary to provide a higher muzzle velocity together with the measured peak chamber pressure.

In a simplified analysis the muzzle exit velocity may be expressed as:

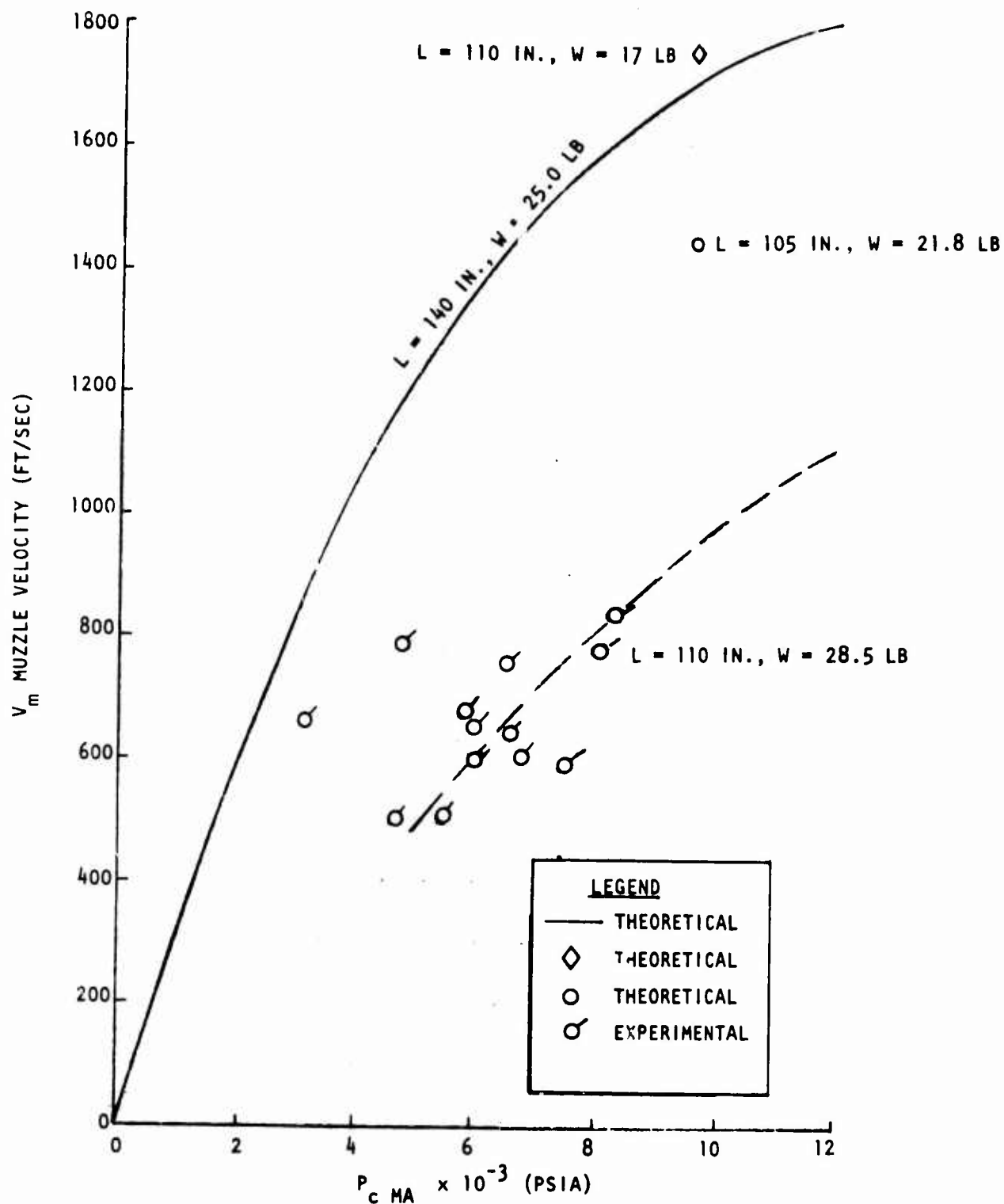$$V_m = K \sqrt{\frac{2 g \bar{P}_c A_B L}{W}} \; ; \quad \bar{P}_c = f (P_c)_{peak}$$

R-9343

C-1

Figure C-1. 105 mm Recoilless Rifle Muzzle Velocity vs Peak
Chamber Pressure

R-9343

where:

K	=	constant
$\overline{P}$	=	mean time integrated pressure
A_B	=	projectile base area
W	=	projectile weight
L	=	barrel length
g	=	gravitational constant
V_m	=	projectile exit velocity

A reduction in muzzle velocity proportional to the square root of the peak pres,ure would be anticipated. If the theoretical muzzle velocity shown in Fig. C-1 could be achieved (1800 ft/sec at 12,000 psia), a reduction to 6000 psia would result in a muzzle velocity reduction to 1270 ft/sec, necessitating only a 330 ft/sec increment to be made up by rocket assistance. As presently shown experimentally for a 6000-psia peak chamber pressure, an added 1000 ft/sec ΔV would be necessary to provide the 1600 ft/séc desired velocity with 500 ft/sec required for a 12,000-psia chamber pressure. It is apparent that modification of the charge burning rate to produce a lower peak pressure for the same exhaust velocity is the best approach.

Rocket-Assist Requirements

For a rocket-assist condition, the rocket exhaust velocity (v_e) can be expressed as:

$$v_e = \eta \sqrt{\left(\frac{2g}{\gamma - 1}\gamma\right)\left(\frac{RT}{M}\right)\left(1 - \frac{P_e}{P_c}\right)^{\frac{\gamma - 1}{\gamma}}}$$

The following conditions were estimated for the rocket-assist mode for a typical propellant (M8) gases:

γ	=	1.23	specific heat ratio
g	=	32.2 ft/sec	gravitational constant
R	=	1545 ft-lb/lb-R	gas constant
T	=	5480 R	isobaric flame temperature
M	=	26.6	molecular weight
P_e	=	13 psia	altitude discharge pressure
P_c	=	500 psia	mean rocket chamber pressure

R-9343

$$\eta \;=\; 0.90 \qquad\qquad \text{overall isentropic efficiency}$$

$$v_e \;=\; 6640 \text{ ft/sec} \qquad\qquad \text{exhaust velocity}$$

An exhaust gas velocity of 6640 ft/sec is calculated for this condition. Typical solid propellant exhaust velocities range from 4500 to 7000 ft/sec.

The exhaust velocity increment was calculated by the relationship:

$$\Delta V \;=\; v_e \; \ln_e \left(\frac{m_i}{m_f} \right)$$

which is shown in Fig. C-2. The incremental velocity is shown bracketed between 700 to 1200 ft/sec. At a typical ΔV design point of 900 ft/sec added velocity, the projectile mass ratio is 1.15, necessitating a 28.7-pound initial projectile weight for a 25-pound burnout weight. This requires a rocket propellant charge of 3.7 pounds.

Rocket-Assist Projectile Dimensions

Based on a typical 500-psia chamber pressure, the specific impulse becomes for the above conditions:

$$I_s \;=\; \frac{v_e}{g} \;=\; \frac{6640}{32.2} \;=\; 206 \text{ seconds}$$

The thrust becomes in terms of the flowrate, $\dot{W}$ (lb/sec):

$$\left(\frac{F}{\dot{W}} \right) = I_{sp}$$

For a 1.0-second burn time reference, the thrust becomes;

$$F \;=\; 762 \text{ pounds}$$

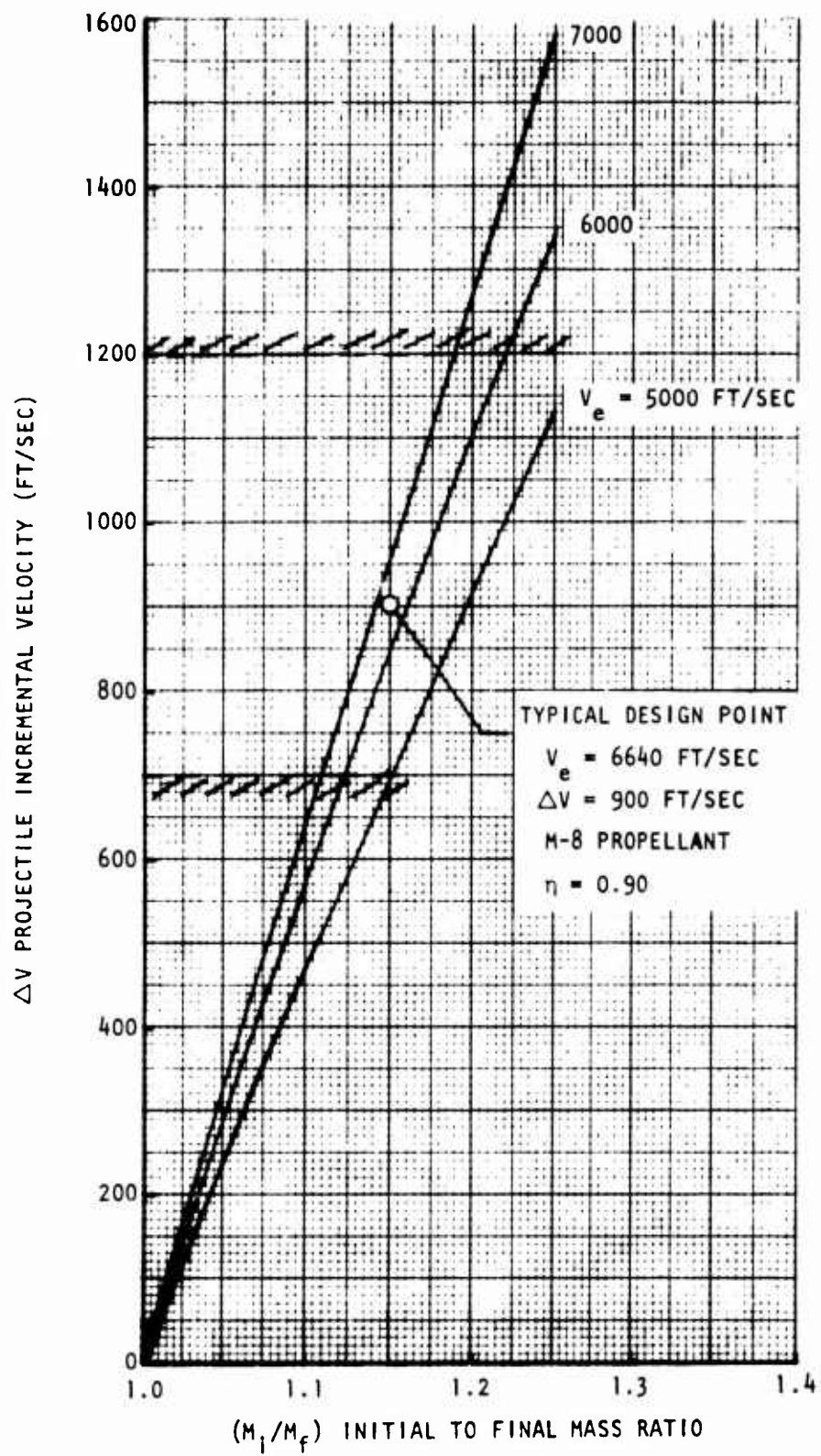$$\dot{W} \;=\; 3.7 \text{ lb/sec}$$

$$I_s \;=\; 206 \text{ seconds}$$

Figure C-2. Rocket-Assisted Projectile Requirements vs Projectile
Incremental Velocity

The initial acceleration of the projectile would be:

$$F = m_i a_i$$
$$a = 26.6 \text{ g's}$$

The final burnout acceleration becomes 30.5 g, which would be acceptable from structural consideration. Figure C-3 illustrates the burn time vs thrust level for a 3.7-pound charge. Figure C-3 illustrates the effect of the burn time on acceleration and thrust level.

Based on typical propellant characteristics, a density of 101 lb/ft^3 and a surface burning rate of 0.8 in./sec at 500 psia pressure, an end-burning solid grain charge design requires:

$$L = \left(\frac{W}{\rho A}\right) = \frac{3.7 \ (1728)}{101 \ (\pi/4) \ (D^2)} = \left(\frac{80.6}{D^2}\right) \text{ inches}$$

Based on a 3.8-inch diameter the length of charge becomes 5.6 inches. At an end-burning rate of 0.8 in./sec, the time required would be $\tau = 7$ seconds. Increasing the rocket chamber pressure to 2000 psia will afford an increase in burning rate to approximately 1.7 in./sec which will reduce the burn time to 3.3 seconds which is a more acceptable time.

Alternate Grain Configurations

Further reductions below a 3.3-second value will be accomplished by providing additional exposed surfaces for burning. A cylindrical hole or star-shaped grain center will result in an increased propellant consumption at the expense of a slightly increased propellant volume. The final selection of grain surface area and type should be made based on the burn time requirements of the rocket assist.
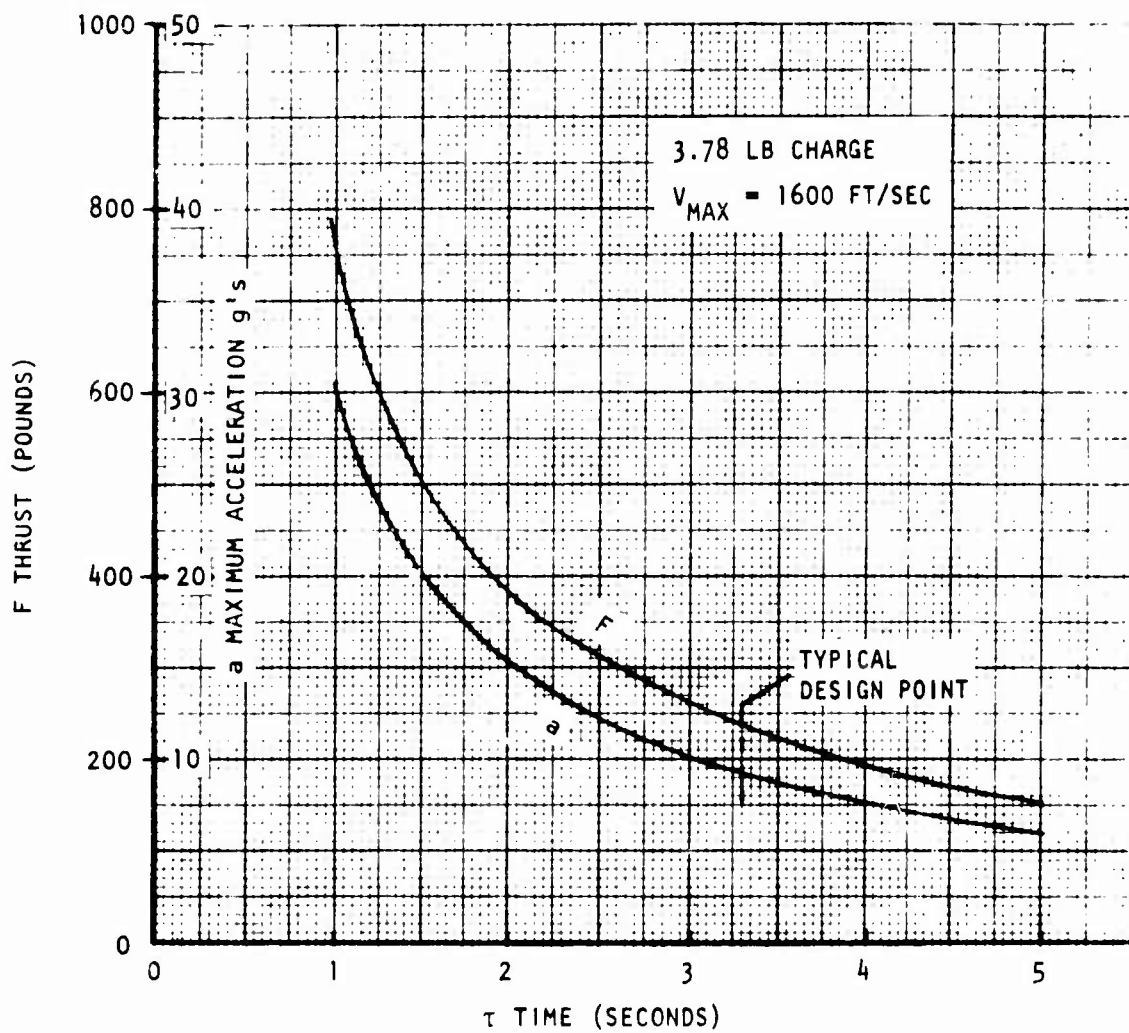
Figure C-3. Rocket Assist Projectile Thrust and Maximum Acceleration vs Burn Time

Assist Nozzle Dimensions

Based on a 2000-psia nominal chamber pressure and a 235-pound thrust, a
nozzle throat area may be defined as:

$$T = P_c A_t C_F$$

For a nozzle thrust coefficient of 1.65, the throat area becomes 0.0712 $in.^2$,
corresponding to a 0.30-inch throat dimension. For a 20:1 nozzle area ratio
the nozzle exit dimension will be 1.34 inch. A typical design configuration
is shown in Fig. C-4. A reduction to 500 psia would result in a throat
diameter of 0.6 inch, with a nozzle exit diameter of 1.7 inch corresponding
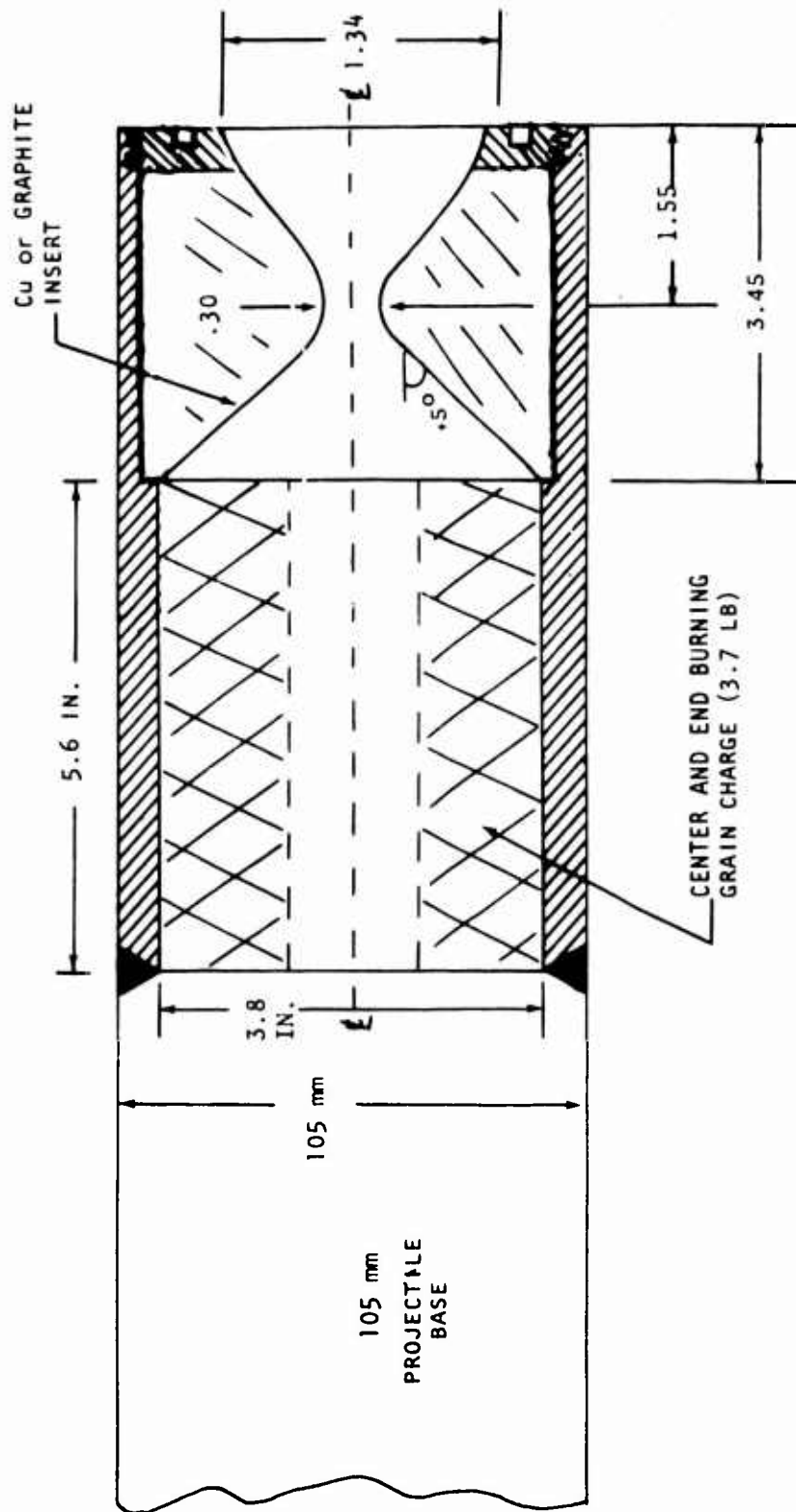to an area ratio of 8.0.

Figure C-4. Typical Rocket Assist Nozzle With Cylindrical Grain Charge for 2000 Psia Pressure